Tribology of Carbon Films as Protective Overcoats
for High Areal Density Disk Drive Applications

by

Walton Fong

B.S. (University of California, Berkeley) 1993
M.S. (University of California, Berkeley) 1999

A dissertation submitted in partial satisfaction of the

requirements for the degree of

Doctor of Philosophy
in

Engineering - Mechanical Engineering

in the

GRADUATE DIVISION

of the

UNIVERSITY OF CALFORNIA, BERKELEY

Committee in charge:

Professor David B. Bogy, Chair
Professor Kyriakos Komvopoulos
Professor Timothy D. Sands

Spring 2002

The dissertation of Walton Fong is approved:

_____

Chair   Date

_____

                                                           Date

_____

                                                           Date

University of California, Berkeley

Spring 2002

Tribology of Carbon Films as Protective Overcoats
for High Areal Density Disk Drive Applications

Copyright © 2002

by

Walton Fong

Abstract

Tribology of Carbon Films as Protective Overcoats

for High Areal Density Disk Drive Applications

by

Walton Fong

Doctor of Philosophy in Engineering – Mechanical Engineering

University of California, Berkeley

Professor David B. Bogy, Chair

Carbon films, either deposited by RF-sputtering or filtered cathodic-arc methods, are examined for use as protective overcoats in high areal density disk drive applications. The tribology and tribochemistry of the head-disk interface are studied in ultra-high vacuum (UHV) drag tests and thermal desorption studies. The material properties of the carbon films and their chemical interaction with the lubricant layer are characterized in nano-indentation, nano-scratch, X-Ray Photoelectron Spectroscopy (XPS), lubricant mobility, film density, and corrosion measurements.

RF-sputtered, nitrogenated carbon (CN_x) films are commonly found as protective overcoats in commercial disk drives. By studying the film's properties, we can extend their use into next generation products, which is desirable from both economic and engineering standpoints. Varying the nitrogen content in the carbon films changes several properties at the head-disk interface: (1) it increases the wear resistance of the CN_x overcoat due to an increase in the sp^3/sp^2 ratio, (2) it decreases the surface mobility of

ZDOL due to an increased dangling bond density in the carbon film, and (3) it decreases the catalytic decomposition of ZDOL in the presence of Al_2O_3 slider material.

As a promising alternative to RF-sputtered carbon films, filtered cathodic-arc carbon (CAC) films are characterized for use as ultra-thin protective overcoats. Their material properties are easily tuned by varying the ion energy during room temperature deposition. The most diamond-like properties occur at ion energies of 120 eV and there is a correlation between film thickness and hardness/elastic modulus. As a corrosion barrier, CAC films significantly outperform CH_x films and provide continuous coverage at a film thickness of 2 nm. CAC films hinder the catalytic decomposition of ZDOL in the presence of Al_2O_3 slider material compared to CH_x films in ultra-high vacuum drag tests. Finally, promising drag test results with 2 nm CAC overcoats on disk media are presented.

Professor David B. Bogy
Dissertation Chair

To my parents

TABLE OF CONTENTS

CHAPTER 4

SUMMARY AND CONCLUSION.. 98

LIST OF FIGURES

ACKNOWLEDGMENTS

I would like to thank my research advisor, Professor David B. Bogy, for his academic and financial support during my career at Berkeley. Throughout my stay at the Computer Mechanics Laboratory, his generosity, guidance, and candor have been invaluable in charting my way through the high seas of tribology research and academia - I am honored to have him as a mentor and a friend.

I am grateful for meeting C. Singh Bhatia, who has provided motivation and unwavering enthusiasm in all my adventures, both professional and personal. I cherish his friendship and look forward to our future collaborations at IBM.

I cannot express enough gratitude to the people at Lawrence Berkeley National Laboratory, IBM, Komag, Hysitron, and Read-Rite for sharing their workplaces, talents, and ideas with me as I fumbled along the course of my research. At LBNL, I am fortunate to have Simone Anders, Othon Monteiro, and Andre Anders introduce me to the world of cathodic-arc deposition. At IBM, my thanks belongs to a wonderful group of people including Jim Belleson, Mike Suk, Don Gillis, Reinhard Wolter, Richard L. White, Robert Waltman, Daryl Pocker, Cherngye Hwang, Andreas Wienss, and Ralph Ohr. I wouldn't be in graduate school without the encouragement of Judy Lin, Tu Chen, and Tom Yamashita at Komag to leave the exciting life of an R&D engineer and begin an endeavor more beneficial to my future. At Hysitron, I thank Lance Kuhn and Tom Wyrobek for their patience in fulfilling all my nano-indentation needs; at Read-Rite, I acknowledge Ashok Kulkarni for access to his deposition chamber for experiments.

I will always have fond memories of the camaraderie and friendships fostered at UC Berkeley: Anil J. Reddy, an all-around great guy who played a large role in my success at this school, I will miss all the fun times and difficult challenges we shared in this chapter of our lives; Brian Thornton, a world-class experimentalist who puts up with my nonsense in the lab and encourages me to stay in school as long as possible; Ryan Grisso and Mark Chapin, two gentlemen who made life in and out of CML more enjoyable; Roger Lo, what more can I say; and, of course, the numerous people who make up the CML crew.

CHAPTER 1

INTRODUCTION

1.1   Magnetic Recording

Magnetic recording technology envelops the everyday lives of our modern society. With the advent of the internet and digital multimedia, consumers rely heavily on storage devices such as hard disk drives, tape drives, and floppy disk drives to record and retrieve data for personal and business applications. Although these examples of magnetic recording in the computing world are the easiest to relate to, there are many more instances of magnetic recording technology at work in the background of our day to day tasks: the video tape we use in our VCRs to record our favorite TV shows, the audio tapes we purchase to play music on our stereos, and, of course, the credit cards we use at banks and retailers for transactions that hold account information in the magnetic stripe on their backs. This technology is omnipresent in our lives, yet consumers hardly think about the physics and engineering involved in designing and manufacturing these outwardly common, but extremely complicated systems. In fact, optical recording technology is much more glamorous and hi-tech to consumers due to the laser assemblies in their designs and, more recently, the influx of semiconductor flash memory cards into digital audio and video products with their almost instantaneous record/retrieval capabilities. However, it is the humble beginnings of magnetic recording over a hundred years ago that offered the fundamental knowledge for today's devices and provided the stepping stone for launching other recording technologies.

Magnetic recording has a long and rich history of creative personalities and technical innovations beginning with Oberlin Smith, a mechanical engineer who first noted his ideas for a magnetic recording device in 1878 [1]. Some evidence suggested that Smith built a prototype device in addition to the experiments he conducted to validate his theory, but it wasn't until Valdemar Poulsen demonstrated and patented his Telegraphone in 1898 that magnetic recording technology was born [2]. In his apparatus, the recording media was a steel wire. Using a telephone microphone as the input device, he fed the electrical current signal to an electromagnet that was moved along the wire "magnetizing" it. To retrieve the voice data, the electromagnet was moved along the wire in the same direction and its output was fed to a telephone earpiece. This simple system is the basis of all magnetic recording devices in the sense that it consists of (1) a recording medium that will retain its magnetization after it is removed from a magnetic field, (2) a recording head that generates a magnetic field during the write process and induces a current when exposed to a magnetized domain in the recording media during the read process, and (3) a mechanism to transport the head over the recording media.

In the next forty years, magnetic recording technology was advanced on steel wire recording products around the world, primarily in Germany, the United Kingdom, and the United States. One of the inherent problems of using steel wire as a recording medium was the inevitable twisting of the wire in between recording and playback, which caused distortion and limited frequency response of the recording. Advances to recording head designs, implementing magnetic coatings on nonmetallic bases, the use of AC bias, and the introduction of steel tape as a recording medium were pioneered as a result of

bypassing the shortcomings of steel wire technology.

During this period of development on steel wire and tape recordings, German inventor Fritz Pfleumer began parallel work on the use of paper impregnated with pulverized iron particles as "sounding paper", or an early version of our modern day audio tape. He patented his tape recorder in Germany in 1928 [1]. Subsequently, Pfleumer approached AEG (German General Electric) with his invention, and, together with BASF, they produced the world's first commercial audio tape recorder called the Magnetophon in 1935, which incorporated the "ring head" and a recording medium based on cellulose acetate coated with carbonyl iron powder. Carbonyl iron powder was eventually replaced with magnetite (Fe_3O_4) and then gamma ferric oxide (γ-Fe_2O_3), which was the material of choice until chromium dioxide in the 1970s. Nowadays, cobalt-doped or coated iron oxides, iron powders and barium ferrite particles may be found in various tape products. This tape recording technology evolved into our modern day cassette tape for audio and data applications. It was also adopted for video recording purposes when Ampex released the rotating-head video recorder in 1955 - we use this technology now in our consumer video cassette recorders (VCRs) albeit in a more mature form.

In the late 1940s, the need for random access mass storage systems was created by the rapid development of electronic data processing systems. Tape systems and punched cards did not provide fast enough access to information, so efforts were focused on developing magnetic drums for storing alphanumeric data. The first magnetic drum devices essentially started out as magnetic tape pasted to the outsides of cylinders

3

rotating at a fixed speed. A housing around the cylinder held the many recording heads at fixed, parallel tracks that allowed access to the information on the drum. Engineering Research Associates (ERA) produced many of these units for government, industrial, and academic users – each customized for a specific application and used spray-painted coatings of ferric oxide particles on the drum as the recording medium. In the latter era of these machines, head transport systems were incorporated into the design allowing a substantial decrease in the number of heads needed to access the data tracks. By this time though, hard disk drives had entered the picture, offering more storage space, and began their domination of the random access mass storage market.

1.2 Hard disk drives

In 1956, International Business Machines (IBM) introduced the first hard disk drive, or Winchester drive, in their RAMAC (Random Access Method of Accounting and Control) product. The IBM 350 held 5 megabytes (MB) of data on a stack of fifty 24-inch diameter disks with an areal density of 2 kb/in^2 [3]. Areal density is defined as the number of data bits per unit area of the recording medium surface and is determined by the linear bit density (bits per inch) along a circumferential track and the track density (tracks per inch) in the radial direction – the higher the areal density, the more information one can store on the same sized disk surface. In the early 1990s, areal density of disk drive products grew 60% annually before escalating to 100% per year just before the millennium, where it remains today [5]. One of the main driving forces for this accelerated growth rate is economics. Increasing the areal density reduces the number of disk and slider components utilized in the drive design, which lowers manufacturing

costs and increases the profit margins made by the drive manufacturers. Competition in this industry has led to practically non-existent profit margins for these companies and any manufacturing or technological advance that cuts costs gives one a significant advantage over the others. At the time of this writing, Fujitsu's latest mobile disk drive product held 40 gigabytes (GB) on two 2.5-inch platters with an areal density of 36.4 Gb/in^2 [6]. In addition to products, there are technology demonstrations where companies like Seagate have shown recently that 100 Gb/in^2 areal densities are achievable [7]!

The picture of a modern disk drive product is shown in Figure 1.1. It basically consists of three components: (1) the rotating, rigid disks that store information, (2) the head-stack assembly (HSA) that holds the read/write heads mounted to suspensions, and (3) the circuit boards/electronics needed to operate the drive. The disks are a multi-layered structure either based on an aluminum-magnesium substrate or one made of glass. In Figure 1.2, a schematic of the disk multi-layers are shown:

(1) Disk substrate – either made of aluminum-magnesium alloy or glass.

(2) Nickel Phosphorus layer – the substrate is chemically plated with nickel phosphorus so that the disk surface may be polished very smoothly and lightly textured, if necessary.

(3) Magnetic layer – typically consists of a multi-phase alloy with base components of cobalt, chromium, platinum, and trace amounts of other elements. An underlayer may be deposited first to promote preferential grain growth in the magnetic layer.

(4) Carbon overcoat layer – an amorphous diamond-like carbon film that

protects the magnetic layer from the environment and damage due to slider contacts.

(5) Lubricant layer – finally, a thin lubricant layer is deposited to protect the carbon overcoat from wear.

The schematic of a typical head-gimbal assembly (HGA) is shown in Figure 1.3. The head (or slider) is attached to the metal suspension, which provides a load on the head against the disk, at the gimbal. Today's heads are made of an alumina and titanium carbide (Al_2O_3-TiC) matrix with an air-bearing rail design etched onto the surface facing the disk, which is then coated with a diamond-like carbon film. During normal drive operation, the slider "flies" on a hydrodynamic air film (air-bearing) that forms between the slider and disk surface – the rail design develops pressure profiles under the slider surface that control its static flying attitude and its responses to dynamic fluctuations at the head-disk interface. Data is recorded and read-back via the read-write transducer located at the rear (trailing edge) of the slider, where the distance between the disk and the slider is smallest.

The distance between the read-write transducer and the magnetic layer is commonly referred to as the magnetic spacing and encompasses everything between these two points: disk carbon overcoat thickness, disk lubricant thickness, air-bearing, slider carbon overcoat thickness, and pole-tip recession (a common phenomenon where the transducer surface is not flush with the slider surface, but recessed slightly). Wallace's spacing loss equation,

$$\text{Spacing loss} = \frac{55d}{\lambda} \; (\text{dB}) \qquad (1)$$

where d = spacing and λ = wavelength, describes the loss in the playback signal due to the physical distance between the read-write transducer and the magnetic bit on the disk [8]. It states that the magnetic spacing needs to decrease exponentially to continue increasing the areal density of future products. Reducing the flying height of the slider has been the simplest way to reduce the magnetic spacing so far, as demonstrated by the drop in flyheight of the original IBM 350 slider at 20 µm down to 10 nm for today's products [3]. Of course, the reality of physics dictates that the minimum value of this spacing is ZERO (physical contact), but we have already observed contact issues well before this hard limit in sliders designed to fly at 7 nm due to the fact that disk surfaces still possess some level of roughness despite our best polishing efforts [9]. The only other alternative for reducing the magnetic spacing involves scaling down the physical layers such as the protective overcoat (on both disk and head surfaces) and the lubricant film. For 1 Tb/in^2, the theoretical models predict that these layers need to be on the order of one to two nanometers [10]. At these levels, the reliability of the head-disk interface (HDI) is jeopardized if careful integration of these layers is not accomplished through the design of a tribologically-robust system – an area of research that has the daunting task of making the seemingly impossible a reality.

1.3   Tribology of the head-disk interface

Tribology is defined as the science of wear and friction between two contacting surfaces moving relative to each other. Research and development in this area is popular in numerous industries - automobile, aviation, and metal cutting to name a few - where moving machine parts have finite lifetimes and extensive effort is focused on materials

selection and lubricant innovation to improve friction, heat generation, and wear life. In a hard disk drive, tribology is critical at the head-disk interface where head contacts with the disk surface during normal operation may cause it to prematurely fail or "crash". These contacts may occur during the aggressive, slider-dragging regime of contact-start-stop (CSS) systems, during steady-state flying over the data zone, or during the dynamic slider loading/unloading in modern load/unload drive designs [9, 11]. These failures include the collection of wear or lubricant debris on the slider surface, which results in increased magnetic spacing and loss of signal, or more commonly, a catastrophic failure of the protective carbon overcoat leading to physical damage of the magnetic layer. Efforts to alleviate the contact stresses at the HDI have led to several key innovations such as laser-textured landing zones on the disk, "padded" sliders, and fast "take-off" sliders [12-14].

The reliability of the HDI hinges upon the physical layers that protect the magnetic layer on the disk – the protective overcoat and the lubricant layer. Amorphous, diamond-like carbon (DLC) films deposited by RF sputtering (reactive and non-reactive), ion-beam deposition (IBD), or chemical vapor deposition (CVD) have been the materials of choice for this overcoat application. Depending upon their deposition conditions, these DLC films provide varying levels of scratch resistance, corrosion protection of the magnetic layer, and, more importantly, chemical compatibility with the lubricant layer. The most popular lubricants for disk drive applications are perfluoropolyethers (PFPEs), which include Ausimont Fomblin ZDOL, Z Tetraol, AM2001, and AM3001. These lubricants were adopted from the aerospace industry where their applications required chemical and

thermal stability to limit decomposition, low surface tension for good coating and high spreading, low vapor pressure to reduce evaporation loss, good viscosity index to insure low change in viscosity over a wide temperature range, and excellent lubricity for reduced friction and wear. The technical challenge presented by the push for higher areal densities is the scaling down of these films to atomic levels while retaining their coveted protective properties.

To compound the problem, more stresses can be expected at the HDI as lower fly-height slider designs generate more mechanical interaction between the disk and slider, increasing friction and heat generation, and accelerating wear of the overcoat. In addition, "tribochemistry" of the HDI becomes significantly more important, where chemical reactions that occur due to repeated head-disk contacts may alter the lubricant layer and its properties. This includes decomposition of the lubricant molecule resulting in poor lubricity, or removal of the lubricant molecule due to poor adhesion to the carbon overcoat surface. Both mechanisms can have serious repercussions on the reliability of disk drives by depleting the supply of lubricant on the disk surface. The chemical interactions between the carbon overcoat and lubricant layer plays a large role in this "tribochemistry" and our research, along with many others, is focused on elucidating the complex mechanisms that occur at this nano-scale level and selecting the appropriate combinations of materials to provide a robust, tribological system for this application.

1.4   Objective

The objective of this research is to evaluate the materials used as protective overcoats for

future high areal density disk drive products. An emphasis is placed on characterization of the material properties of the overcoats, their interaction with the lubricant layer, and the resulting tribological and tribochemical phenomena that occur in head-disk contacts to determine the reliability of the HDI.

1.5   Dissertation outline

This dissertation is divided into four chapters. The first chapter is an introduction and outlines the history of magnetic recording leading to the development of the hard disk drive and the motivation for the research presented in this manuscript. Chapter 2 is an investigation of sputtered, nitrogenated carbon (CN_x) overcoats and the effects of nitrogen content on the tribological performance at the HDI. Chapter 3 is an investigation of cathodic-arc carbon films as a promising alternative to sputtered carbon films for protective overcoat applications. Finally, Chapter 4 presents the conclusions of the dissertation.

rigid disks

head-stack assembly

circuit boards/electronics

Figure 1.1. Picture of typical disk drive product consisting of 3 primary components: (1) rigid disks, (2) head-stack assembly, and (3) circuit boards/electronics [4].

Lubricant layer

Carbon overcoat layer

Magnetic layer

Nickel Phosphorus layer

Al-Mg or glass substrate
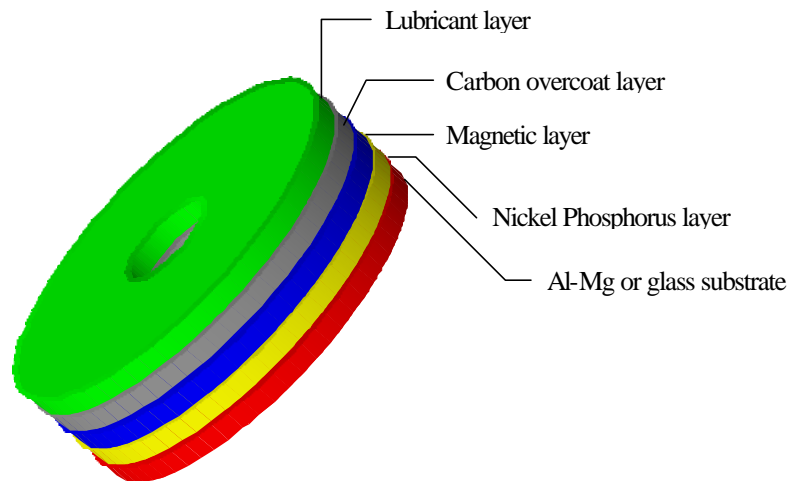
Figure 1.2. Schematic of disk multilayers: (1) Al-Mg or glass substrate, (2) Nickel Phosphorus layer, (3) magnetic layer, (4) carbon overcoat layer, and (5) lubricant layer. (picture not to scale)

11
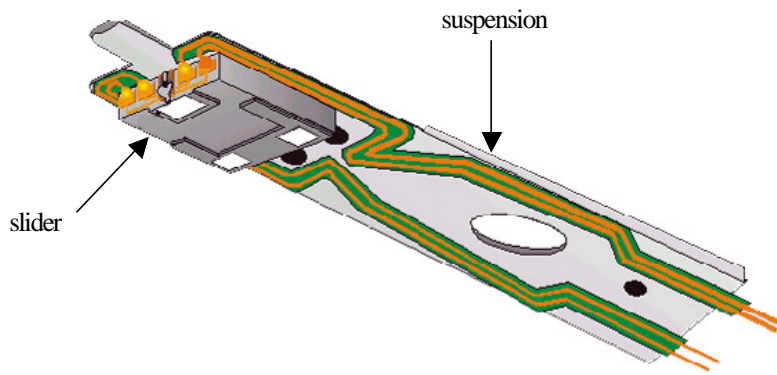
Figure 1.3. Schematic of head-gimbal assembly (HGA) consisting of (1) slider and (2) suspension [5].

CHAPTER 2

SPUTTERED NITROGENATED CARBON (CN$_X$) FILMS AS PROTECTIVE OVERCOATS

Abstract

A study on the effects of nitrogenation in sputtered, amorphous carbon overcoats (CN$_x$) on tribological performance in UHV drag tests is presented. To explain the phenomena observed in these tests, further characterization of the CN$_x$ material properties and their interaction with ZDOL lubricant was carried out using the following techniques: (1) ESCA/XPS analysis, (2) Hysitron nano-scratch tests, and (3) Candela OSA lubricant mobility measurements. It was found that increasing the nitrogen content from 0 to 16 at. % in the carbon film effectively changes three properties at the head/disk interface: (1) it increases the wear resistance of the CN$_x$ overcoat due to an increase in the sp^3/sp^2 ratio, (2) it decreases the surface mobility of ZDOL due to an increased dangling bond density in the carbon film, and (3) it decreases the catalytic decomposition of ZDOL in the presence of Al$_2$O$_3$ slider material. A mechanism for the reduced catalytic decomposition is proposed. In UHV drag tests, the wear life of CN$_x$ disk samples tested with DLC-coated sliders is governed by the first two properties, while tests with uncoated sliders are governed by all three.

2.1   Introduction

As a human civilization, we have accumulated approximately 12 exabytes (12 x 10^{18} bytes) of information in the last 300,000 years. However, with the advent of the internet

and digital media applications, analysts predict that this number will double in the next 2.5 years [15]! To keep up with this blistering information growth, the need for storage is enormous. As noted previously in Chapter 1, the areal densities of disk drive products have increased year after year at a rate of 100% since 1997 with no indications of decelerated growth in years to come [16]. Because Wallace's spacing loss equation dictates that the spacing between the read/write transducer on the head and the magnetic layer on the disk exponentially decreases as a function of areal density, the protective overcoats on these surfaces must be reduced also [17]. In fact, for 100 Gb/in^2 and 1 Tb/in^2 areal densities, recording performance models predict magnetic spacings of 10 and 6.5 nm, respectively [18, 19]. Overcoats on both the disk and slider, in turn, are on the order of 1 nm thick for the latter case!

Amorphous diamond-like carbon (DLC) films are popular choices as overcoat layers on these substrates and may be deposited by various techniques including DC magnetron sputtering [20-22], ion-beam deposition [23-25], and filtered cathodic-arc deposition [26-28]. Of particular interest to the disk drive industry is the use of sputtered DLC films as overcoats because the majority of media and head manufacturers would like to extend the life of existing sputtering tools in their process lines. However, at film thicknesses of 1 nm, sputtered carbon films may not possess the tribological properties required of a protective overcoat: (1) wear resistance, (2) corrosion protection, and (3) chemical compatibility with the lubricant.

Excellent wear resistance of the protective overcoat is a necessity -- with slider flyheight

designs approaching 3.5 nm, intermittent contact between the head and the disk during normal operation is inevitable [29]. The addition of hydrogen and nitrogen to the carbon overcoat has allowed researchers to enhance the material properties of these DLC films for this need and much work has been published on this topic [21, 30-44]. Because of its properties, the use of CN_x films as a protective overcoat (5 to 10 nm thick) is widespread in the disk drive industry now and focus on developing thinner films without sacrificing performance continues today.

The magnetic alloy (usually a combination of cobalt, chromium, platinum, and other elements) used for the storage medium on disk media is highly susceptible to corrosion from the environment [17]. The oxides that form on this surface accumulate on the ABS and impair the stability of the slider's operation resulting in degradation of the readback signal and possibly failure of the HDI [45]. Hence, the need for an overcoat that acts as a barrier between the magnetic layer and the environment. Until recently, the porous nature of ultra-thin (< 5 nm) sputtered DLC overcoats prevented them from protecting the magnetic layers sufficiently, but by varying the deposition parameters during film preparation, researchers have been able to manipulate the microstructure of CN_x films extensively for various applications [39, 46, 47]. For disk drive applications, Guruz et. al demonstrated that by applying a pulsed bias voltage to the target and substrate during deposition, they were able to mono-energetically bombard the growing CN_x films and produce films as thin as 2 nm with excellent corrosion resistance [48]. With the addition of substrate tilt and rotation, Li et. al were able to extend that level of corrosion protection to 1 nm films [49]. These latest developments with sputtered CN_x films make

them a viable overcoat candidate for future disk drive products.

In addition to the increased mechanical interaction with low slider flyheights, the chemical reactions that occur at the HDI during those contacts are significant. The lubricant layer's role on the disk media is to reduce wear and friction during normal operation conditions and its durability must match that of the expected lifetime of the drive [17]. Lubricant evaporation, degradation, and diffusion are all factors that may be detrimental to the lifetime of the lubricant, especially in current disk media designs where the lubricant layer is only a few atoms thick, and they are influenced by their interaction with the underlying carbon surface. We use the term "tribochemistry" to describe these chemical interactions between the lubricant and carbon overcoat layers at the HDI and their effect on tribological performance [50]. The tribochemical studies of ZDOL, a popular PFPE lubricant for disk media, with carbon overcoats has led to the adoption of DLC-coatings on slider surfaces for extended life of the HDI. Kasai et. al showed how ZDOL lubricant decomposes differently in the presence of Al_2O_3 material versus pure thermal stimulation [51], and Yun et. al verified those findings in actual drag tests with disks and sliders (with and without DLC-coatings) in ultra-high vacuum [52]. Chen extended those studies to include the effects of various lubricant and overcoat parameters on drag life and lubricant decomposition [53]. Many others have conducted a myriad of experiments ranging from lubricant mobility measurements [54-56] to triboelectron-stimulated degradation of lubricant [57, 58] to in-situ monitoring of lubricant redistribution in flyability tests [59, 60] – all with the express purpose of gaining insight into understanding the chemistry at the HDI. On the theoretical side, a large repository of

work is available on models for lubricant and carbon overcoat interaction from Waltman [61-64], Kasai [65, 66], and others.

In this study, we investigate the effects of nitrogenation in sputtered DLC overcoats on the wear durability, friction, and lubricant decomposition in drag tests with an ultra-high vacuum tribochamber. Others have focused primarily on scratch-resistance of CN_x films or on the lubricant interaction with CN_x overcoats – it is our goal in this chapter to demonstrate the combined effects of lubricant decomposition and material properties of the CN_x films on actual drag tests with disks and sliders. Analysis of the CN_x overcoats and lubricant layers provide supporting evidence for the phenomena observed in these experiments.

2.2   Experimental methods

2.2.1   Sample preparation

In this work, the disk samples were commercially-available, 65 mm aluminum disks with a "super-smooth" data zone (rms surface roughness of 0.349 nm). All samples were manufactured identically up to the carbon overcoat layer (i.e. plating, polish, texture, magnetic layer), whereupon an 11 nm CN_x overcoat was sputter-deposited with different nitrogen contents ranging from 0 to 16%. Processing of the CN_x overcoats was done by Richard L. White (IBM San Jose) in a commercial, single-disk sputter tool (BPS Circulus M12) with a base pressure of 3 x 10^{-7} Torr, using high purity graphite targets in Ar/N_2 gas mixtures. To control the nitrogen percentage in the films, the partial pressure of N_2 was varied from 0 to 2 mTorr, while holding the total deposition pressure to approximately 6

mTorr. The deposition rate was ~ 1 nm/s. A total of five sets of CN_x overcoats with nitrogen contents of 0, 6, 9, 13.6, and 16% were fabricated. Nitrogen content in the CN_x overcoats was determined using Auger electron spectroscopy.

Upon completion of the CN_x overcoat process, all samples were lubricated with 1.4 nm of perfluoropolyether (PFPE) ZDOL by a dip-coating process and subjected to the same post-processing steps. The molecular weight of the ZDOL was 2000 AMU and its chemical formula is given below:

$$CH_2OH\text{-}CF_2O\text{-}(CF_2O)_m\text{-}(CF_2CF_2O)_n\text{-}CF_2\text{-}CH_2OH \text{ where } n/m = 2/3 \qquad (2)$$

To insure uniform total lubricant thickness across the five sets of disks, the samples were drawn out of the lubricant bath at various pull rates ranging from 4.5 to 9.0 mm/s. Subsequently, a post-test measurement of all the disks revealed "bonded" lubricant thicknesses between 0.42 to 0.48 nm and "mobile" lubricant thicknesses ranging from 0.37 and 0.55 nm. Figure 2.1 gives the specific details for each cell. We defined the "bonded" lubricant as the portion remaining on the disk after a stripping process in a solvent bath. Subtracting the "bonded" lubricant thickness from the total lube thickness yielded the "mobile" lubricant contribution. All lubricant thicknesses were measured with Fourier transform infrared spectroscopy (FTIR) by Robert Waltman (IBM San Jose).

In addition to the disk samples, a second set of 5 nm CN_x overcoats was deposited on Si <100> wafer substrates with the full disk structure described earlier. These samples had

nitrogen contents of 0, 6.5, 10.8, 16, and 20.5% in the CN_x overcoat. However, half the samples from each cell were lubricated at a constant pull rate of 1.7 mm/s, while the second half remained unlubricated. These samples were used in the nano-scratch tests and ESCA/XPS analysis.

2.2.2 X-Ray Photoelectron Spectroscopy (XPS) analysis

Surface analysis of the 5 nm CN_x samples with and without ZDOL lubricant was done with a Phi Quantum 2000 Electron Spectroscopy for Chemical Analysis (ESCA) system equipped with a monochromatic Al Kα (1486.7 eV) x-ray source, which was operating at 99.7 W. Near-perpendicular (75°) and grazing (2°) photoelectron take-off angles were used to sample the bulk (characteristic sampling depth of 1.9 nm) and surface of the CN_x films, respectively. Also, both low- and high-resolution scans were done at corresponding analyzer pass energies of 58.70 and 29.35 eV with an aperture of 100 µm. C 1s, O 1s, N 1s, F 1s, and Cr 3p spectra were collected for each sample.

2.2.3 Hysitron nano-scratch tests

Due to the thinness of the CN_x films under investigation, conventional nano-indentation tests for hardness and elastic modulus were not applicable. In addition, it was difficult to directly correlate such numbers with the wear durability of carbon films -- toughness of the material was a more relevant parameter. Thus, we evaluated the wear resistance of the CN_x films in nano-scratch tests, where diamond tips were used to scratch test surfaces at very light loads to gauge their resistance to wear.

The Hysitron system [67] is a portable add-on to commercially available atomic force microscopes (AFM). We used a Digital Instruments Nanoscope III in our laboratory. The Hysitron lateral force transducer is centered around a capacitative force/displacement sensor that provides high sensitivity, a large dynamic range, and a linear force/displacement output signal. In these nano-scratch tests, we utilized the 5 nm CN_x films deposited on the Si wafers. A Berkovich diamond tip with a nominal radius of 331 nm was used to make 2 µm long scratches into the sample surface with a ramped loading force of 100 µN. Figure 2.2 shows the loading force and lateral displacement of the tip over the surface for each scratch. Before and after the nano-scratch tests, 200 µN indents were made into a reference fused quartz surface to confirm no changes or damage to the diamond tip shape. The TriboScope 3.5FL software was used to specify the scratch test parameters, record load/displacement data during scratching, and analyze data afterwards.

2.2.4 Candela Optical Surface Analyzer (OSA) lubricant mobility measurements

As mentioned earlier, the mobility of the lubricant on a disk's surface is a significant factor in the tribology of the head-disk interface. Good lubricant mobility allows the re-flow of lubricant to areas of the disk surface where head-disk contacts may have removed the lubricant temporarily. This occurs during the contact-start-stop cycles of disk drives that do not utilize load/unload technology and, more recently, during flying/seeking over the data zone with low flyheight slider designs. However, too much mobility is detrimental to the overall life of the HDI, as spin-off of the lubricant prevents it from protecting the overcoat surface. This is becoming increasingly important as spindle speeds in current disk drives are 15,000 rpm and expected to go higher.

Lubricant mobility is a function of the interaction between the lubricant molecules and the carbon overcoat surface. Although there is no consensus on the exact specifics of this lubricant/carbon interaction, we expect changes in the carbon overcoat composition to affect its surface properties such as surface energy and dangling bond density, and hence its interaction with the lubricant molecule.

The Candela Optical Surface Analyzer (OSA) is a commercially-available measurement system capable of ellipsometry, reflectometry, scatterometry, and Kerr effect microscopy for imaging and metrology applications related to the inspection of disk media. The system was originally designed by Meeks et. al for in-situ imaging and analysis of the surface of a thin film disk, specifically lubricant depletion/degradation and carbon wear [68].

In our laboratory, we utilize a modified Candela 5100 OSA system that allows the use of additional fixtures and stages to mount HGAs for dynamic studies and in-situ monitoring of the head-disk interface. Several data channels may be monitored including P and S polarized light, Q polarized light (comprised of both P and S polarized light components), the M channel for magnetic characterization, and the Z channel for topology measurements. For lubricant thickness measurements, the Q polarized light channel offers the most sensitivity with a resolution of 0.1Å and works on the principal of ellipsometry – the instrument measures the phase shift between the P and S components of a Q polarized wave before and after it reflects off the sample surface. The difference is

what is recorded in the phase shift image and is affected by the multi-layers of the disk sample including the lubricant and carbon overcoat.

Samples were prepared prior to test by removing the mobile lubricant from a radial track of the disk surface with a swab soaked in 3M HFE-7100 solvent, which is commonly used to strip disks of their lubricant layer. A fixture was designed to insure the track was straight and repeatable between samples. With the Candela TS software version 2.3.9, we acquired the QAbsPhase channel data at 5 minute intervals from a 2 mm by 30° angular section of the test track located at a radius of 26 to 28 mm. The total test duration was 15 hours and the disk was stationary between measurements to reduce the effects of centrifugal force and air shear on lubricant movement. Using the following parameters, our spatial resolution was 3.7 µm in the radial direction and 2.6 µm in the circumferential direction: 10,000 rpm spindle speed, "medium" resolution setting, 64X encoder multiplier, 10.923 MHz sample rate, 541 tracks, and 5482 pixels/track. The measured images are subtracted from the initial image (t=0) to insure that the only differences observed are due to the lubricant and none of the other underlying films on the disk surface (i.e. carbon overcoat). An angular average of the data over the sample area is calculated to provide a cross-section of the test track with increased signal/noise ratio. Finally, plotting this data as a function of time allows us to monitor the flow of lubricant back into the test track.

2.2.5 Ultra-high vacuum (UHV) tribochamber drag tests

The UHV tribochamber consists of a disk spindle, a slider actuator, a substrate heater,

and a Balzers QMG 420 high-resolution quadrupole mass spectrometer (QMS) in a stainless-steel vacuum chamber. A base pressure of less than 2×10^{-8} Torr was achieved through the use of a Balzers TPU 330 turbo-molecular pump that was backed by a Balzers DUO 016B mechanical pump. The chamber pressure was monitored with two Varian gauges: a 524-2 cold cathode ionization gauge and a UHV-24 Bayard-Alpert type ionization gauge. The disk spindle was driven by a DC motor at rotational speeds of 50 to 64 rpm through a UHV-compatible feedthrough. A slider was mounted on the slider actuator, which has a strain arm instrumented with semiconductor strain gauges to measure forces in the vertical and horizontal directions, and its XYZ position was controlled via linear stages. More specific details of this system were described in an earlier CML report [69].

The QMS provided in-situ detection of the gaseous products generated at the HDI during drag tests. The QMS can monitor simultaneously 15 different atomic mass units (a.m.u.s) ranging from 1 to 500. We simultaneously obtained friction data from strain gauge transducers. Based on earlier work [69], specific a.m.u.s were monitored during drag tests to examine the decomposition mechanisms of ZDOL: 2 (H_2), 12 (C), 19 (F), 20 (HF), 28 (N_2 or CO), 31 (CF), 44 (CO_2), 47 (CFO), 50 (CF_2), 51 (CF_2H), 66 (CF_2O), 69 (CF_3), 100 (C_2F_4), 116 (C_2F_4O), and 119 (C_2F_5).

The following test procedure was used to conduct drag tests in the tribochamber. Initially, the tribochamber was heated to 423 K at high vacuum for 24 hours. The chamber was then backfilled with Argon gas as the disk and slider samples were mounted inside. The

23

sliders used in this study were 30% (1.25 mm by 1 mm) Al_2O_3-TiC sliders with and without 7 nm amorphous diamond-like carbon (DLC) films on their air bearing surfaces (ABS). Next, the chamber was pumped down to a base pressure of 2 x 10^{-8} Torr and the channels of the QMS were assigned to the selected AMUs. The background intensities were recorded before the drag tests were initiated with the following parameters: 0.2 m/s drag speed, a load of 2.5 grams, and a sliding time until failure. The mass spectrum and friction data were collected every 2 seconds by a computer connected to the QMS via a serial connection.

2.3   Results and discussion

2.3.1   X-ray Photoelectron Spectroscopy (XPS) analysis

The first analysis was conducted on the unlubricated 5 nm CN_x films with near-perpendicular take-off angles (75°) to examine the bulk structure of the overcoats. Figures 2.3 through 2.5 correspond to the C1*s*, O1*s*, and N1*s* high-resolution spectra, respectively. In Figure 2.3, we noted a broadening of the C1*s* spectrum with the addition of nitrogen to the overcoats – this pattern was expected as more highly nitrogenated C moities formed at higher nitrogen concentrations in the overcoat. Unfortunately, this broadening of the C1*s* spectrum makes it impossible to deconvolute the peaks that correspond to various C-N bonds such as those found in β-C_3N_4 and graphitic C_3N_4 structures. Instead, we turn to the N1*s* spectra in Figure 2.5, where increasing the nitrogen content of the overcoats correlated with the relative change of two distinct peaks in the N1*s* spectrum at 398.5 eV and 400.5 eV. The unambiguous assignment of all the peaks observed in this spectrum to specific film microstructures is nearly impossible, but a

useful compilation by Hellgren [47] of the published work in this field (both experimental and theoretical) allowed us to identify these two features. The 400.5 eV peak corresponds to nitrogen bonded to sp^2-coordinated carbon in an aromatic structure, whereas the 398.5 eV peak may be associated with nitrogen bonded to sp^3-coordinated carbon. Hence, the ratio of these two peaks provides an indication of the sp^3/sp^2 content in the CN_x films and we observed that increasing the nitrogen in the overcoats corresponded to an increase of the sp^3 content in the films.

Analysis of the lubricated 5 nm CN_x samples provided information about the lubricant's bonding behavior to the carbon surface. Figures 2.6 through 2.8 are the F1s, C1s, and O1s low-resolution spectra, respectively, taken at near-perpendicular take-off angles (75°). From the F1s spectra and the peaks on the left-hand side of the C1s and O1s spectra (associated with the lubricant), we noted no significant change in the lubricant's structure as a function of nitrogen content in the overcoat. Also, the lubricant thickness did not vary with the addition of nitrogen to the overcoat as it ranged from 14.19 to 14.98 Å.

2.3.2   Hysitron nano-scratch tests

Figure 2.9 is a plot of the normal displacement vs. time for a scratch on the 0% N_2 overcoat sample, which was representative of the data taken with this instrument. The tilt of the sample, due to mounting and other set-up errors, was taken into consideration and subtracted from the data using the software functions. Since we had clearly scratched through the carbon film layer and into the underlying substrate layers with a load of 100 µN, we chose to compare the normal displacement at a load of 5 µN for each of the

overcoat samples to evaluate the scratch resistance of the carbon films. A summary of the results is plotted in Figure 2.10 as a function of % N_2 in the overcoat. Each data point is the average of eight measurements.

The normal displacement we measured in these nano-scratch tests included the effects of both elastic and plastic deformation of the sample surface. As the nitrogen content in the CN_x overcoat was increased above 6%, we observed an increase in the scratch resistance of the carbon film as exhibited by the decrease in the tip's normal displacement into the sample surface. Further addition of nitrogen into the overcoat past 16% resulted in no appreciable increase in scratch resistance. Our results matched those reported by Wienss et. al, where they conducted scratch tests on similar samples with a normal load of 3 μN in their scanning force microscope (SFM) [70]. Using Raman spectroscopy to observe the shift of the G-peak position, they attributed the increased scratch resistance to increased sp^3 bonding in the carbon films. In our own XPS analysis described earlier, we also observed an increase in sp^3 bonding as a function of nitrogen content in the carbon overcoat. In addition to improved scratch resistance, this change in the carbon film's microstructure has been correlated to increases in hardness and elastic modulus, density, and other material properties [39, 40].

2.3.3   Candela Optical Surface Analyzer (OSA) lubricant mobility measurements

Figure 2.11 is a typical QAbsPhase image taken immediately after removing the lubricant from the test track – this one corresponds to the surface of the 18% N_2 disk. Brighter colors on the image (the light vertical strip) indicate less lubricant in the test track, while

the darker hues represent the normal lubricant thickness on the disk. An angular average of the test area is shown in Figure 2.12 for this disk. As can be seen from the plot, averaging the data over the test area allows us to quantify the amount of lubricant in and out of the test track. Positive reflectivity values indicate less lubricant on the disk. By subtracting this original image from all the subsequent measurements, we arrive at the plot shown in Figure 2.13 of the reflectivity difference at the test track (positive differences indicate more lubricant on the disk surface in this plot). As time progresses, the lubricant slowly re-flows back to the test track from the surrounding areas.

To study the effects of nitrogenation in the overcoat on lubricant mobility, we compared the integrated intensities of the test track reflectivity differences for low nitrogen (9.5 at. %) and high nitrogen (18 at. %) CN_x disks as a function of time. In Figure 2.14, we observe that more lubricant re-flows into the test track for the low nitrogen disk – hence, the surface mobility of ZDOL decreases as the amount of nitrogen in the overcoat increases. Ma et. al noted similar results in their micro-ellipsometry studies of ZDOL spreading on amorphous carbon surfaces with hydrogen and nitrogen doping [56]. These experimental results were later confirmed in their theoretical model involving the solution of the two-dimensional diffusion equation using the finite-difference method [71].

The surface mobility of ZDOL is dependent upon the number of adsorption sites on the carbon film surface where the lubricant molecule may interact or bond – for hydrogenated amorphous carbon films (CH_x), this was shown to be carboxyl end groups

(COOH) and dangling bonds (unpaired electrons) based on XPS and electron spin resonance (ESR) studies [54]. Increasing the number of these high-energy bonding sites provides places for the lubricant molecules to anchor themselves and, effectively, reduce their motion over the carbon surface. For dangling bonds in the carbon film, Kasai demonstrated that ZDOL attaches itself via the transfer of a hydrogen atom from the active hydroxyl endgroup to a dangling bond site, linking the molecule as an alkoxyl group [72]. From our XPS analysis, we found that increasing the nitrogen content of CN_x overcoats increases the amount of sp^3-coordinated C in the films. This data may be coupled with the fact that the dangling bond density of carbon surfaces correlates with the sp^3 content of the sample, as observed by Yanagisawa in his ESR studies [73], to infer that increasing the N_2 content of films increases the dangling bond density on the CN_x overcoat. It is this increase in the dangling bond density that results in the decreased surface mobility of the ZDOL lubricant as a function of nitrogen content in the overcoat. Other detailed mechanisms proposed for the bonding of the ZDOL hydroxyl endgroups and its ether linkages to nitrogenated carbon surfaces may be found in work by Tyndall et. al and Paserba et. al [74, 75].

2.3.4 Ultra-high vacuum (UHV) tribochamber drag tests

Figure 2.15 shows a plot of the friction coefficient vs. drag time for the 0% N_2 overcoat case tested with uncoated and 7 nm DLC-coated sliders, which is representative of the data taken from the strain gauge transducer. From this friction data we extracted two sets of information: (1) the maximum friction coefficient observed at the head-disk interface (HDI) during the test and (2) the time of failure of the HDI, which is marked by a rapid

drop in the friction along with the formation of a wear track on the disk. Compiling the data from each of these tests into summary plots allowed us to discern any trends with N_2 content in the overcoats.

Figure 2.16 is a plot of wear life vs. N_2 content in the overcoat for tests with the DLC-coated sliders; a similar plot for drag tests with the uncoated sliders is shown in Figure 2.17. In tests with the DLC-coated sliders, we noted a peculiar trend in wear life that was neither monotonically increasing nor decreasing as a function of % N_2 in the overcoat. Hence, we tested these samples again except in reverse order (i.e. from 16% to 0 %, whereas the first set of tests were from 0% to 16%) and acquired a similar set of data points. For the uncoated slider tests, we observed an increase in wear durability for nitrogen content in the overcoats greater than 9%.

A summary of the maximum friction coefficient observed in each test is presented in Figure 2.18. No changes in the friction coefficient were observed as a function of % N_2 in the overcoat in tests with the DLC-coated sliders. However, we noted a drop in the maximum friction coefficient as the N_2 content of the overcoat exceeded 9%.

A post-test analysis was done of the slider ABS under an optical microscope at 50X magnification for each test. A summary of the results is shown in Figure 2.19 for both the DLC-coated and uncoated sliders. Even though comparisons of the amount or type of debris on the slider ABS are subjective in nature, we noted a visual difference in the debris composition from tests on disks with different % N_2 overcoats. Sliders from tests

on the lower % N_2 overcoats had debris that consisted of smears or liquid-like material, whereas sliders from tests with high % N_2 overcoats had particulate-like debris embedded on the rail surfaces. The change in the overcoat from an sp^2- to sp^3-rich microstructure with the addition of nitrogen to the overcoat, as observed in the XPS analysis, may account for this transition in debris generation.

Figure 2.20 is a summary of the mass spectra taken from the QMS for drag tests on the 0% N_2 overcoat disk with DLC-coated and uncoated sliders, which is representative of the data taken with this instrument. Four mass fragments were monitored specifically to determine the extent of the ZDOL lubricant decomposition that occurs at the HDI during these drag tests: CFO (47 a.m.u.), CF_2O (66 a.m.u.), CF_3 (69 a.m.u.), and C_2F_5 (119 a.m.u.). We categorized the decomposition of ZDOL lubricant into two mechanisms, a thermal decomposition or mechanical scission of the molecule and a catalytic decomposition. CFO and CF_2O are associated with the thermal decomposition or mechanical scission of the lubricant molecule due to friction generated at the HDI. CF_3 and C_2F_5 are the end products of the catalytic decomposition of ZDOL in the presence of slider material Al_2O_3-TiC. A complete outline of the decomposition mechanisms will be discussed later in Section 3.4.4.

For the DLC-coated slider case, we observed the immediate generation of CFO and CF_2O at the beginning of the drag test, which coincided with the initiation of friction. As the test progressed, the intensity of these fragments declined as the amount of lube available for this decomposition mechanism was depleted from the wear track. Finally,

catastrophic failure of the HDI occurred when the amount of lubricant could no longer protect the overcoat and the carbon film was worn away. Insignificant amounts of CF_3 and C_2F_5 were observed because the DLC-coating on the slider surface prevented any interaction between the Al_2O_3-TiC material and the lubricant on the disk.

For the uncoated slider case, friction at the HDI initiated the generation of CFO and CF_2O similar to the DLC-coated slider case. However, at the same time, we noted the production of CF_3 and C_2F_5, indicating the presence of the catalytic decomposition mechanism. As this decomposition progressed, the intensities of these fragments continued to increase – a similar trend was also observed in the CFO and CF_2O spectra because (1) these fragments are also generated in small amounts as a by-product of the catalytic decomposition, and (2) the friction at the interface increased significantly. Failure of the HDI took place when carbon wear occurred after the lube was depleted from the test track.

Therefore, the dominant lubricant decomposition mechanism for tests with DLC-coated sliders is a thermal decomposition or mechanical scission of the molecule. For tests with uncoated sliders, it is the catalytic decomposition that dictates the lifetime of the lubricant. To determine the effects of overcoat nitrogenation on lubricant decomposition, we need a method of quantifying the extent of these two mechanisms. First, we integrate the intensity of each mass fragment over the duration of each individual test to determine the overall amount of lubricant decomposition that occurred at the HDI. Figures 2.21 through 2.24 show the integrated spectra for CFO, CF_2O, CF_3, and C_2F_5, respectively, as

a function of nitrogen content in the overcoats when tested with DLC-coated and uncoated sliders. From these plots, we observe that less lubricant is decomposed at the HDI as the nitrogen content increases in the carbon overcoat. This stems from the fact that the surface mobility of ZDOL decreases with increasing nitrogen content based on our Candela measurements -- more lubricant re-flows back into the test track of samples with lower nitrogen overcoats providing more material to participate in the decomposition, which results in more mass fragments being generated and counted by the quadrupole mass spectrometer. For the uncoated slider case, where failure times were fairly short, the effects of lubricant re-flow are most likely minimal, and the substantial decrease in the catalytic decomposition at higher % N_2 in the overcoat may be attributed to other factors.

One possible scenario for the reduced catalytic decomposition is based on the bonding characteristics of the ether linkages in the ZDOL backbone to the carbon film and supported by our work with hydrogenated and nitrogenated carbon overcoats in the UHV tribochamber. Paserba et. al indicated in their temperature-programmed desorption experiments that ethers interact with carbon films through electron donation from the oxygen lone pair electrons [75]. Nitrogen is electronegative relative to carbon and its addition to a carbon film depletes electrons from the film - hence, enhancing the bonding between the ZDOL ether linkages and the carbon surface. For hydrogen, which is electropositive relative to carbon, its addition to carbon films donates electrons to the film, which weakens the ether bonding [76]. Evidence of the effects of this bonding mechanism on the catalytic decomposition may be found in drag tests with uncoated

sliders in our UHV tribochamber. In Chen's dissertation [53], the addition of hydrogen to carbon overcoats resulted in an increase in the catalytic decomposition of ZDOL in drag tests with uncoated sliders and he suggests that it is the presence of acetal units, -O-CF$_2$-O-, in ZDOL that is the source of the decomposition, but he does not elaborate on the specifics. As can be seen from our explanation, the addition of hydrogen weakens the ether bonding at the carbon/lubricant interface resulting in increased catalytic decomposition of the ZDOL backbone, explaining Chen's results, while the addition of nitrogen enhances this bonding mechanism, reducing the catalytic decomposition in our results. Thus, increasing the % N$_2$ in the carbon overcoat reduces the catalytic decomposition in the presence of Al$_2$O$_3$ material.

Since the comparison of the integrated intensity does not take into account the disparate time scales to failure (hours versus minutes), it does not present an accurate picture of the severity of these decomposition mechanisms. For instance, in the 0% N$_2$ case, tests with the uncoated and the DLC-coated slider resulted in a similar "amount" of CFO mass fragments produced at the HDI, suggesting no significant difference between the two sliders, but the uncoated slider case produced that "amount" in 1/30th of the time of the DLC-coated slider test case – a significant factor to consider in this comparison. To incorporate this temporal dependence in our analysis, a more appropriate "number" to compare this set of data was an "average decomposition rate", which was the integrated mass spectrum for each fragment normalized by the time to failure. This is comparable to plotting the average mass fragment intensity generated per revolution of sliding on the disk surface.

Figures 2.25 through 2.28 are the average decomposition rates for CFO, CF_2O, CF_3, and C_2F_5, respectively, as a function of nitrogen content in the overcoats when tested with DLC-coated and uncoated sliders. The trends are similar to those observed in Figures 2.21 through 2.24, but now we can clearly see how much more aggressive the catalytic decomposition process is compared to the thermal decomposition/mechanical scission at the HDI. The decomposition rates for the uncoated sliders were one order of magnitude higher than the DLC-coated sliders, which give an indication as to how long the interface lasted before failure in each test. Until recently, most sliders in disk drive products were coated with a significant amount of DLC that insured the isolation of the Al_2O_3 material on the slider from the lubricant on the disk surface. With the push for reduced magnetic spacing, this coating has been reduced (< 5 nm) and our tests have shown that at these levels, the DLC coatings may be worn off, exposing the Al_2O_3 material and initiating this more devastating decomposition mechanism. This is a significant concern for future products as the catalytic decomposition of ZDOL lubricant will shorten the life expectancy of the HDI.

In addition to these drag tests, a 2nd series of tests were conducted with similar CNx disks, but WITHOUT the lubricant layer. Obviously, the removal of the lubricant from the disk structure isolates only the material properties of the overcoat in determining the wear life of the HDI. Figure 2.29 is a plot of the wear durability vs. nitrogen content for these disks tested with DLC-coated and uncoated sliders. From this data, it is clear that increasing the % N_2 in the overcoat improved its resistance to wear via sliding. This data

correlates well with the improved scratch resistance demonstrated in the Hysitron nano-scratch test results and may be explained by the increase in sp^3 content of the carbon film from our XPS analysis.

Incorporating our myriad of results into a simple schematic, as shown in Figure 2.30, we can finally explain the drag test trends observed in the UHV tribochamber. Increasing the nitrogen content in the CN_x overcoat effectively changes two properties of the carbon film: (1) increased wear resistance of the overcoat itself, as demonstrated by unlubricated CNx disk drag tests, Hysitron nano-scratch tests, and XPS analysis, and (2) decreased surface mobility of ZDOL lubricant due to an increase in the dangling bond density.

For the uncoated slider case, increasing the % N_2 in the overcoat improved wear durability because the aggressive nature of the catalytic decomposition negated any benefits of improved ZDOL surface mobility, and only the wear resistance of the carbon films was reflected in the trends.

For the DLC-coated slider case, the superposition of these two phenomena resulted in our observations as shown in Figure 2.30. At low nitrogen concentrations, the surface mobility of the ZDOL lubricant is enhanced which allows for replenishment of the wear track after the slider passes over the disk and provides continued protection of the overcoat layer. Since the scratch resistance of the overcoat itself is not optimal in this regime, it is the lubricant layer that plays the dominant role in determining wear life. As the N_2 content is further increased in the overcoat, ZDOL mobility decreases and we

observe a decrease in wear life. A transition occurs at approximately 9% N_2 content though – the ZDOL mobility continues to decrease, but the inherent scratch resistance of the overcoat increases and becomes the source of the improved wear durability noted at the HDI for higher N_2 concentrations. Because no catalytic decomposition of the lubricant is observed in these tests with DLC-coated sliders, only the thermal decomposition/mechanical scission of the lubricant is possible. The rate of this reaction is comparable among the disks, as the friction at the HDI is similar for these series of tests, so we neglect any contributions from lubricant decomposition in this explanation.

2.4   Conclusions

The effects of nitrogenation in sputtered, amorphous carbon overcoats (CN_x) on tribological performance in UHV drag tests were investigated. In this chapter, we demonstrated that increasing the nitrogen content from 0 to 16% effectively changes three properties at the head/disk interface: (1) increases the wear resistance of the CN_x overcoat due to an increase in the sp^3/sp^2 ratio as observed by Hysitron nano-scratch tests, ESCA/XPS analysis, and drag tests with unlubricated disk samples, (2) decreases the surface mobility of ZDOL due to an increased dangling bond density in the carbon film, and (3) decreases the catalytic decomposition of ZDOL in the presence of Al_2O_3 slider material. A mechanism for the reduced catalytic decomposition is presented that illustrates the behavior observed in our tests and previous studies by other researchers. In UHV drag tests, the wear life of CN_x disk samples tested with DLC-coated sliders is governed by the first two properties, while tests with uncoated sliders are governed by all three.
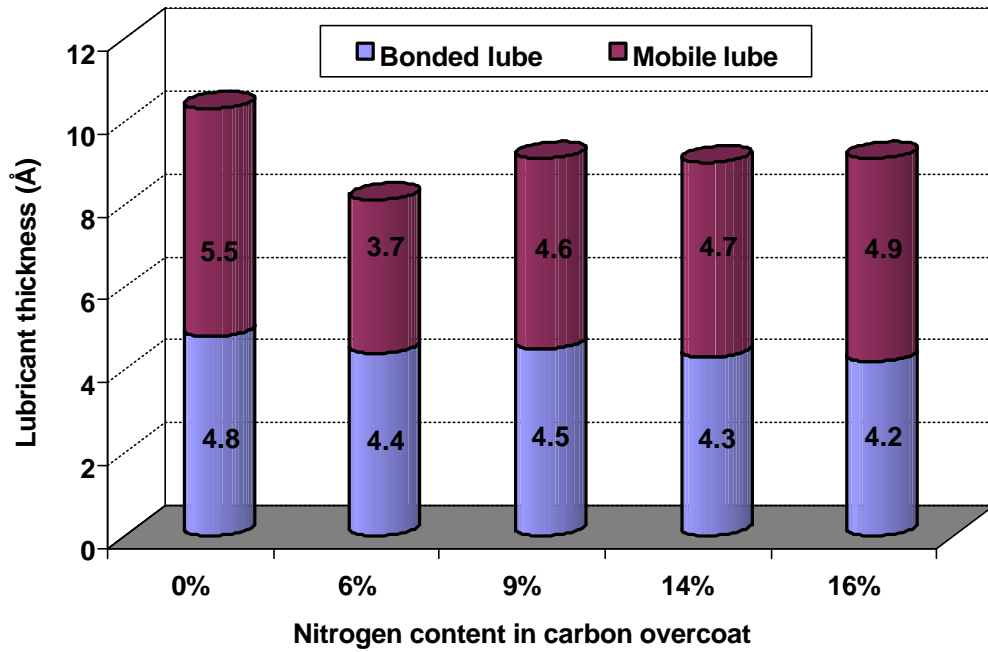
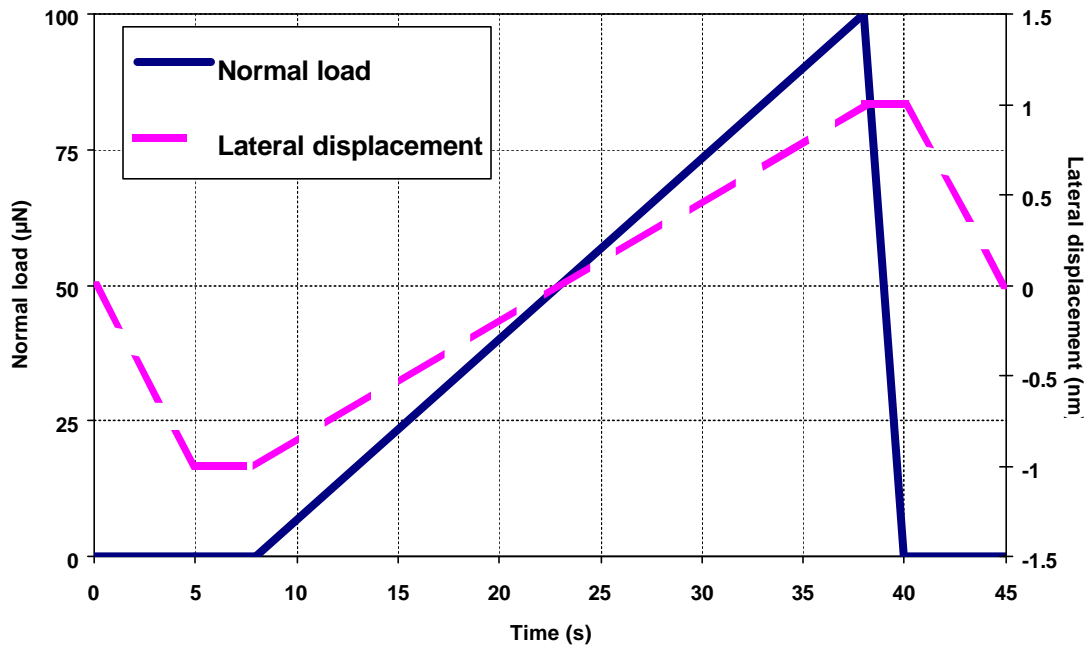Figure 2.1. "Bonded" and "mobile" lubricant thicknesses vs. nitrogen content in CN_x overcoat.

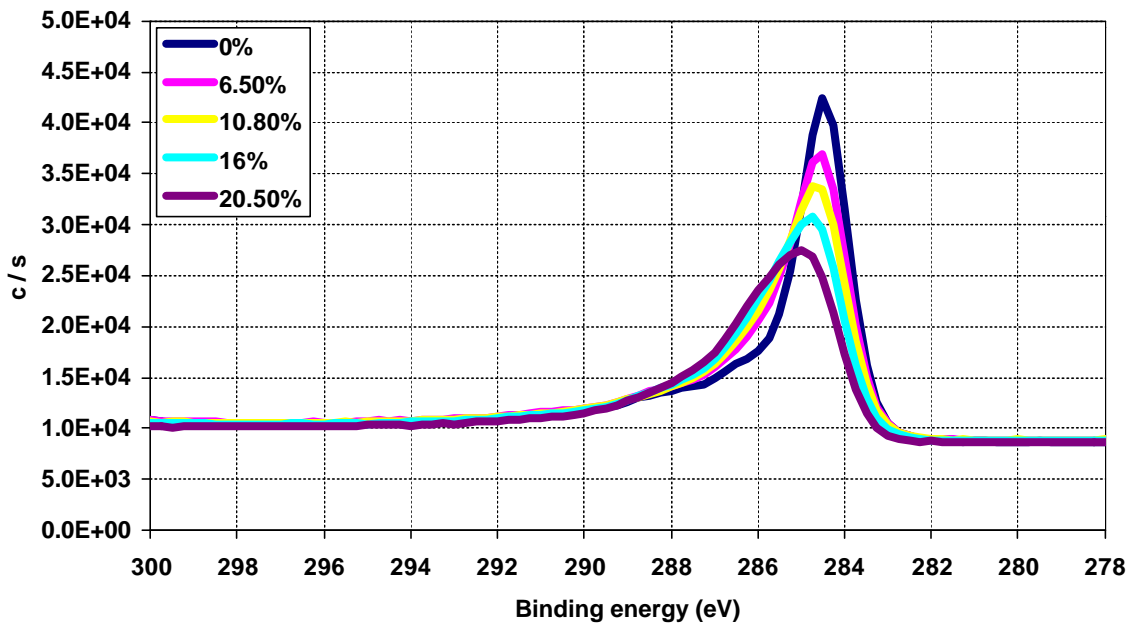Figure 2.2. Hysitron nano-scratch test loading and displacement profiles.

Figure 2.3. High-resolution C1*s* spectra of unlubed CN$_x$ overcoat samples.
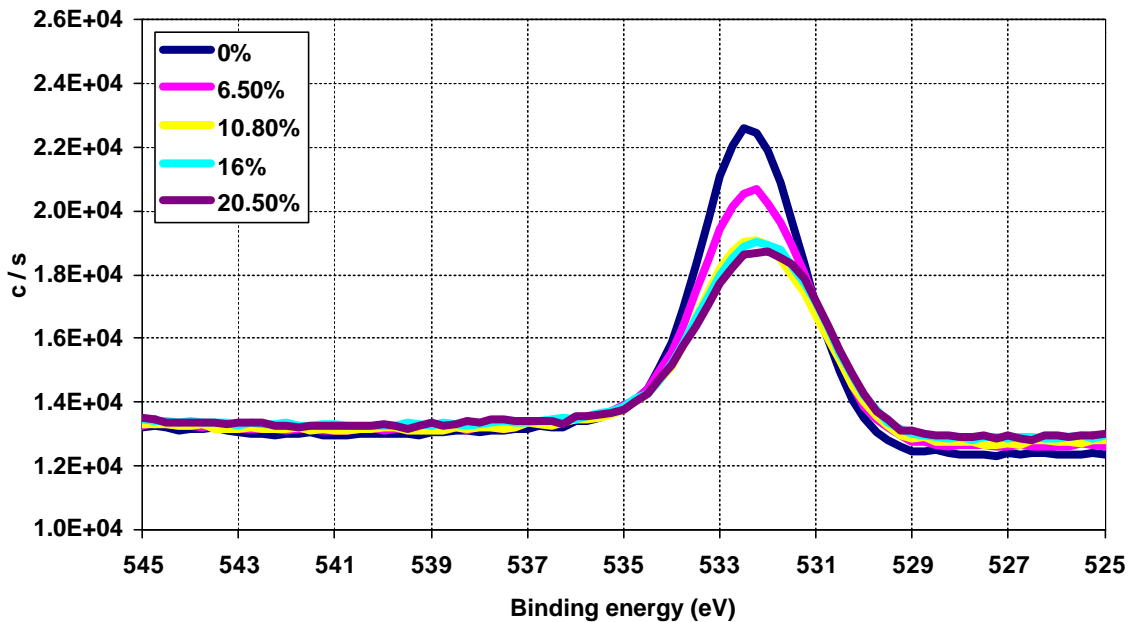

Figure 2.4. High-resolution O1*s* spectra of unlubed CN$_x$ overcoat samples.

Figure 2.5. High-resolution N1*s* spectra of unlubed CN$_x$ overcoat samples.
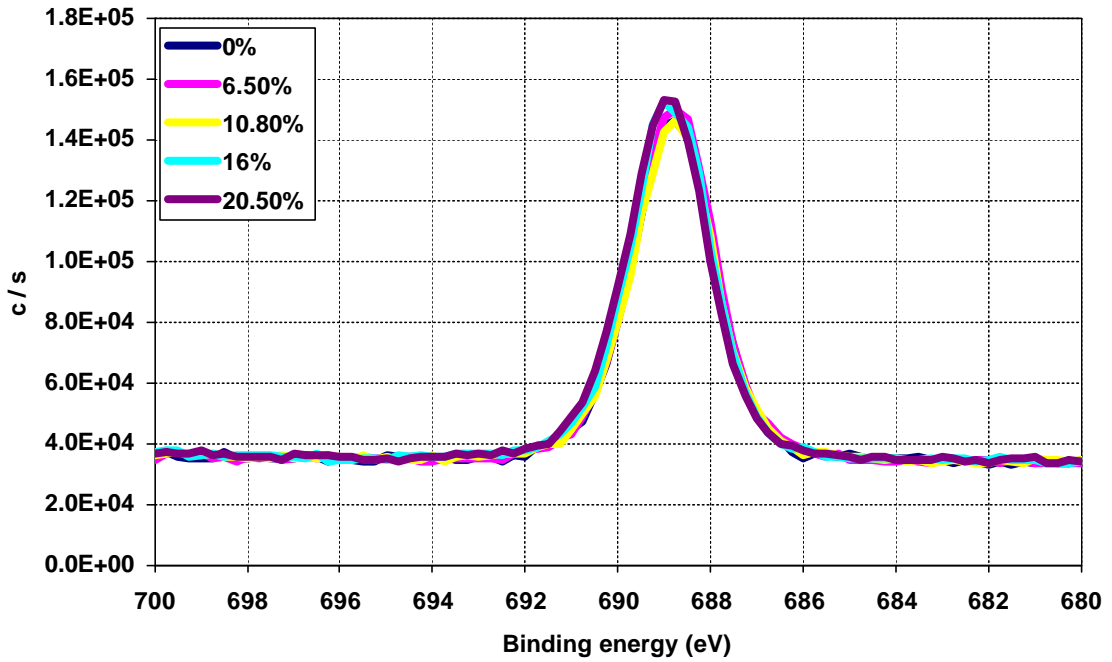
Figure 2.6. Low-resolution F1*s* spectra of lubed CN$_x$ overcoat samples.
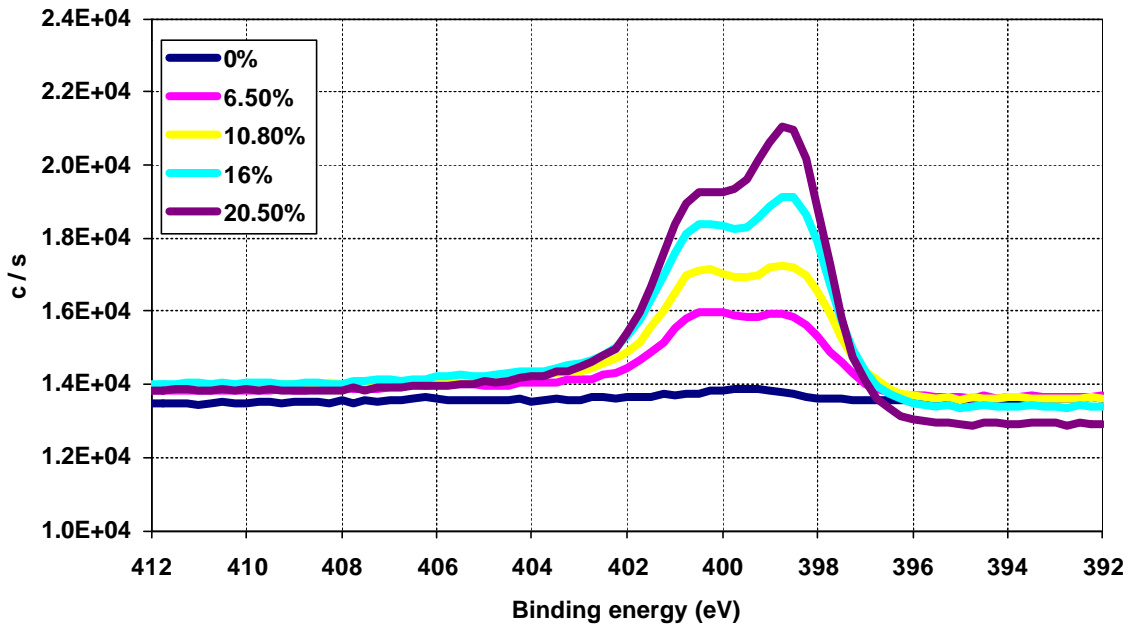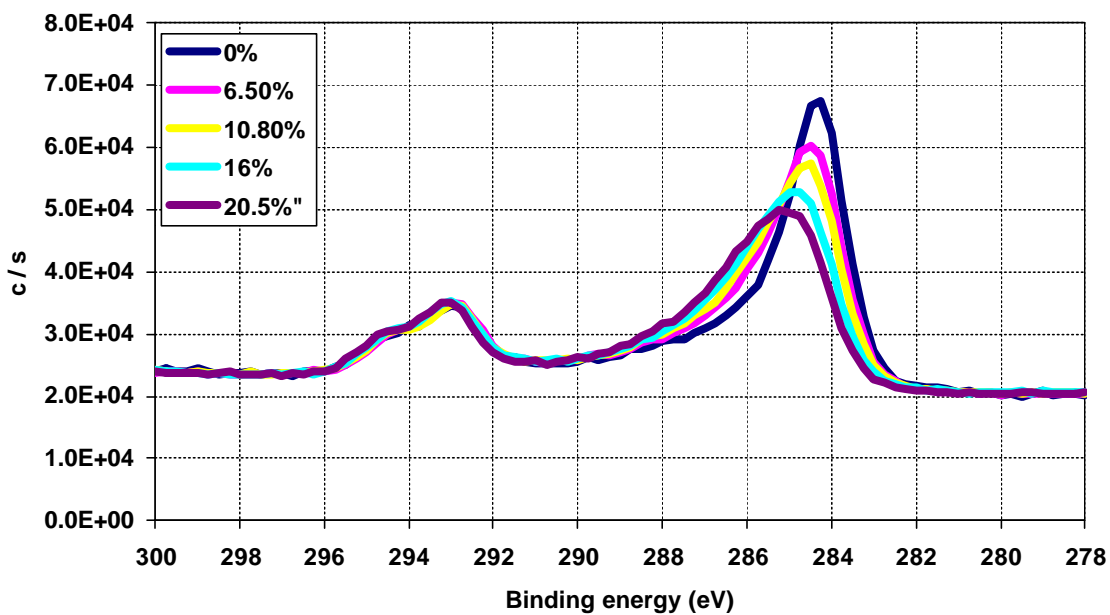
Figure 2.7. Low-resolution C1*s* spectra of lubed CN_x overcoat samples.
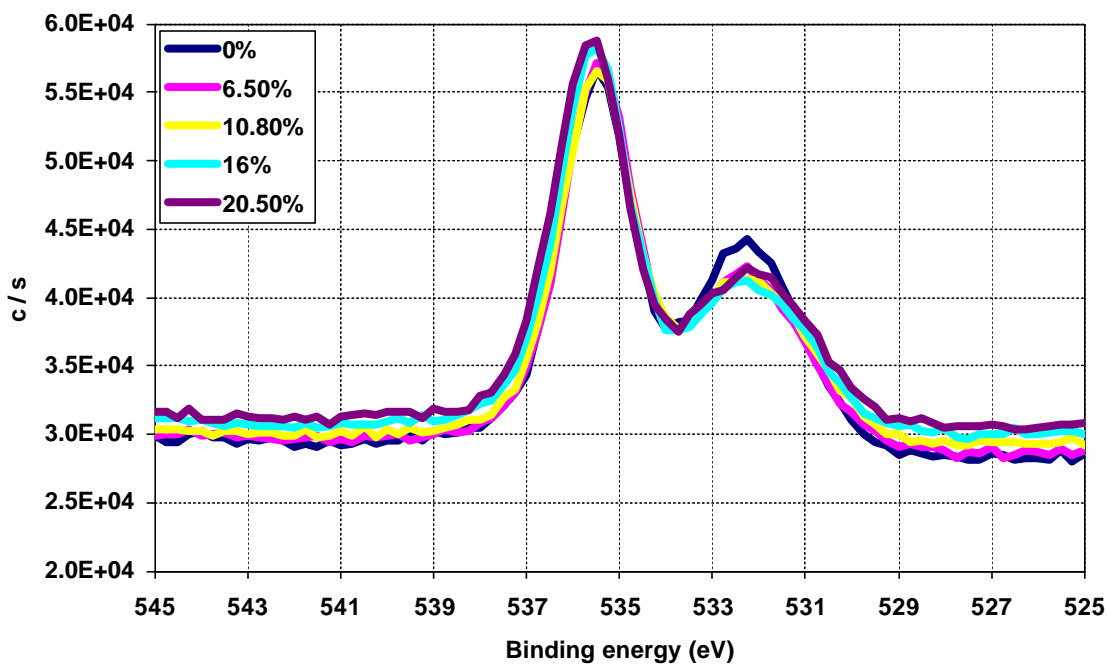
Figure 2.8. Low-resolution O1*s* spectra of lubed CN_x overcoat samples.
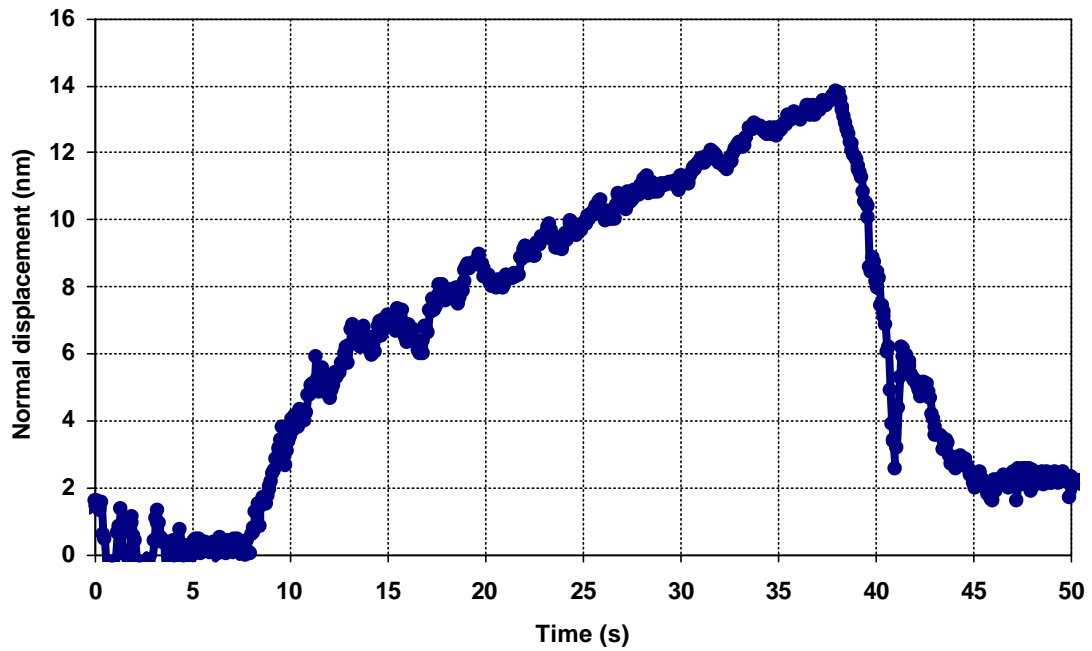
Figure 2.9. Normal displacement vs. time in Hysitron nano-scratch test of 0% N_2 overcoat sample.
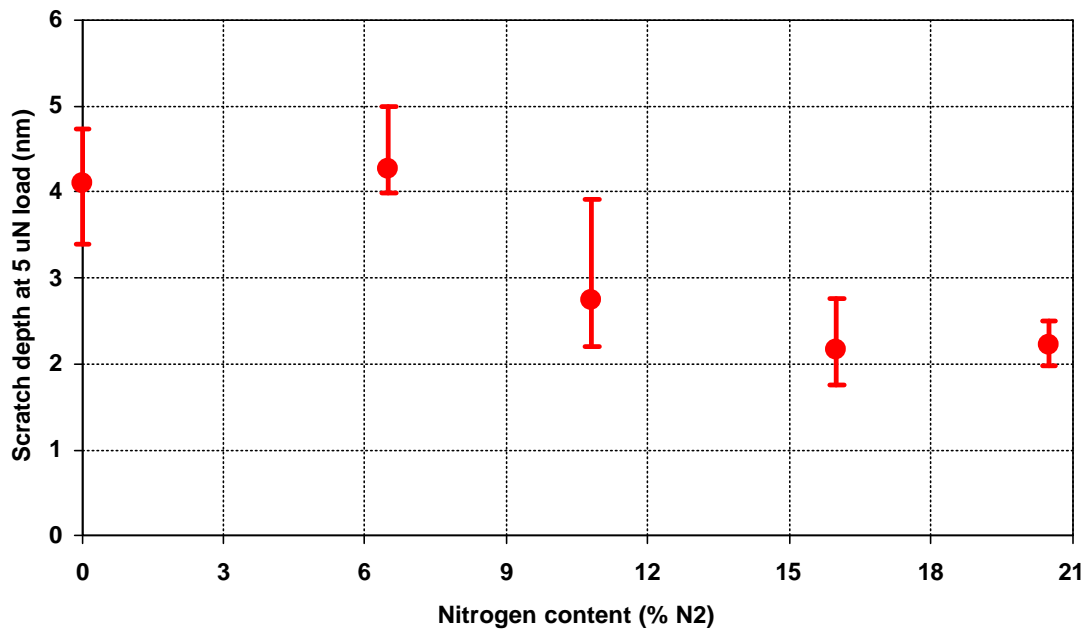
Figure 2.10. Scratch depth at 5 μN load vs. nitrogen content in CN_x overcoat in Hysitron nano-scratch tests.
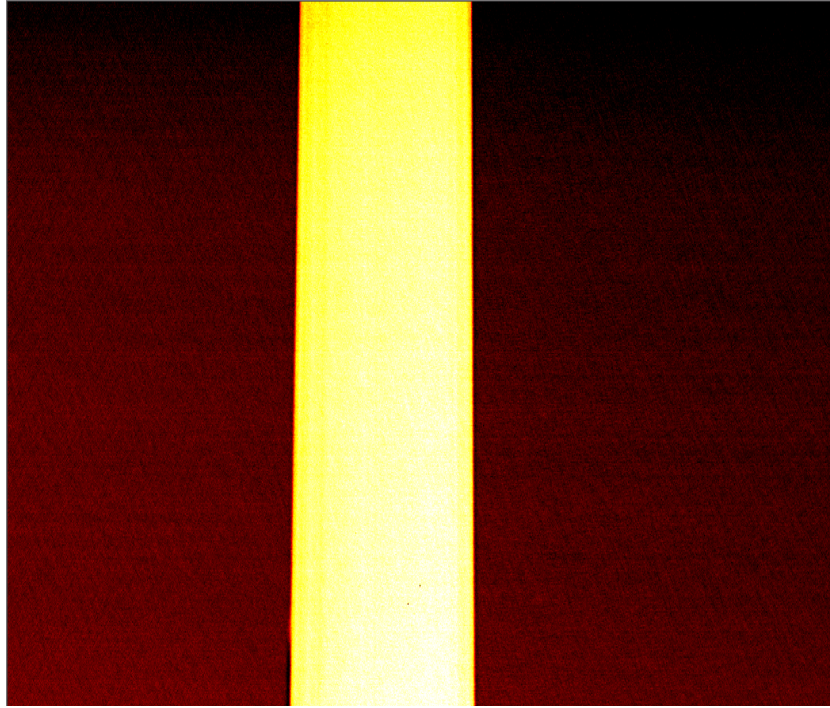
Figure 2.11. QAbsPhase image of the removed lubricant track from the 18% N_2 disk.
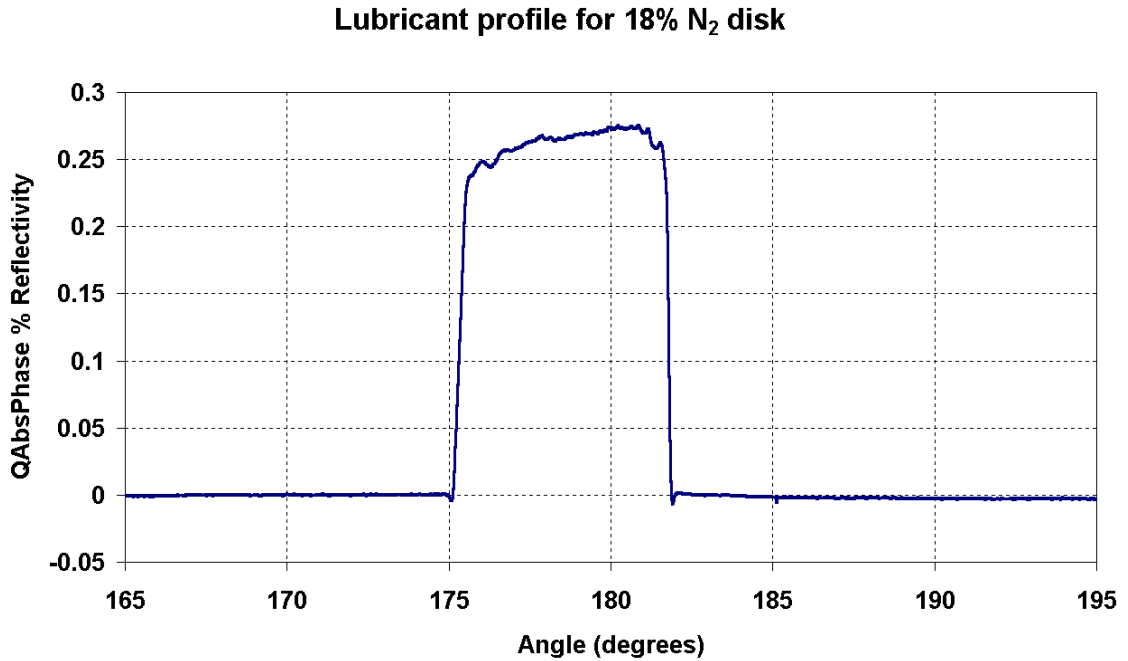
Figure 2.12. Angular average of QAbsPhase % reflectivity data for the removed lubricant track from the 18% N_2 disk.
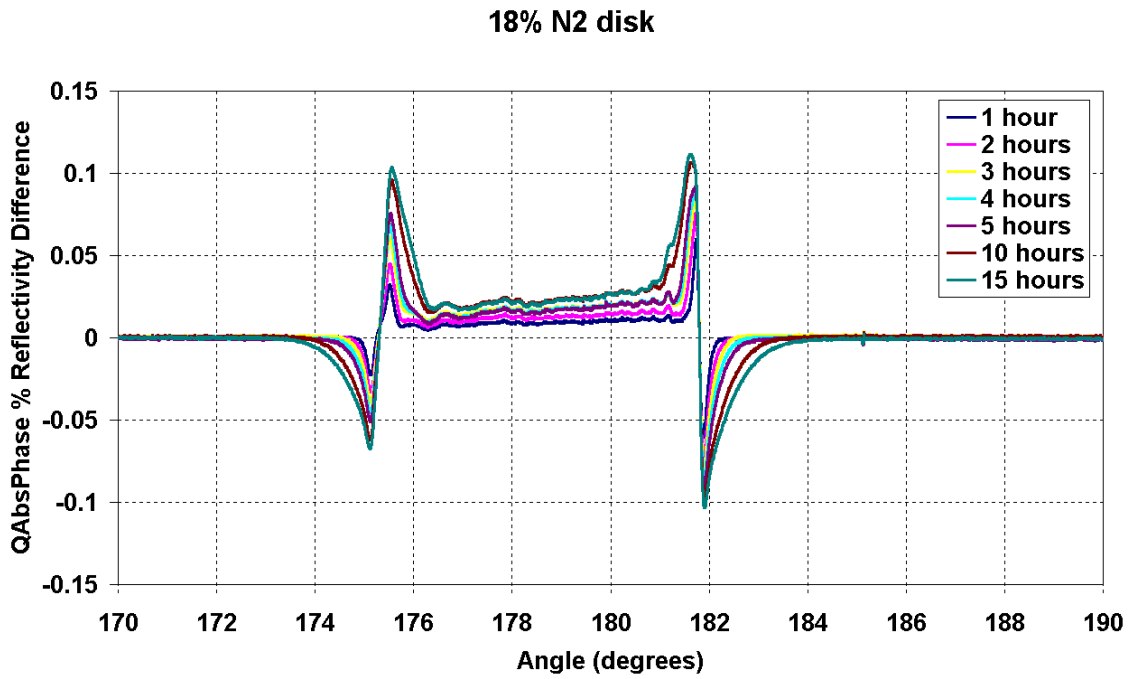
18% N2 disk

Figure 2.13. QAbsPhase % reflectivity difference at various time intervals after removal of lubricant from 18% N₂ disk surface. Positive values are associated with re-flow of lubricant, while negative values indicate lubricant removal.
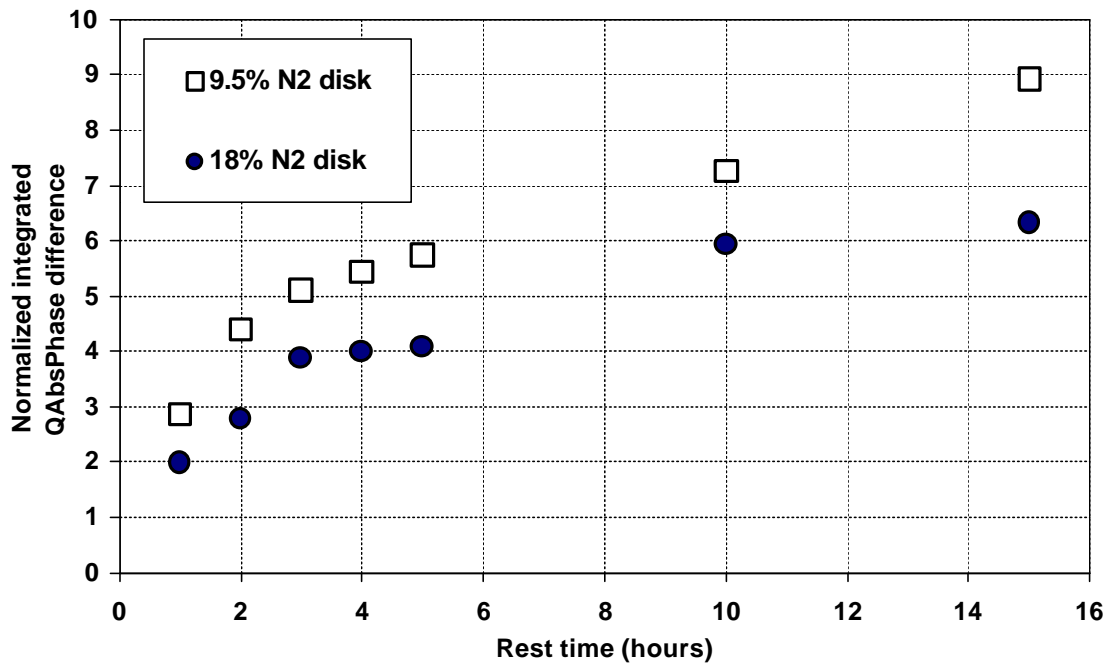
Figure 2.14. Normalized integrated QAbsPhase difference from test tracks of 9.5 and 18% N₂ disks vs. rest time (hours) after lubricant removal.
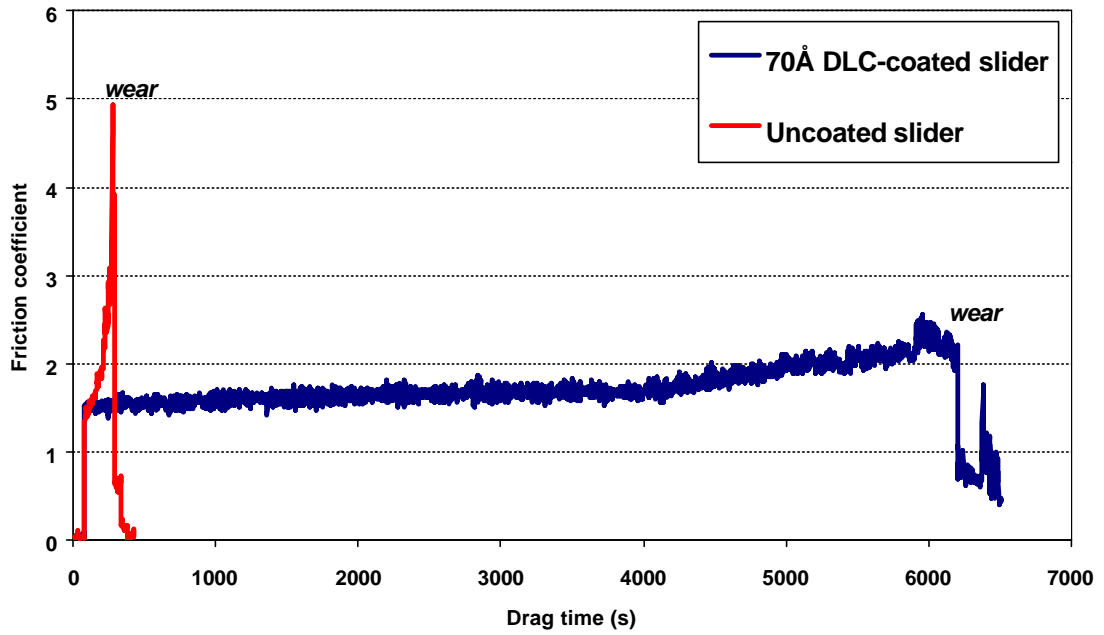
Figure 2.15. Friction coefficient vs. drag time for 0% N_2 overcoat tested with uncoated and 7 nm DLC-coated sliders.
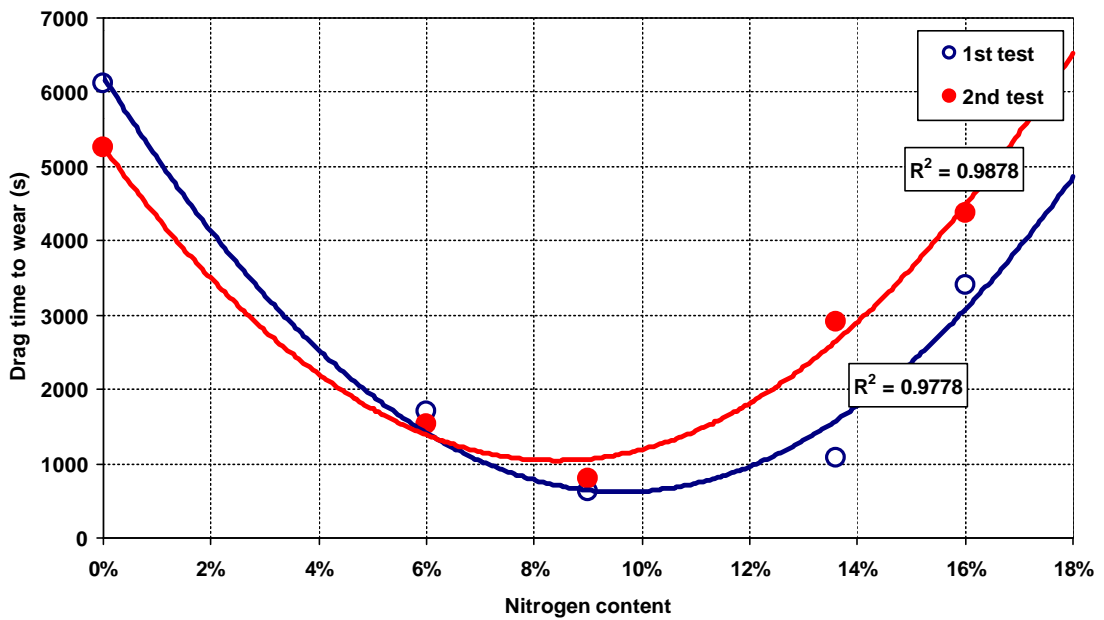
Figure 2.16. Wear life vs. N_2 content in overcoat for 7 nm DLC-coated slider tests.
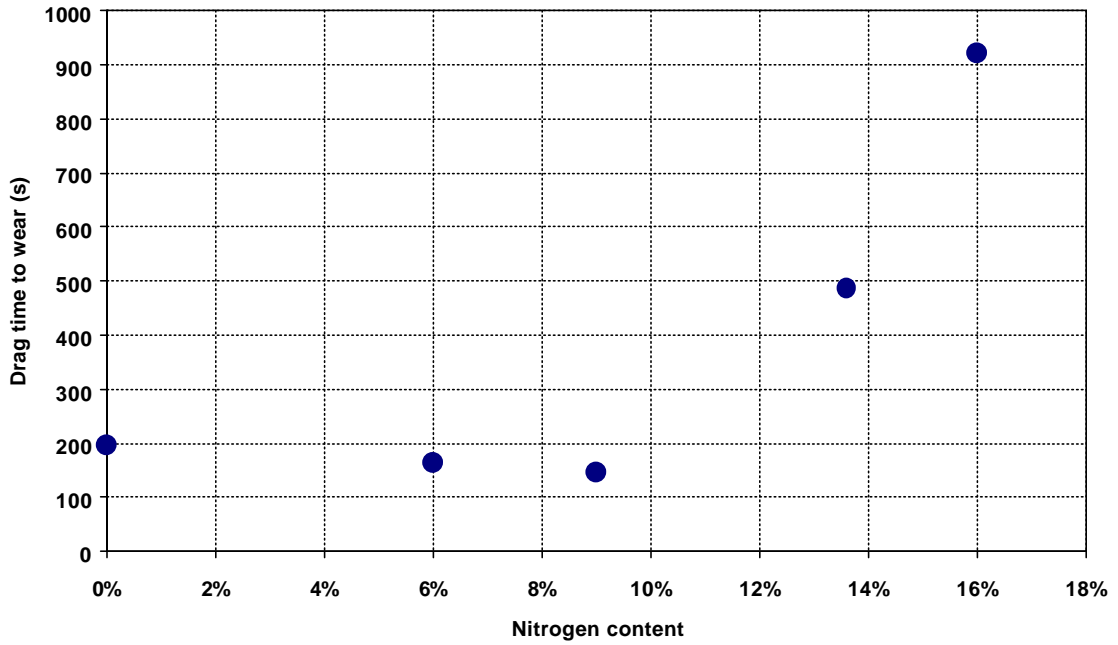
Figure 2.17. Wear life vs. N_2 content in overcoat for uncoated slider tests.
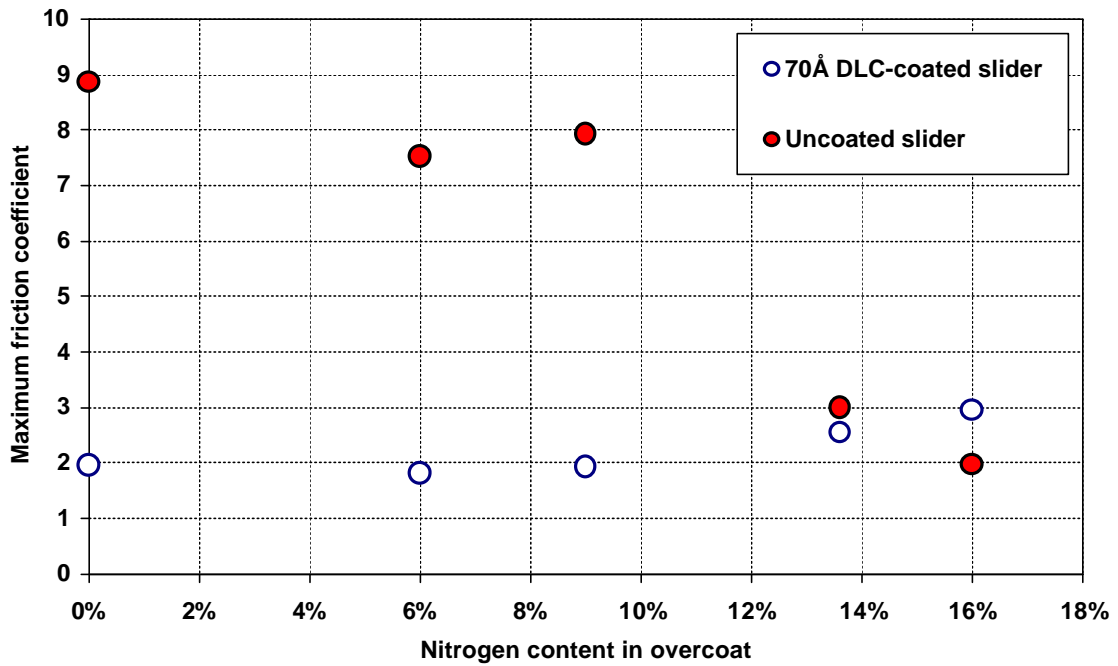
Figure 2.18. Maximum friction coefficient vs. N_2 content in overcoat for tests with uncoated and 7 nm DLC-coated sliders.
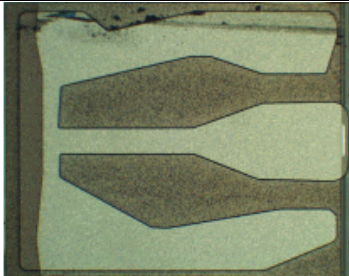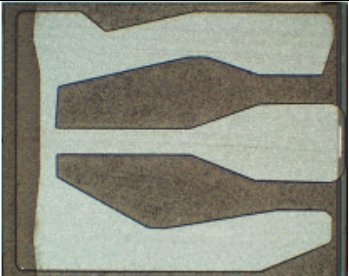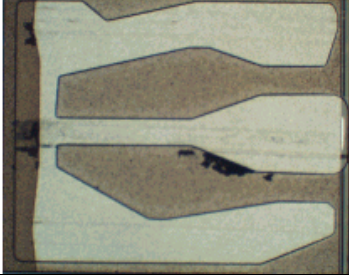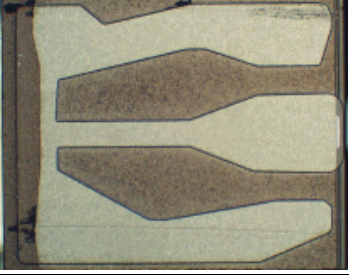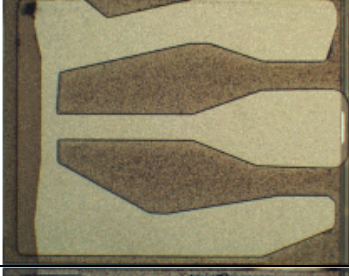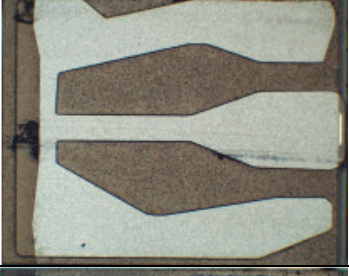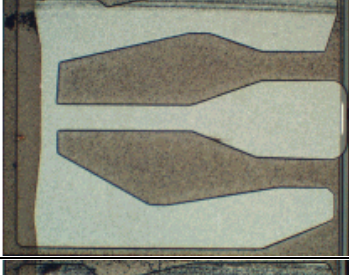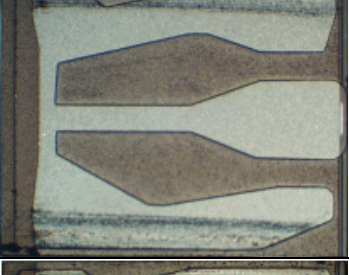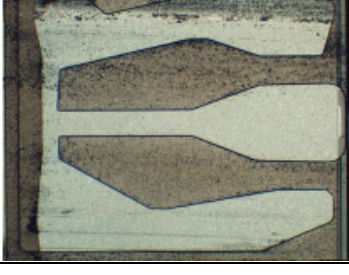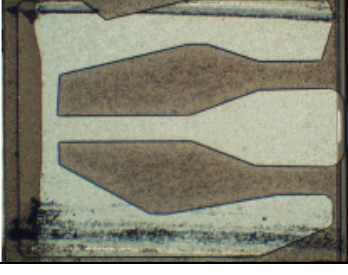
% N_2 in overcoat	70Å DLC-coated slider	Uncoated slider
0		
6		
9		
13.6		
16		

Figure 2.19. Microscope pictures of 70Å DLC-coated and uncoated ABS after drag tests.
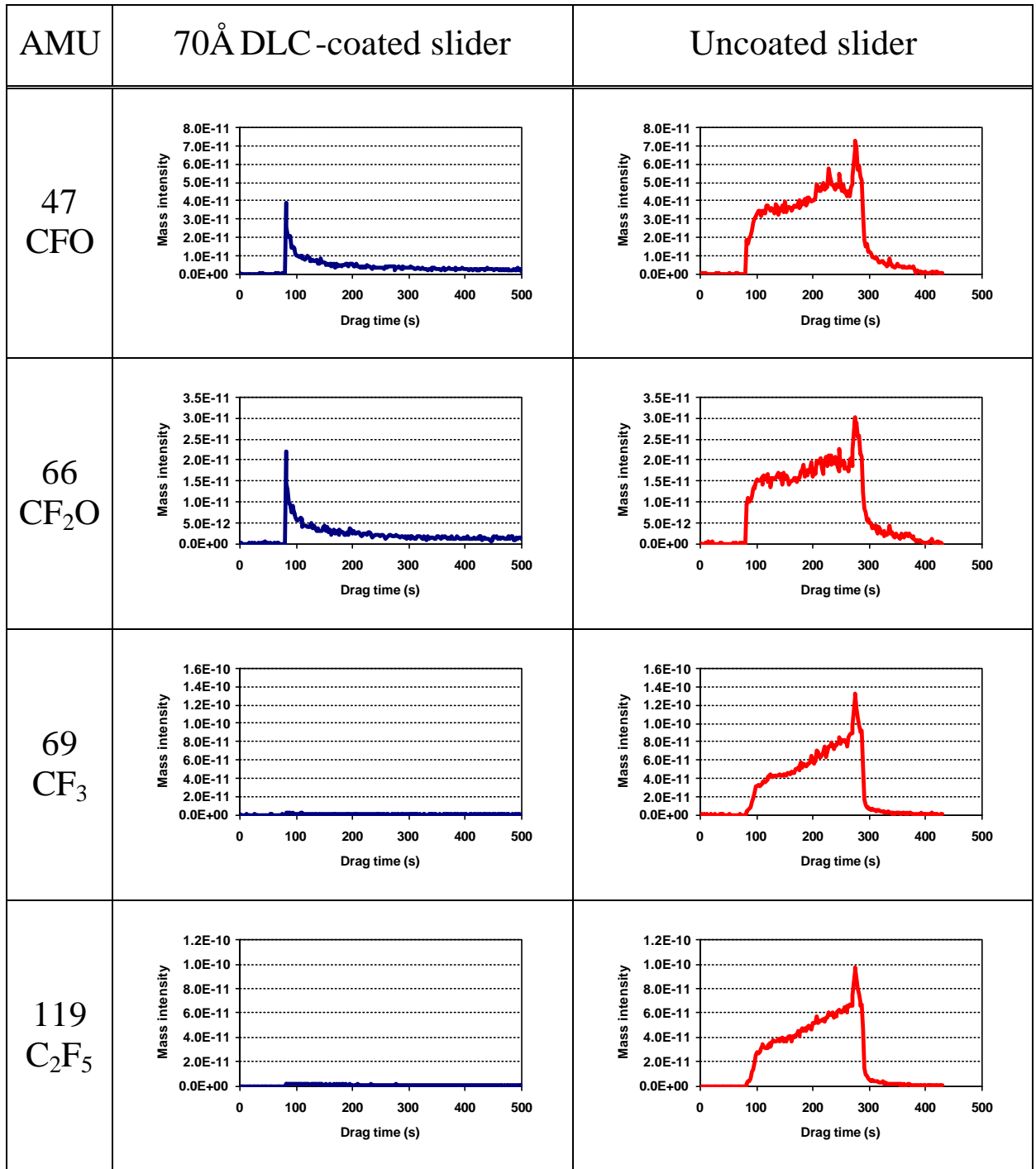
Figure 2.20. Mass spec data for drag tests with DLC-coated and uncoated sliders on 0% N_2 overcoat disk.
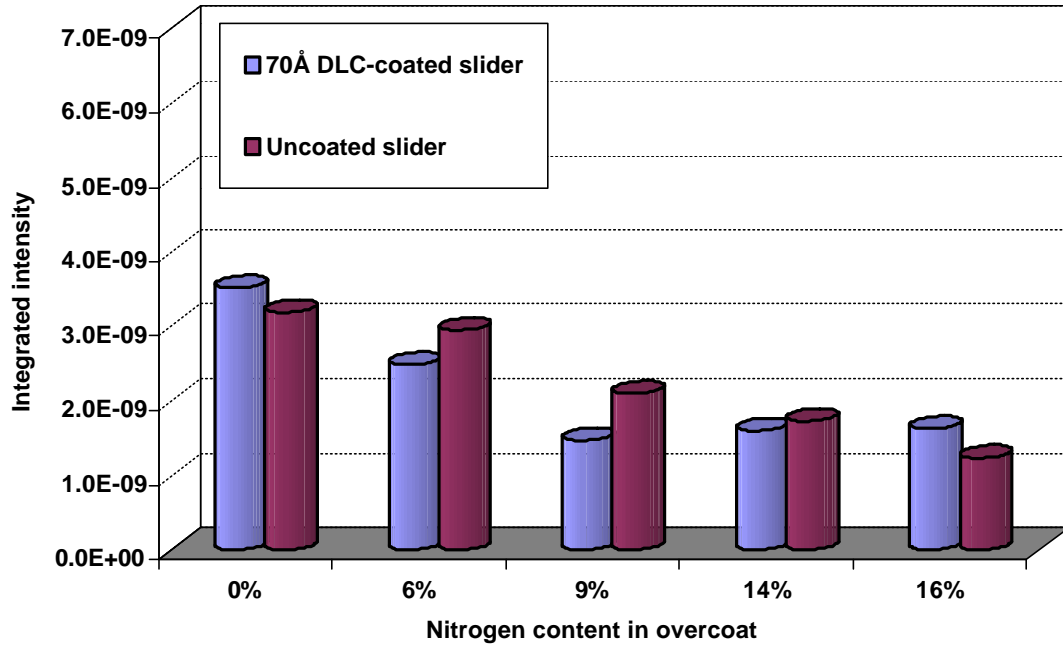
Figure 2.21. Integrated intensity for CFO (47 a.m.u.) vs. % N_2 in overcoat.
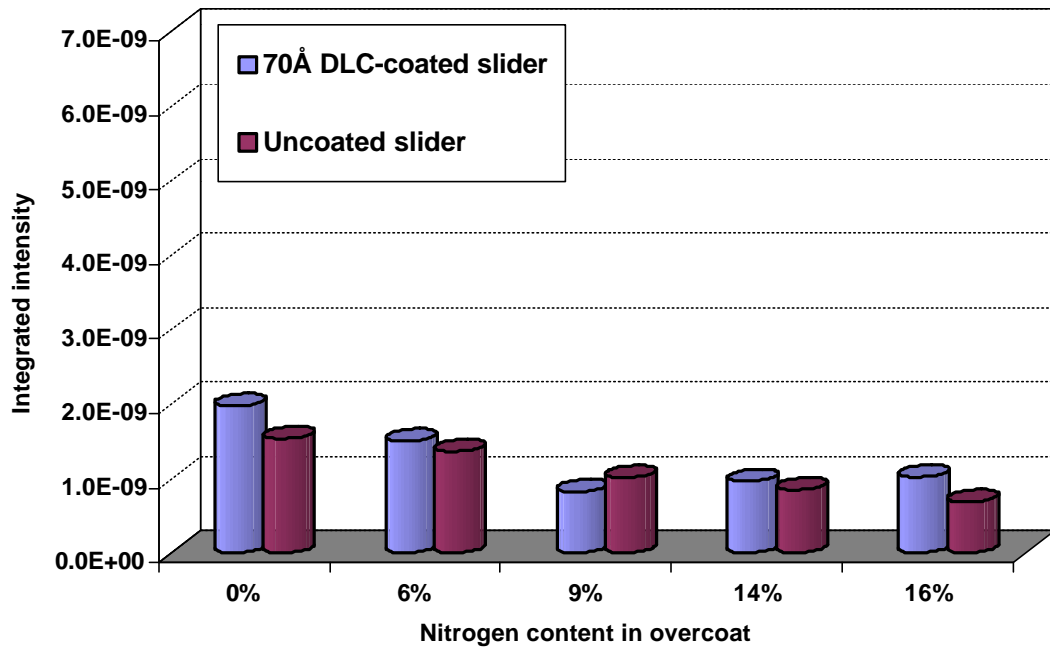
Figure 2.22. Integrated intensity for CF_2O (66 a.m.u.) vs. % N_2 in overcoat.
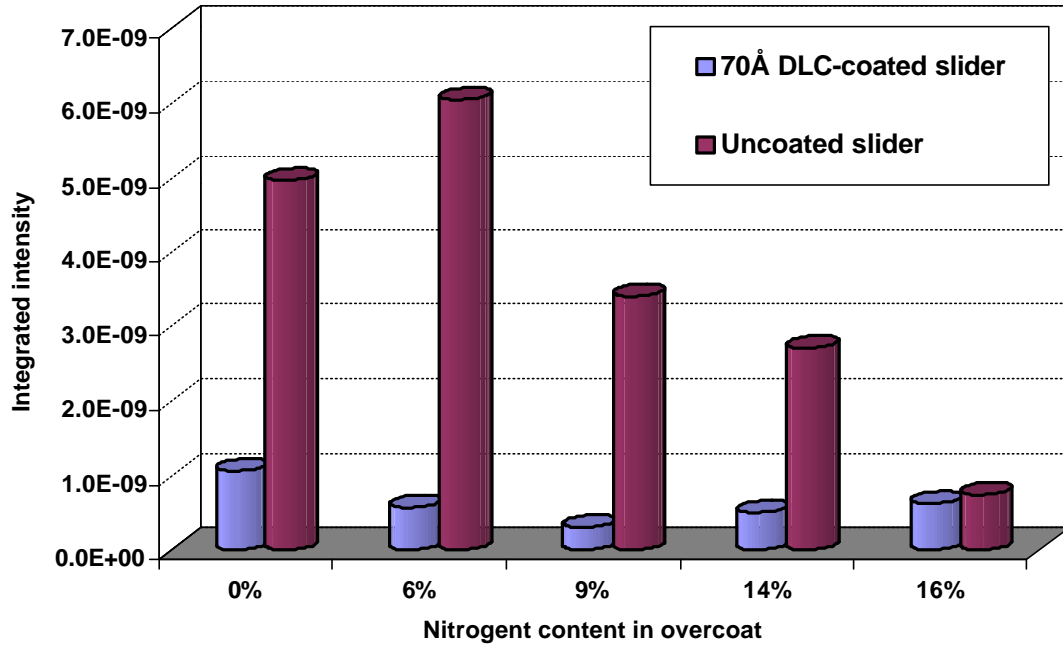
Figure 2.23. Integrated intensity for CF_3 (69 a.m.u.) vs. % N_2 in overcoat.
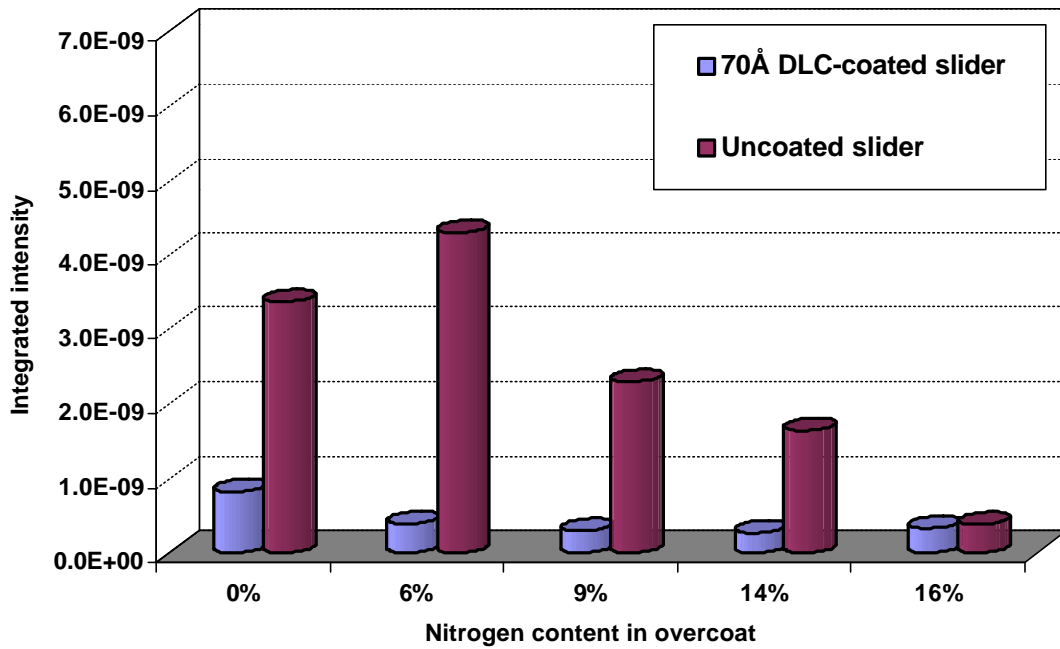
Figure 2.24. Integrated intensity for C_2F_5 (119 a.m.u.) vs. % N_2 in overcoat.
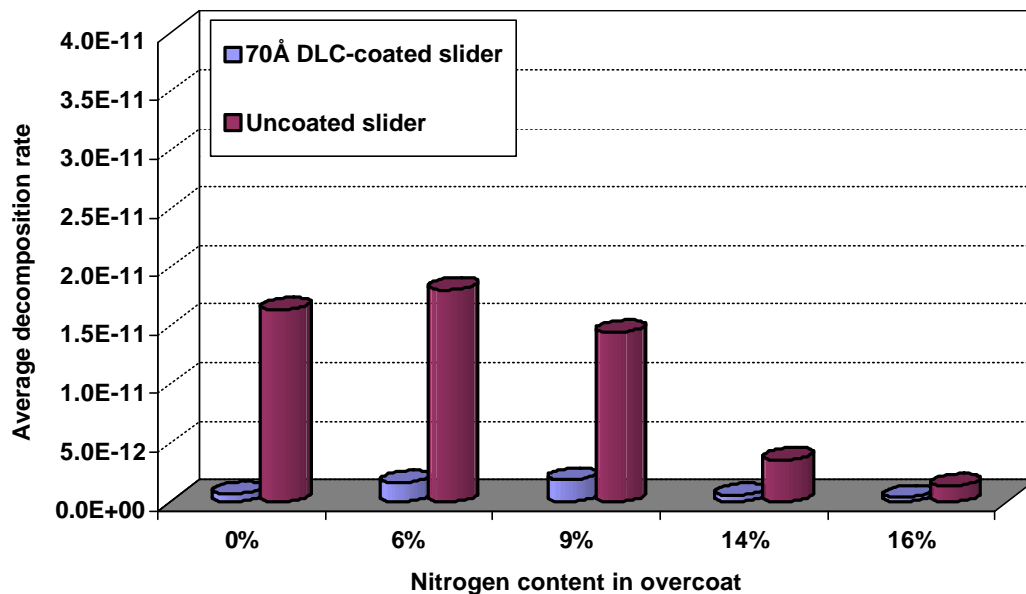
Figure 2.25. Average decomposition rate for CFO (47 a.m.u.) vs. % N_2 in overcoat.
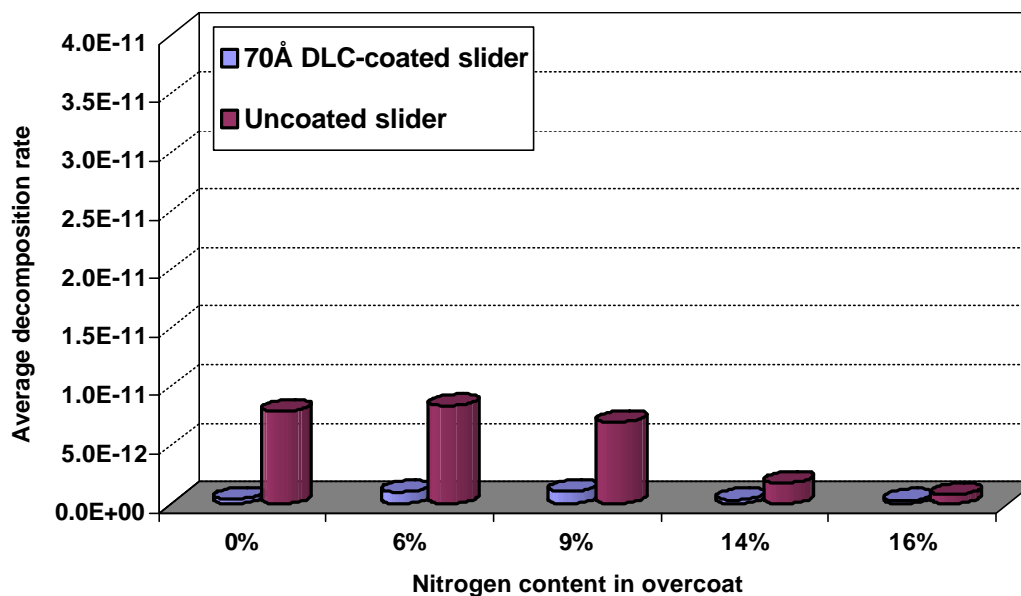
Figure 2.26. Average decomposition rate for CF_2O (66 a.m.u.) vs. % N_2 in overcoat.
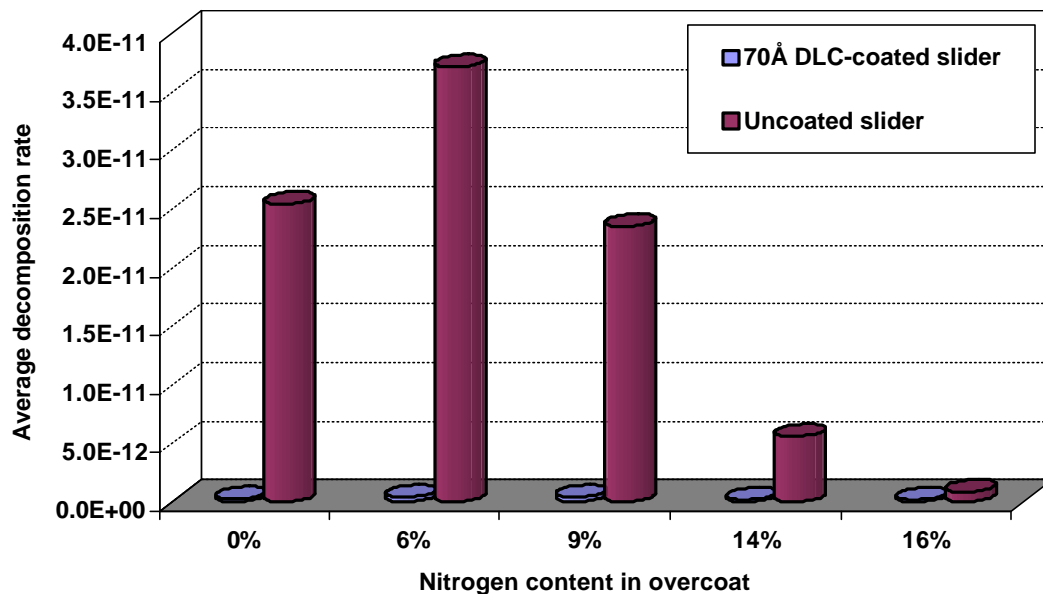
Figure 2.27. Average decomposition rate for CF_3 (69 a.m.u.) vs. % N_2 in overcoat.
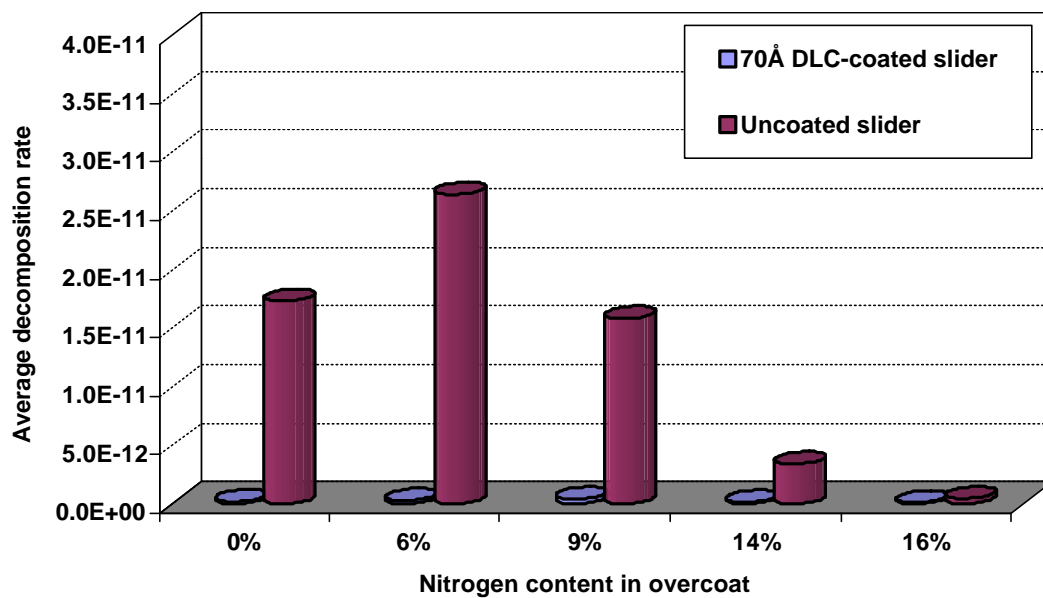
Figure 2.28. Average decomposition rate for C_2F_5 (119 a.m.u.) vs. % N_2 in overcoat.
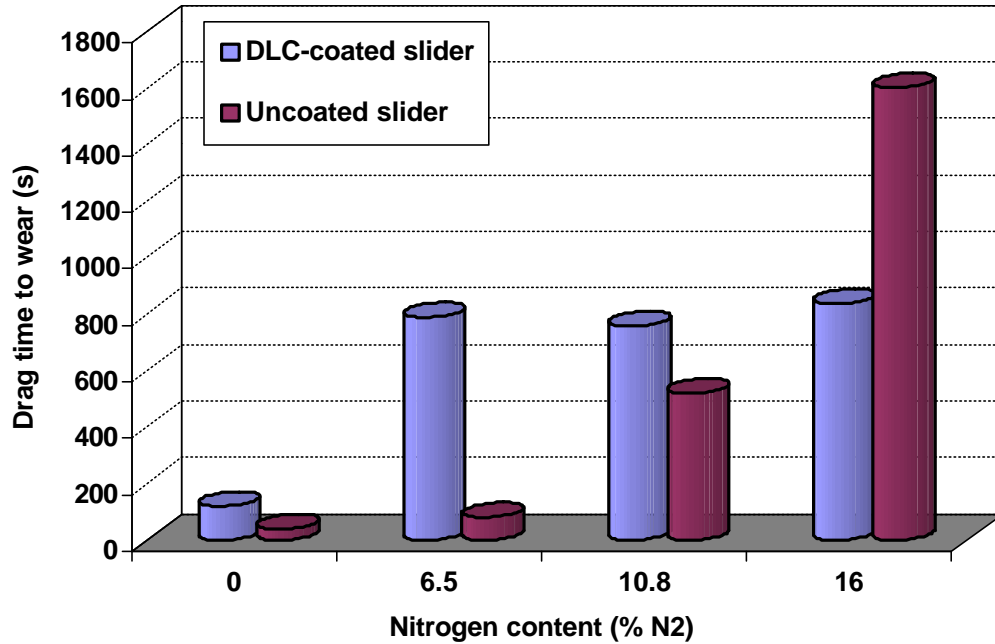
Figure 2.29. Wear life vs. nitrogen content for unlubricated CN_x disks.
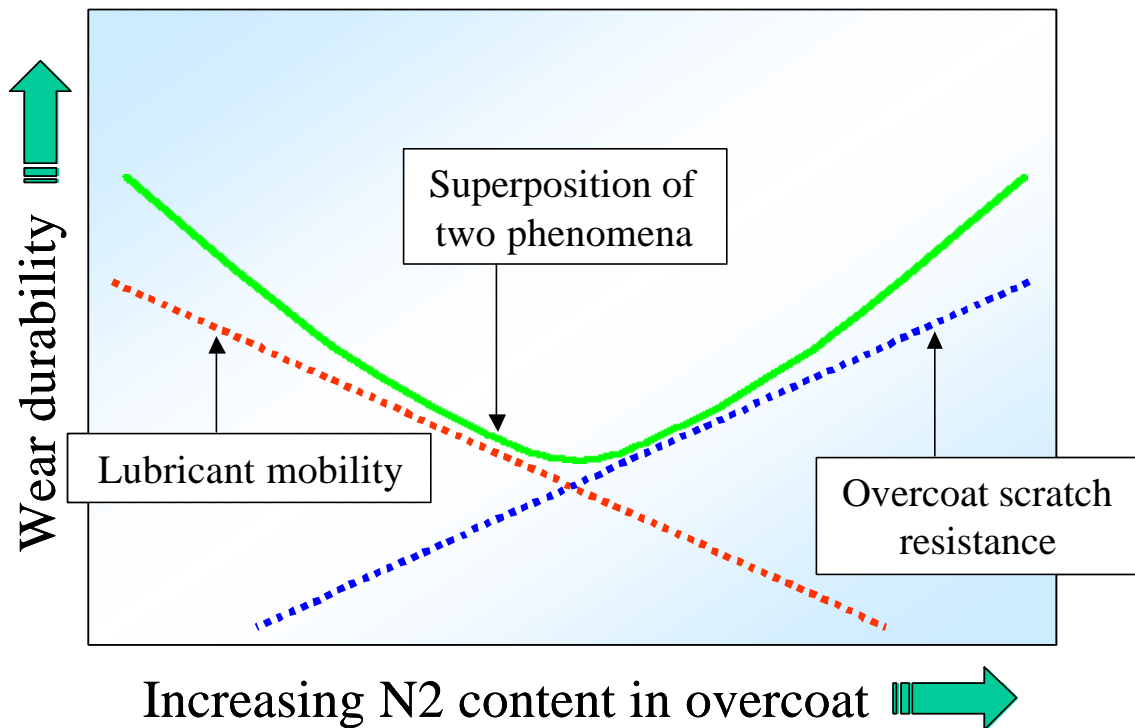
Figure 2.30. Schematic of material and lubricant properties dependent upon % N_2 in CN_x overcoat.

CHAPTER 3

CATHODIC-ARC CARBON (CAC) FILMS
AS NEXT GENERATION PROTECTIVE OVERCOATS

Abstract

An evaluation of cathodic-arc carbon (CAC) films used as protective overcoats on disk drive media is presented. The material properties of these carbon films are studied first as a function of ion energy during room temperature deposition and then as a function of film thickness. It is shown that the most diamond-like properties occur at ion energies of 120 eV and that there is a correlation between film thickness and hardness/elastic modulus. Next, the corrosion performance of these cathodic-arc carbon films is determined by a NaCl decoration test and compared to sputtered, hydrogenated carbon (CH_x) films. The CAC films significantly outperformed the CH_x films and provided continuous coverage at a film thickness of 2 nm. Disks were fabricated with 5 nm CAC overcoats and tested against similar CH_x disks in ultra-high vacuum tribochamber drag tests and thermal desorption studies. The CAC overcoat prevented the catalytic decomposition of ZDOL in drag tests with uncoated sliders. A mechanism for the observed phenomena is described with supporting evidence from thermal desorption tests. Finally, promising drag test results with 2 nm CAC overcoats are presented, which indicate that CAC is a viable candidate to replace sputtered carbon overcoats for future high areal density applications.

3.1   Introduction

In Chapter 2, we explored the role of nitrogen in sputtered, amorphous diamond-like carbon (DLC) films on the tribology and tribochemistry at the head-disk interface. Because of the continuing demand for increased areal density in hard disk drives, advances in slider and media technology are a never-ending process ranging from improvements in pseudo-contact slider designs to manufacturability of thinner protective overcoats – all with the express purpose of reducing magnetic spacing [77-79]. On the media side, much of that work focuses on developing protective overcoats that provide continuous coverage of the disk and the material properties required for acceptable tribological performance in the ultra-thin regime (film thickness < 5 nm).

Currently, carbon overcoats on commercially available disk drive media are deposited by various sputtering techniques. RF sputtering, DC magnetron sputtering, and reactive sputtering are most commonly used for this application [80]. The incorporation of hydrogen and nitrogen during deposition has led to carbon films with improved tribological performance at the head-disk interface (HDI) and spawned the widespread use of amorphous hydrogenated carbon (a-C:H) and nitrogenated carbon (a-C:N) overcoats [21, 30-44].   More recently, ion-beam and filtered cathodic-arc deposition techniques have been investigated in the fabrication of carbon films [81-85]. The interest in these alternative techniques stems from the fact that both can deposit mono-energetic carbon atoms to the surface at $\sim$100 eV, which is suitable for the formation of sp^3 bonds in the resulting carbon film [81, 86]. These unhydrogenated, highly sp^3 bonded films are commonly referred to as tetrahedral amorphous carbon (ta-C).

Cathodic-arc or vacuum-arc deposition has been in use since the late 1800s and, in the past forty years, most commonly employed to coat cutting tool surfaces [87, 88]. In the early 1990s, Anders et al. pioneered the use of filtered cathodic-arc deposition for disk drive applications with the incorporation of a 90° bent magnetic filter of the Aksenov type to remove the macroparticles (large micron-sized droplets that solidify during flight) generated at the cathode surface [89]. In other experiments, they also demonstrated the benefits of using a pulsed substrate bias to deposit carbon ions at various ion energies [85]. By varying the energy of the carbon ions, one can easily tune the material properties of the carbon film. At ion energies of ~120 eV, the cathodic-arc carbon (CAC) films had an sp^3 content of 85%, hardness of 60 GPa, elastic modulus of 400 GPa, and a density of 3 g/cm^3 [85, 90]. In addition, films fabricated under these conditions exhibited low friction coefficients and extended wear durability.

Since then others have actively conducted research in this area. Various characterization techniques have been applied to studying the material properties and film structures of CAC films including Raman spectroscopy [91, 92], Electron Energy Loss spectroscopy [93], nano-indentation [90], Rutherford backscattering [94], elastic recoil scattering [94], ellipsometry [94], and Fourier Transform IR Spectroscopy [95], to name a few. Of notable mention is the work done by McKenzie et. al. They reported parallel findings to those in Anders et. al [85] in the material properties of CAC films and extended their efforts into understanding the film stresses generated during deposition and how they affected the film structure [96-98].

A potential drawback of using the cathodic-arc deposition technique is the intrinsic generation of large residual compressive stresses in thicker carbon films that eventually lead to the delamination of the films from the substrate due to adhesion failure at the interface [80]. Anders et. al [99] reported success in counteracting the generation of these stresses using a multilayer approach, depositing alternating layers of hard and soft carbon while retaining the high hardness and elastic modulus of monolithic films. Another technique for relieving these compressive stresses was adopted by Friedmann et. al [100] in their *ex situ* rapid thermal annealing studies of pulsed-laser deposited carbon films. Also, the use of ion implantation during the initial stages of deposition to create an intermediary "mixed" layer at the substrate/film interface alleviated the poor adhesion dilemma by removing the site of the failure [101, 102].

Overall, there is a large and wealthy repository of information in the literature related to CAC films and their properties. Unfortunately, the bulk of this work encompasses CAC films that ranged in thickness from 20 nm to 0.2 µm, a regime that is not directly applicable for use in the future disk drive industry. As we focus on protective carbon overcoats on the order of a few nanometers, questions arise as to whether or not the bulk properties measured previously remain the same in this ultra-thin regime. We are not as concerned about generating large residual compressive stresses from such thin films, but we still insist on good adhesion between the film and the substrate, good film homogeneity to protect the magnetic layer from environmental effects, and also superior wear durability for long product life. Hence, in this chapter, we examine the material

properties of ultra-thin CAC films specifically for disk drive applications, including hardness, elastic modulus, film density, corrosion resistance, wear durability, and surface chemistry. The experimental methods employed include the use of nano-indentation, NaCl decoration tests, high-precision scales (10^{-7} g), UHV tribochamber drag tests, and thermal desorption. In closing, we report promising new data with 2 nm CAC films that demonstrate good levels of wear durability in drag tests.

3.2   Cathodic-Arc Deposition Technique

We begin by reviewing the general working principle of cathodic-arc deposition before continuing with the specific details of our carbon film depositions. The cathodic-arc deposition method is a plasma discharge that occurs between two electrodes in a vacuum. A trigger creates a spark that initiates a high current, low voltage arc. The arc current is concentrated at tiny, discrete spots on the cathode surface, where the cathode material is converted into a plasma that plumes away from the cathode surface [88]. Macroparticles, liquid droplets that are ejected from the surface and solidify during flight, are also created. Various macroparticle filters are incorporated to remove these unwanted particles and to guide the plasma to the substrate surface where high quality thin films are generated [28]. For deposition of uniform films over a large surface area, magnetic ducts are typically placed between the exit of the filter and the substrate for enhanced plasma expansion. A schematic of this deposition method is shown in Figure 3.1.

To control the energy of the incident carbon ions, a pulsed substrate bias is applied during deposition. Upon exit from the cathode gun, carbon ions have energies on the order of 20

to 30 eV [85]. As they enter the high voltage sheath encompassing the substrate, the carbon ions are accelerated rapidly to energies of 100 eV and higher depending upon the voltage applied to the substrate. Subsequently, by varying the substrate bias, we can easily control the carbon ion energy during deposition and thereby control the film's material properties.

In this chapter, the films studied were deposited at one of two facilities: (1) Lawrence Berkeley National Laboratory (Berkeley, CA), or (2) IBM (Mainz, Germany), where the deposition chamber was located in a production cleanroom environment. All films deposited for characterization and the 1st set of disks fabricated for the UHV tribochamber studies (5 nm overcoat) were done at Lawrence Berkeley National Laboratory. The only samples manufactured at IBM (Mainz, Germany) were the 2nd set of disks for the UHV tribochamber studies (2 to 4 nm overcoat).

3.2.1   Lawrence Berkeley National Laboratory deposition system

This deposition system consists of a stainless steel vacuum chamber outfitted with various feedthrough ports for power and water-cooling. A base pressure of 1 x 10^{-6} Torr is achieved through the use of a CTI-Cryogenics Cryoplex 8LP cryopump that is backed by a Trivac D25BCS mechanical pump. The chamber pressure is monitored with a Granville-Phillips 307 vacuum gauge controller and Electron Technology Inc. Bayard-Alpert type ionization gauge.

The following set-up is used to fabricate the cathodic-arc carbon film samples for our

studies. A 99.99% pure graphite rod is used as the cathode material and source of C atoms. A General Radio 1340 pulse generator outputs a 5 ms / 1 Hz square wave that is fed into three devices: (1) a Hewlett-Packard 214A pulse generator operating in gated mode that provides a 2 µs ON / 6 µs OFF square wave signal, (2) a custom arc supply that provides the arc current, and (3) a Hewlett-Packard 5532A electronic counter that tracks the number of pulses during a deposition. The custom arc supply provides a discharge from two capacitor banks – the first capacitor bank discharges 600 V to create the spark while the second bank discharges 350 V to supply the voltage for the duration of the arc. The average current generated by the arc supply during a 5 ms pulse is 250 A. From the HP 214A, the gated signal is then fed into a Cober 605P high power pulse generator that amplifies the voltage from 100 to 2000 V before reaching the water-cooled substrate holder. Hence, the pulsed substrate bias is generated during deposition. Tektronix 2201 and 2430 digital oscilloscopes are used to monitor the arc and substrate bias signals, while a Pearson transformer is implemented to measure the arc current. A flowchart of the deposition process is shown in Figure 3.2.

To prevent macroparticles from reaching the substrate during deposition, we use a macroparticle filter. Due to the evolution of these magnetic filters during our work, several different designs are used to direct plasma to the substrate while ejecting the macroparticles. The basic working principle of these magnetic filters in guiding the plasma is the same, however [103]. As current flows through the coils of the filter, a magnetic field is generated. Electrons in the plasma entering the filter spiral along these magnetic field lines because their gyration radius is much smaller than the filter size and

their collision frequency is smaller than the gyration frequency. The carbon ions in the plasma are not affected by the magnetic field lines, but they follow the guided electrons towards the exit of the filter to keep the plasma quasineutral.

The first of these filters is an open-walled 90° bent filter, shown in operation in Figure 3.3. This filter design allows approximately 25% of the plasma entering the filter to be transmitted to the exit [89]. Because the substrate is not in the line-of-sight of the plasma source, macroparticles generated on the cathode surface travel straight through the open-walls of the filter due to their momentum, while the plasma is guided to the filter's exit. However, due to collisions with the coil, some macroparticles reflect off and land on the substrate.

An improvement on this design is the solid-walled S-duct filter, which is two 90° bent filters in series with a bellows wall. As expected, the plasma transmission efficiency of this filter is poor at 6% (0.25 x 0.25 = 0.0625) [104], but the addition of a bellows wall allows macroparticles to be captured or reflected enough times to prevent their emergence at the filter's exit. This filter design is the first to achieve suitable levels of filtration to accommodate the deposition of carbon films for disk drive applications.

Third, an open-walled S-duct filter in a smaller form factor (radius and curvature) coupled with a physical barrier at the exit provides better filtering of macroparticles. By increasing the number of coils in the filter at specific locations and reducing the overall length of the filter, the plasma is focused better and transmission efficiency increases to

12-15% [105]. A picture of this S-duct filter in operation is shown in Figure 3.4.

Finally, the twist filter is an open-walled S-duct filter with the two 90° bent filters rotated out-of-plane. This fourth generation macroparticle filter offers significant advances in plasma transmission and particle reduction. A picture of the twist filter is shown in Figure 3.5 and further details of its development may be found in our paper [27].

At the exit of the filter, the plasma expands freely before impinging on the substrate to form carbon films. However, for 65 mm and larger disk substrates, thickness uniformity of the deposited film over these surface areas is critical so we use a magnetic bucket or homogenizer to expand the plasma rapidly over a short distance to obtain more uniform coatings.

3.2.2   IBM (Mainz, Germany) deposition system

This deposition system is a commercially-available, Unaxis Circulus M12 single disk sputtering tool designed specifically for the hard disk drive industry. Its 10 disk processing stations allow for high-throughput manufacturing of 600 disks per hour. For our studies, one of the processing stations was retrofitted with a cathodic-arc source and macroparticle filter for deposition of the carbon overcoat, while the other stations remained unchanged and continued to sputter-deposit the other layers of the disk media. All disk samples processed at this site were done by Ralph Ohr et. al (IBM in collaboration with IWS Dresden).

3.3   Experimental methods

3.3.1   Nano-indentation

One of the benefits of the cathodic-arc technique for depositing carbon films is the ease in modifying the material properties of the resulting ta-C films. By varying the pulsed substrate bias during deposition, one changes the energy of the impinging carbon ions, which is a critical parameter in depositing predominantly sp^3-bonded films [86]. Changes in the bonding structure of the cathodic-arc carbon films affect material properties such as hardness, which is a material's resistance to plastic deformation, and elastic modulus [90]. In this investigation, we implement the use of a commercially available Hysitron Triboscope system to determine the hardness and elastic modulus of the cathodic-arc carbon films as a function of substrate bias and film thickness.

We use the same Hysitron system and Digital Instruments Nanoscope III described in Section 2.2.3 for nano-scratch tests, but equipped with a single-axis transducer [67]. The Hysitron single axis tester is centered around a capacitative force/displacement transducer that provides high sensitivity, a large dynamic range, and a linear force/displacement output signal. A corner of a cubic diamond tip with a nominal radius of 50 nm is used to indent into the sample surface at loads of 1 µN to 10 mN. The TriboScope 3.0 software is used to specify the loading functions, record load/displacement data during indentation, and calculate hardness and elastic modulus of the films.

We define hardness H as

$$H = \frac{P_{max}}{A}$$ (3)

62

where P_{max} is the peak load during indentation and A is the projected contact area at the peak load. Elastic modulus is determined from the following relation (Sneddon) [106]:

$$S = \frac{dP}{dh}\bigg|_{Pmax} = 2\sqrt{\frac{A}{\pi}}E_r \qquad (4)$$

where S is the contact stiffness or slope of the unloading curve at the maximum load, E_r is the reduced modulus, and h is the penetration depth. The reduced modulus is related to the elastic modulus E of the material by

$$\frac{1}{E_r} = \frac{1-v^2}{E} + \frac{1-v_i^2}{E_i} \qquad (5)$$

where v_i and E_i are the Poisson's ratio and elastic modulus of the indenter, respectively.

The contact area A is a function of contact depth h_c during indentation (i.e. $A=A(h_c)$) and may be found experimentally for a given indenter shape. With this information, the method in Lo and Bogy [67] is used for analyzing the load/unload curve to determine the contact stiffness and subsequently the elastic modulus. Since the possibility of indenter deformation exists with the use of an extremely sharp tip on cathodic-arc carbon films, a correction technique by Lo and Bogy [107] is also incorporated to compensate for this behavior and to calculate true hardness and elastic modulus. Otherwise, an overestimate of the hardness and elastic modulus may occur.

3.3.1.1 Material properties versus substrate bias

To understand the effects of substrate bias on hardness and elastic modulus, three cathodic-arc carbon films are deposited on low-resistivity, 1" diameter Si <100> wafer substrates. The carbon films are deposited at substrate biases of -100, -500, and –1000 V.

We implement the open-walled 90° bent filter for macroparticle reduction and use the following deposition parameters: (1) a base pressure of 1 x 10^{-5} Torr, (2) an arc current of 300A in 5 ms durations at a frequency of 1 Hz, and (3) a pulsed substrate bias with a 33% duty cycle (2 µs ON / 6µs OFF). The first 10% of the deposition is done at a substrate bias of -2000 V for good adhesion between the carbon film and Si wafer. Film thickness is measured with a Dektak IID profilometer. The film thicknesses of the -100, -500, and – 1000 V bias samples are 71.5, 122.5, and 98.5 nm, respectively. Hardness and elastic modulus of the CAC films are measured with the Hysitron system. All measurements are limited to indentations with residual depths less than 20% of the total film thickness.

3.3.1.2 Material properties versus film thickness

To understand the effects of film thickness on hardness and elastic modulus, eight cathodic-arc carbon films are deposited on low-resistivity, 1" diameter Si <100> wafer substrates with film thicknesses ranging from 6.6 to 66 nm. We implement the open-walled 90° bent filter for macroparticle reduction and use the following deposition parameters: (1) a base pressure of 1 x 10^{-5} Torr, (2) an arc current of 300A in 5 ms durations at a frequency of 1 Hz, and (3) a pulsed substrate bias of –100 V with a 33% duty cycle (2 µs ON / 6µs OFF). The first 10% of the deposition is done at a substrate bias of -2000 V for good adhesion between the carbon film and Si wafer. Film thicknesses are measured with an n & k Analyzer 1100 reflectance spectrometer and Dektak IID profilometer. The film thicknesses of the eight films are 6.6, 10.4, 17.7, 18.2, 23.5, 44, 49, and 66 nm. Hardness and elastic modulus of the CAC films are measured with the Hysitron system. As before, all measurements are limited to indentations with

residual depths less than 20% of the total film thickness.

3.3.2 Density measurements

Another material property closely related to the carbon ion energy during deposition is the film density. Pharr et. al [90] indirectly measured the film density with Electron Energy Loss Spectroscopy (EELS) where the mass density is taken from the valence electron density, which in turn is derived from the valence plasmon. In our investigation, film density measurements are made directly with a high-precision scale with 10^{-7} gram accuracy.

The experimental procedure is as follows. The weights of three low-resistivity, 1" diameter Si <100> wafer substrates are measured with the scale prior to deposition. Next, a small circular area is masked off with a Sharpie permanent ink marker. The carbon films are deposited at substrate biases of -100, -500, and –1000 V. We implement the open-walled 90° bent filter for macroparticle reduction and use the following deposition parameters: (1) a base pressure of 1 x 10^{-5} Torr, (2) an arc current of 300A in 5 ms durations at a frequency of 1 Hz, and (3) a pulsed substrate bias with a 33% duty cycle (2 μs ON / 6μs OFF). The first 10% of the deposition is done at a substrate bias of -2000 V for good adhesion between the carbon film and Si wafer. The samples are then submerged in an ultrasonic bath of acetone for fifteen minutes to remove the ink and any contamination on the film surface. These wafers are then weighed again and a Dektak IID profilometer is used to determine the film thickness. The film thicknesses of the -100, -500, -1000V bias samples are 71.5, 122.5, and 98.5 nm, respectively. Density values are

then calculated directly from the weight difference and film volume as determined by the thickness measurement.

3.3.3   Corrosion tests

Until recently, one of the shortcomings of sputter-deposited, amorphous carbon films is their low density and subsequent porous film structure [83]. This results in poor corrosion protection of the magnetic layer as overcoats are reduced to thicknesses less than 10 nm. Cathodic-arc carbon films are well suited for this application as their intrinsic density approaches that of diamond [28, 85, 90, 108], but proper precautions are needed to prevent macroparticles from contaminating the film during deposition. As such, the corrosion resistance of cathodic-arc carbon films is studied in a series of samples with film thicknesses ranging from 2 nm to 40 nm.

These films are deposited on low-resistivity, 1" diameter Si <100> wafers that were previously coated with a layer of 100 nm permalloy (80% Ni / 20% Fe). The CAC films are deposited at a base pressure of 1 x 10^{-5} Torr under these conditions: (1) an arc current of 300 A in 5 ms durations at a frequency of 1 Hz, and (2) a pulsed substrate bias of –100 V with a 33% duty cycle (2 µs ON / 6 µs OFF). The first 10% of the deposition is done at a substrate bias of –2000 V for good adhesion between the carbon film and magnetic layer. To evaluate the effects of macroparticles on corrosion performance, three sets of films are fabricated with these filter designs:

1.   Solid-walled S-duct filter.

2. Open-walled S-duct filter.

3. Twist-filter.

Sputter-deposited CH_x films (30 atomic % H_2) are used as a reference for this study. Film thicknesses are measured with an n & k Analyzer 1100 reflectance spectrometer and Dektak IID profilometer.

The corrosion performance of these films is based on a simple, yet effective decoration technique – a sodium chloride (NaCl) dip test. Samples were immersed for 24 hours in a pre-mixed solution consisting of 0.5 mol NaCl, 0.5 mol $(NH4)H_2PO_4$, 1 gram Liquinox, and 1000 grams of deionized H_2O. Upon removal, the specimen is rinsed in an ultrasonic bath of deionized water for five minutes and dried with a N_2 air gun. Inspection of the sample surface is done under an Olympus Vanox optical microscope at 100x magnification, where an image analysis system counts the defect density (number of defects per unit area) in a 0.8 x 1 mm^2 area and defect size (percent area occupied by defects). The image analysis system consists of a Sony Hyper HAD CCD camera interfaced to a computer by a frame grabber board and a Media Cybernetics' Image-Pro Plus software package.

3.3.4   Ultra-high vacuum (UHV) tribochamber tests – 5 nm CAC films

As the disk drive industry approaches near-contact and contact recording, the reduced fly height of slider designs results in more intimate contact between the slider and disk surface for prolonged periods of time [78]. In this regime, not only are mechanical

interactions between the slider and disk important, but also chemical reactions between the two surfaces and the lubricant layer. As such, much research is being conducted in this area of tribo-chemistry of the head-disk interface (HDI) [50-60, 109-111]. A useful tool for studying these tribo-chemical phenomena, especially the decomposition of perfluoropolyether (PFPE) lubricant ZDOL in various environments, is the ultra-high vacuum (UHV) tribochamber in our laboratory [69]. We utilize this system to study the tribological performance of 5 nm CAC overcoats on disk and slider substrates.

The UHV tribochamber consists of a disk spindle, a slider actuator, a substrate heater, and a Balzers QMG 420 high-resolution quadrupole mass spectrometer (QMS) in a stainless-steel vacuum chamber, as pictured in Figure 3.6. A detailed description of this system may be found in Section 2.2.5 of this dissertation.

3.3.4.1 Drag tests

The following test procedure is used to conduct drag tests in the tribochamber. Initially, the tribochamber is baked out at 423 K at high vacuum for 24 hours. The chamber is then backfilled with Argon gas as the disk and slider samples are mounted inside. Next, the chamber is pumped down to a base pressure of 2×10^{-8} Torr and the channels of the QMS are assigned to the selected AMUs. The background intensities are recorded before the drag tests are initiated with the following parameters: 0.1 m/s drag speed, a load of 2.5 grams, and a sliding time of 20 minutes. The mass spectrum and friction data is collected every 2 seconds by a computer connected to the QMS via a serial connection.

The disks used in this study are commercially available, 65 mm smooth thin-film disks. Two sets of disks are tested – both sets are identically manufactured up to the magnetic layer, whereupon one set is sputter-deposited with a 5 nm amorphous, hydrogenated carbon overcoat (CH_x) and the second is deposited with 5 nm of cathodic-arc carbon. The cathodic-arc carbon is deposited at a base pressure of 1×10^{-5} Torr with the solid-walled S-duct filter under the following conditions: (1) an arc current of 300A in 5 ms durations at a frequency of 1 Hz, and (2) a pulsed substrate bias of -100 V with a 33% duty cycle (2 µs ON / 6µs OFF). The first 10% of the deposition is done at a substrate bias of -2000 V for good adhesion between the carbon film and magnetic layer. Both sets of disks are lubricated with ZDOL by a dipping process and subjected to the same post-processing steps. The molecular weight of ZDOL is 2000 a.m.u. and its chemical formula is given below [113]:

$$CH_2OH\text{-}CF_2O\text{-}(CF_2O)_m\text{-}(CF_2CF_2O)_n\text{-}CF_2\text{-}CH_2OH \text{ where } n/m = 2/3 \qquad (6)$$

Fourier transform infrared spectroscopy (FTIR) measurements indicated lubricant thicknesses of 0.85 nm on the disks.

The sliders used in this study are 50% (1.6 mm by 2 mm) negative-pressure Al_2O_3-TiC sliders with and without amorphous diamond-like carbon (DLC) films on their air bearing surfaces (ABS). The carbon-coated sliders are further separated into two groups: (1) 10 nm commercially coated DLC sliders and (2) 5 nm CAC-coated sliders fabricated in-house. The deposition parameters for the CAC film on the sliders are identical to those

described earlier for the disk samples. A picture of the ABS is shown in Figure 3.7(a).

3.3.4.2 Thermal desorption tests

Prior to conducting thermal desorption tests in the UHV tribochamber, the substrate heater is baked at 589 K in high vacuum for 4 hours to remove any residual contaminants on the heater surface after the previous thermal desorption test. A 2 cm x 2 cm square test sample is cut from each disk. Each sample is mounted on the heater where a thermocouple in contact with the heater is used to monitor the temperature during testing. As with the drag tests, the tribochamber is pumped down to a base pressure of 2×10^{-8} Torr and the channels of the QMS are assigned to the selected AMUs described earlier. The sample is heated at a rate of 0.2 K/s from room temperature to 550 K, while the mass spectrum and temperature data is collected every 2 seconds by a computer connected to the QMS via a serial connection.

The test samples used in this study are cut from commercially available, 65 mm smooth thin-film disks. Two sets of disks are tested – each set is identically manufactured up to the magnetic layer, whereupon one set is sputter-deposited with a 10.5 nm amorphous, hydrogenated carbon overcoat (CH_x) and the second is deposited with 10.5 nm of cathodic-arc carbon. The deposition parameters for the cathodic-arc carbon are described earlier in Section 3.3.4.1. Both sets of disks are lubricated with ZDOL (MW 2000) by a dipping process and subjected to the same post-processing steps. FTIR measurements indicated lubricant thicknesses of 1.2 nm on the disks.

3.3.5   Ultra-high vacuum (UHV) tribochamber tests – 2 nm CAC films

For 1 Tb/in^2 areal densities, we noted earlier that the protective overcoat must be on the order of 1 to 2 nm depending upon the model used for the calculation. In this study, we examine the performance of 2 to 4 nm CAC films optimized for wear durability and deposited on disk media in tribochamber drag tests. The drag test procedure is identical to that described in Section 3.3.4.1 with the following exceptions: a load of 3.0 grams and sliding until failure of the HDI occurs.

The disks used in this study are commercially available, 95 mm glass thin-film disks with a super-smooth data zone (r.m.s. roughness of ~ 0.6 to 0.8 nm). They are fabricated in the deposition system at IBM (Mainz, Germany) described previously in Section 3.2.2. Three sets of disks are tested – all sets are identically manufactured up to the magnetic layer, whereupon a cathodic-arc carbon overcoat is deposited at a film thickness of 2, 3, or 4 nm. The cathodic-arc carbon is deposited at a base pressure of 7.5 x 10^{-4} Torr and a temperature of 220°C with a 120° bent filter under the following conditions: (1) an arc current of 4 kA in 1.6 ms durations at a frequency of 100 Hz, and (2) no applied substrate bias. These parameters resulted in a carbon ion energy of ~ 40 eV. The film thickness is varied by changing the number of pulses in the deposition and is measured with X-ray reflectometry (XRR) / ellipsometry. All disks are lubricated with ZDOL (MW 4000) by a dipping process and subjected to the same post-processing steps. FTIR measurements indicated lubricant thicknesses of 1.2 nm on the disks. As a reference, a set of disks was also processed identically but with sputtered 5 nm CN_x overcoats.

The sliders used in this study are 50% (1.6 mm by 2 mm) negative-pressure Al_2O_3-TiC sliders with and without amorphous diamond-like carbon (DLC) films on their air bearing surfaces (ABS). A picture of the ABS is shown in Figure 3.7(b).

3.4   Results and Discussion

3.4.1   Nano-indentation

Figure 3.8 is a plot of the hardness versus substrate bias during deposition of cathodic-arc carbon films. Figure 3.9 is a similar plot of the elastic modulus of these films. From the charts, we note that the highest hardness (68 GPa) and elastic modulus (244 GPa) belongs to the sample deposited at a –100 V bias, which corresponds to an ion energy of ~120 eV. Weiler et. al [114] and Fallon et al. [115] have published similar hardness levels for carbon films deposited with various methods at ion energies of 90 to 140 eV per incident carbon atom. In addition, the hardness of our film approaches the 90 GPa value typically quoted for polycrystalline diamond [116]. As we increase the substrate bias, both hardness and elastic modulus decrease due to increased graphitization (higher sp^2/sp^3 bonding ratio) of the film. Electron Energy Loss Spectroscopy (EELS) is typically used to determine the sp^3 content of carbon films [81] and an analysis by Pharr et. al [90] on similar films demonstrated that CAC films deposited with a –100 V bias have an sp^3 content of 81% while films deposited at –2 kV had a substantially lower value of 39%.

To determine the effects of film thickness on these two material properties, we refer to Figures 3.10 and 3.11, plots of hardness and elastic modulus vs. film thickness for a fixed substrate bias of –100 V. As we decrease the film thickness from 66 to 6.6 nm, the nano-

indentation tests clearly show a reduction in both hardness and elastic modulus. Initial review of this data suggests that the substrate is affecting the nano-indentation measurements, i.e. the underlayer contribution to the hardness of the film increases as the film becomes thinner, which is a common explanation for this phenomenon. However, Lo et. al [117] demonstrated the existence of a surface layer for CAC films that is predominantly sp^2 bonded, whereas the bulk of the film is sp^3 bonded. The ratio of this surface layer thickness to the total film thickness increases for thinner films and hence results in lower hardness values in our nano-indentation tests.

The growth mechanism of this surface layer is still under investigation but we present two popular hypotheses here for discussion. Robertson [81, 118] suggests a subplantation or ballistic model whereby incident ions penetrate the surface into an interstitial site causing a local increase in density. At high enough energies, atoms can migrate back to the surface to relax the excess density forming the sp^2 bonded surface layer. The higher localized densities in the bulk of the film result in sp^3 bonded regions. Thus, a dual-layered film is grown with a softer surface layer over a harder bulk layer. The second model is based upon a similar idea but depends on total film thickness. As film thickness increases, the compressive stress also increases in the film, promoting the formation of sp^3 bonds. This was demonstrated by McKenzie et. al [98] in their studies of compressive-stress-induced formation of ta-C films. For thin films, no appreciable amount of stress is generated so the films remain in an sp^2 bonded state. Hence, thicker films are relatively harder than thinner films due to their higher sp^3 content. Both growth models support our data, but at this time, we cannot determine which model is correct or

73

if a combination of the two is also possible.

3.4.2 Density measurements

Figure 3.12 is a plot of film density versus substrate bias during deposition. Similar to the results from the hardness and elastic modulus study, the highest film density (3.0 g/cm^3) is noted at a pulsed substrate bias of –100 V and decreases to 2.4 g/cm^3 as the bias is increased to – 1 kV. For comparison, the densities of graphite and diamond are 2.25 and 3.51 g/cm^3, respectively. This decrease in film density is the result of a reduction in the compressive stresses of the film. Using a simple theory that accounts for stress generation and stress annealing by ion impacts, Davis [119] demonstrated that the compressive stress increases initially with ion energy and then decreases with further increase of ion energy for ta-C films. For CAC films deposited in our system, we know that this peak corresponds to a substrate bias of – 100V based on earlier work by Ager III et. al [91]. With reduced stress, McKenzie et. al's model [98] predicts less sp^3 hybridization in the films and subsequently lower film density. Moreover, our film density measurements are the first to confirm those predicted indirectly by several others with EELS [85, 90, 94, 98].

3.4.3 Corrosion tests

Figure 3.13 is a plot of corrosion pinhole count versus film thickness for a fixed substrate bias of –100 V during deposition. Higher pinhole counts imply poorer corrosion-resistance of the film. Three sets of data are plotted on the graph corresponding to the various macroparticle filters used during each deposition. Also on the plot is a line

marking the average pinhole count of 100 for a 7 nm RF-sputtered CH_x film (30 atomic %). This CH_x film is chosen as a reference because it possesses a performance level that is deemed acceptable for disk drive applications based on drive-level testing in the field.

The first set of data, represented by circles, corresponds to films deposited with the solid-walled S-duct filter. No significant difference in corrosion performance is noted for film thicknesses between 4 and 40 nm (the plot only displays data from 0 to 6 nm to zoom in on details at ultra-thin regime), which indicates a continuous film on the sample surface even at 4 nm. However, below 4 nm, the pinhole count rises an order of magnitude, which coincides with the values for an uncoated sample, indicating a breakdown of the film continuity/coverage. Hence, the corrosion performance of a 4 nm CAC film with this filter is acceptable for use in today's disk media products.

The second set of data, represented by squares on the plot, corresponds to films deposited with the open-walled S-duct filter. In the 2 to 5 nm film thickness regime, we note that the use of this filter significantly improves the corrosion performance of films compared to those deposited by the solid-walled S-duct filter by reducing the amount of macroparticle contamination. Pinhole counts are in the hundreds instead of the thousands, which is a substantial decrease from the counts we would typically expect for an uncoated sample and also for a 4 nm CH_x film.

Finally, utilizing the twist filter, we achieve the best levels of corrosion performance to date for cathodic-arc carbon films – better than the 3 nm CAC films deposited on sliders

and tested using the "Batelle" method in our previous work [27]. The data corresponding to this third set of films is marked with triangles on the plot. We observe continuous coverage of the surface down to film thicknesses of 2 nm, as exhibited by no significant changes in the number of pinhole counts for films in the 2 to 5 nm thickness regime, and acceptable levels of corrosion protection for this application (pinhole counts ≤ 100).

3.4.4   Ultra-high vacuum (UHV) tribochamber tests – 5 nm CAC films

Figure 3.14 is a plot of the friction coefficient versus drag time for the 5 nm CAC disk tested with three different types of sliders: (1) uncoated, (2) commercially carbon-coated, and (3) CAC-coated. For the uncoated slider case, the maximum friction coefficient is 2.3 before visual wear is observed after 46 s of dragging. With the addition of a carbon-coating to the slider surface, both wear durability and friction performance improves. The maximum friction coefficient before visual wear for the commercially carbon-coated and CAC-coated slider cases are 0.82 and 0.80, respectively. Also, the wear life for each is extended to 72 s and 60 s of dragging before failure of the head-disk interface is observed.

Figure 3.15 is a similar plot of the friction coefficient versus drag time for the 5 nm CH_x disk tested with the same three types of sliders. Once again, the worst performance is observed with the uncoated slider case, where maximum friction hits 2.7 before failure occurs after 100 s of dragging. For the commercially available carbon-coated and CAC-coated slider cases, their maximum friction coefficients are 0.75 and 0.29 before failure after 870 s and 140 s of dragging, respectively.

A comparison of the wear durability between the CAC and CH_x disks shows that the CH_x disk outperforms the CAC disk in every slider case. These results are surprising because others have reported enhanced wear performance with CAC films. Tsui et. al [120] reported superior scratch resistance of CAC films in nano-scratch tests compared to CH_x films with hydrogen contents ranging from 20 to 40 atomic percent. In another related experiment, Anders et. al [108] demonstrated that disks coated with CAC films reduced the amount of slider ABS erosion compared to CH_x films, which would prevent the formation of particles, initiation of tri-body wear, and subsequent failure of the interface. However, in those studies, their films were much thicker than those of interest here, and citing our earlier nano-indentation results, the difference in material properties due to the film thickness effect are significant. These differences may account for the poor wear durability in our drag tests with the CAC films.

In terms of friction, the use of various different sliders greatly affects the values recorded during the drag test. For both CAC and CH_x disks, the highest coefficient of friction (COF) is observed with the uncoated sliders due to the material incompatibility between the slider (Al_2O_3-TiC) and disk (carbon) surface. Using sliders with a carbon-coating reduces the COF and prolongs the life of the head-disk interface as expected [121, 122]. On the CAC disk, no significant difference in friction performance is noted between the commercially available carbon-coated slider and CAC-coated slider. However, on the CH_x disk, the CAC-coated slider provides a COF half that of the commercially available carbon-coated slider, an observation noted by others in similar experiments [123].

Next, we examine the effects of the carbon overcoat on the decomposition mechanisms of the ZDOL lubricant layer. The decomposition of ZDOL may be broken down into two primary mechanisms, frictional/thermal decomposition and catalytic decomposition. CFO (47 a.m.u.) and CF_2O (66 a.m.u.) are recorded to monitor the extent of the frictional or thermal decomposition of ZDOL. A synopsis of the frictional decomposition mechanism is listed below and is based on extensive work in our laboratory by Chen et. al [109-111], Wei et. al [112], and Yun et. al [69]. Further details of the decomposition may be found in their papers.

$$-O-/-CF_2-O-/-CF_2-CF_2-O-/-CF_2- \Rightarrow CF_2=O \ (66) + -CF_2-CF_2-O- \ (116) \qquad (7)$$

$$-CF_2-CF_2-O- \ (116) \Rightarrow -CF_2- \ (50) + CF_2=O \ (66) \qquad (8)$$

$$CF_2=O \ (66) \Rightarrow CFO \ (47) + F \ (19) \qquad (9)$$
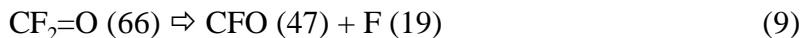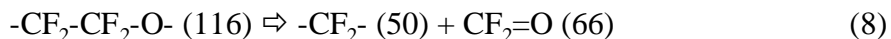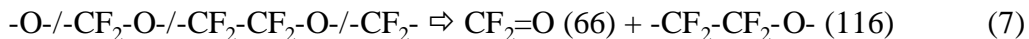
In this process, the ZDOL molecule decomposes under friction action alone by chemical reactions 7 and 8. The gaseous by-products from these reactions are then further cleaved by electron bombardment in the mass spectrometer as described in reaction 9.

The catalytic decomposition mechanism is much more complex. We monitor CF_3 (69 a.m.u.) and C_2F_5 (119 a.m.u.) during the drag tests to determine the extent of this reaction. Once again, this mechanism is based on the work by Chen et. al [109-111], but important components are also derived from the results of Kasai et. al's [51] chemical studies with ZDOL in the presence of slider material Al_2O_3-TiC. It begins with the by-

products generated by frictional stimulation of the interface described in reaction 7. In addition, the formation of hydrofluoric acid (HF) occurs. The $CF_2=O$ and HF from these two reactions then interact with the Al_2O_3 from the slider surface to produce Lewis acid AlF_3 as shown in reactions 10 and 11.

$$Al_2O_3 + 6\ HF \Rightarrow AlF_3 + 3\ H_2O \qquad (10)$$

$$Al_2O_3 + 3\ CF_2O \Rightarrow 2\ AlF_3 + 3\ CO_2\ (44) \qquad (11)$$

Rapid reactions along the main ZDOL chain take place on the AlF_3 surface to form CF_3-O-, CF_3CF_2-O- compounds, and R-CF=O:

$$\begin{array}{c} F \\ R\text{-}CF_2\text{-}O\text{-}CF_2\text{-}R \Rightarrow R\text{-}C=O + CF_3\text{-}R \\ (CF_3\text{-}R:\ CF_3\text{-}O\text{-},\ CF_3CF_2\text{-}O\text{-}) \end{array} \qquad (12)$$
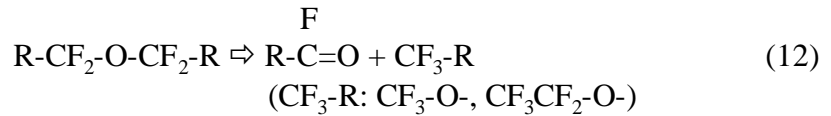
Subsequent electron impacts in the mass spectrometer lead to CF_3 (69) and C_2F_5 (119) fragments.

Figure 3.16 is a plot of the integrated mass spectrum over the first eighty cycles of dragging on the CH_x disk for four different mass fragments: 47 (CFO), 66 (CF_2O), 69 (CF_3), and 119 (C_2F_5). Three sets of data are plotted in this figure corresponding to the various sliders used during the drag test. First, we observe that the highest intensities are associated with the uncoated slider. CF_3 and C_2F_5 are an order of magnitude higher than that for the carbon-coated slider cases – this is expected as the carbon film on the slider

surface acts as a physical barrier between the lubricant and the Al_2O_3-TiC slider material to prevent the catalytic decomposition from occurring. CFO and CF_2O are also higher than that for the carbon-coated slider cases and this difference is due to the higher COF we observe during the drag tests, i.e. higher friction results in more shearing/scissioning of the ZDOL molecule. No significant difference is noted between the results for the commercially available carbon-coated slider and CAC-coated slider. Both coatings prevent the catalytic decomposition of ZDOL from occurring.

Figure 3.17 is a similar plot of the integrated mass spectrum for the CAC disk. We note a slightly more than two-fold decrease in the intensities of CF_3 and C_2F_5 compared to those for the CH_x disk, indicating that the use of a CAC overcoat reduces the catalytic decomposition of ZDOL. These results confirm our earlier reports of a two-fold reduction in the catalytic decomposition of ZDOL when using CAC instead of CH_x overcoats on disks in drag tests [50]. Surprisingly, for the carbon-coated slider cases, both sliders exhibit higher intensities in CFO and CF_2O for the CAC disk compared to the CH_x disk. No significant differences in the friction coefficient could account for this increase. Instead, a measurement of the lubricant thickness via FTIR on both disks revealed that the CAC disk had twice as much lubricant as the CH_x disk (1 nm vs. 0.5 nm). Chen et. al [124] reported that the mass fragment intensities measured in these types of studies are highly dependent on lubricant thickness – the intensity scales with lubricant thickness. Thus, we observe consistently higher intensities for all the masses in the carbon-coated slider cases of the CAC disk compared to the CH_x disk. Remarkable, though, is the fact that the CAC disk significantly decreases the catalytic decomposition of ZDOL with

uncoated sliders compared to the CH_x disk when we account for this lubricant thickness disparity between the two samples.

To understand why CAC films prevent the catalytic decomposition of ZDOL in drag tests, we turn to the thermal desorption experiments. Figure 3.18 is the thermal desorption profile for H_2, i.e. the intensity of H_2 as a function of temperature, for both the CAC and CH_x disks. We observe that the amount of hydrogen evolving from the CAC sample (interpreted as the area under the curve) is orders of magnitude lower than that for the CH_x sample – this stems from the fact that these CAC films only possess 1 to 3 at. % of hydrogen in their composition compared to the 30 at. % for the CH_x film. Figures 3.19 and 3.20 are similar desorption profiles for fluorine (F) and hydrofluoric acid (HF), respectively. We again note that the CAC sample generates much less F and subsequently less HF than its CH_x counterpart. As described in Section 2.3.4, the addition of hydrogen to carbon films weakens the ether bonding (at the acetal units) between the ZDOL molecule and the carbon surface, which evidences itself by the increased generation of F in the thermal desorption test with the CH_x film. Hence, the CAC film evolves less H_2 and F than CH_x films, which hinders the catalytic decomposition mechanism of ZDOL described earlier. Without a source of hydrogen and flourine, HF production is limited and prevents the formation of the Lewis acids required for the rapid decomposition of the ZDOL chain. This is a significant result in our understanding of the critical components of the decomposition of ZDOL and this knowledge may be applied to the development of better overcoat/lubricant systems for a more robust HDI.

3.4.5   Ultra-high vacuum (UHV) tribochamber tests – 2 nm CAC films

Figure 3.21 is a summary of the wear durability in drag tests with DLC-coated and uncoated sliders for the 2, 3, 4 nm CAC overcoats and the 5 nm CN_x film. In tests with the DLC-coated sliders, the trends observed for the CAC overcoats are counter-intuitive – wear durability increases as the protective films become thinner! The 2 nm CAC film approaches the durability of the 5 nm CN_x film, which demonstrates the potential of this carbon material as a useful protective overcoat for 1 Tb/in^2 applications. For the tests with uncoated sliders, the trends were similar, but the differences between the cells were less significant. The coefficient of friction (COF) during dragging for all sets of disks, both CAC and CN_x, were similar with an average of ~ 1.5. The only exception was the CN_x disk tested with the uncoated slider – it's COF began at 1.5 and grew rapidly to 3.4 before failure. In addition to these results, AFM nano-scratch tests were conducted by Ralph Ohr (IBM, Mainz, Germany) on similar films deposited onto silicon wafers (with the accompanying disk underlayers) using the technique developed by Wienss et. al [70]. In Figure 3.22, we note that the inherent scratch resistance (defined as normal load divided by the cross-sectional area of the scratch) of these films decrease as they become thicker, correlating well with the behavior we observe in our drag tests.

Because our characterization studies have focused primarily on varying ion energy to tune the material properties of CAC films, the introduction of elevated deposition temperature as a variable adds changes to the film structure that we have yet to explore. It is known that there is a transition temperature for ta-C films where graphitic films begin to form instead of the sp^3-rich films we expect at room temperature depositions [126].

With deposition parameters that are relatively close to the ones used for these films, Kleinsorge et. al have reported in their studies that at temperatures of approximately 200°C there is a sharp transition from ta-C films with a sp^3 matrix and the beginnings of sp^2 clusters to ones with a sp^2 matrix and graphitic structures [127]. Coupling this observation with the fact that the substrate temperature rises for the thicker films due to longer deposition times suggests that the decrease in wear resistance noted in both drag tests and nano-scratch experiments may be attributed to a transformation of the CAC overcoat from a sp^3- to sp^2-rich film microstructure.

Figures 3.23 and 3.24 are the integrated intensities of the mass fragments generated at the HDI associated with the thermal and catalytic decomposition of ZDOL from tests with DLC-coated and uncoated sliders, respectively: CFO (47 a.m.u.), CF_2O (66 a.m.u.), CF_3 (69 a.m.u.), and C_2F_5 (119 a.m.u.). For the DLC-coated slider test case, we clearly observe an increase in the overall amount of decomposition components as CAC thickness increases suggesting more re-flow of lubricant back to the test track. As noted before in Section 2.3.3, lubricant mobility is related to the dangling bond density on the carbon film surface, which is a function of the sp^3 content in the film. This increased lubricant mobility supports our aforementioned statement that the CAC films are becoming more sp^2-rich with increasing thickness. For the uncoated slider test case, no significant difference was observed in the lubricant decomposition among the CAC samples due to the aggressive nature of the catalytic decomposition and relatively short wear lives. We do note a significant decrease in the catalytic decomposition of ZDOL on the CAC overcoats compared to the CN_x sample. We attribute this to the high friction

observed with the CN_x disk, which generates more of the precursor mass fragments that fuel the catalytic decomposition mechanism resulting in the increased production of CF_3 and C_2F_5.

This data is reported to demonstrate the feasibility of producing 2 nm CAC films with good wear durability - the promising results observed definitely warrant further studies in this area to characterize the effects of temperature on the material properties of CAC films and their optimization for enhanced tribology at the HDI in high areal density applications.

3.5   Conclusions

The use of cathodic-arc carbon (CAC) films as a protective overcoat for disk drive media as an alternative to conventionally sputtered, hydrogenated (CH_x) and nitrogenated carbon films (CN_x) is investigated. In this chapter, we demonstrated that the material properties of CAC films are highly dependent upon ion energy of C atoms during room temperature depositions and that the most diamond-like films are observed when this energy is approximately 120 eV. Moreover, these material properties are dependent upon the thickness of the CAC film due to the inherent formation of a dual-layered film structure with an sp^2-bonded surface layer and an sp^3-bonded bulk layer. At a film thickness of 2 nm, CAC films remained continuous, provided acceptable levels of corrosion resistance by today's disk drive standards, and significantly outperformed CH_x films. 5 nm CAC disks also prevented the catalytic decomposition of ZDOL in UHV drag tests with uncoated sliders by generating less H_2 and F at the head/disk interface. This

reduced hydrogen and fluorine evolution in turn hindered the formation of hydrofluoric (HF) and Lewis acids (AlF_3) required to decompose the ZDOL molecule. Finally, 2 nm CAC disks optimized for wear durability show excellent levels of wear durability that approach that of 5 nm CN_x films in drag tests, making them a viable option for future high areal density applications.
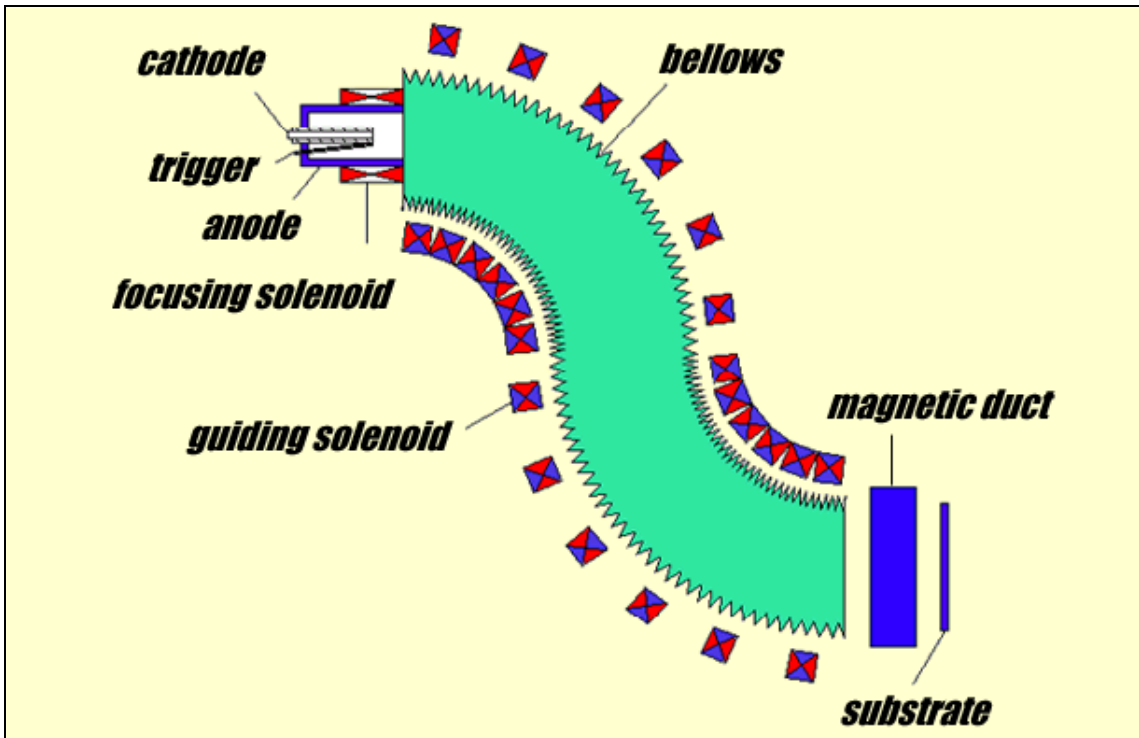
Figure 3.1. Schematic of cathodic-arc deposition method with solid-walled S-duct filter.
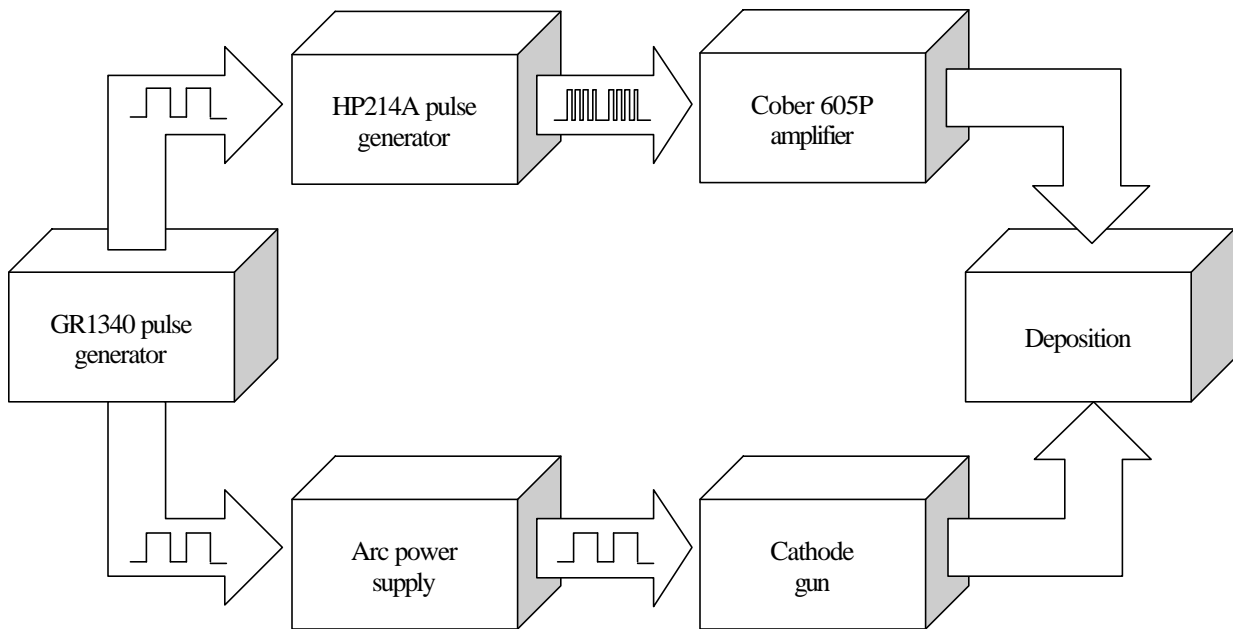
Figure 3.2. Cathodic-arc deposition flowchart.
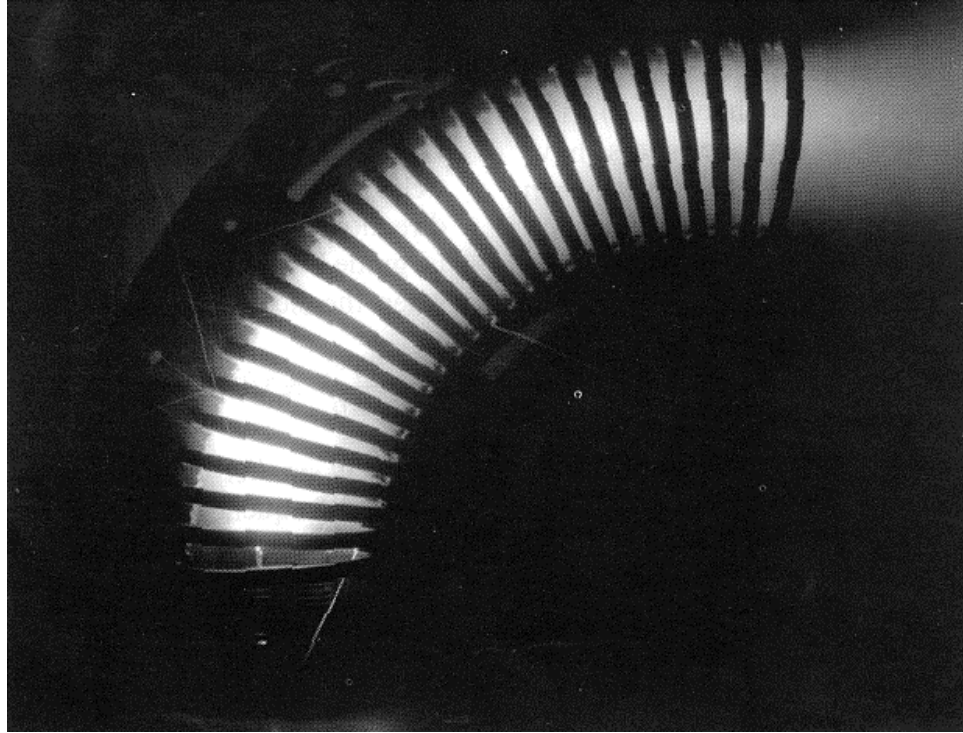
Figure 3.3. Open-walled 90° bent filter in operation [84].
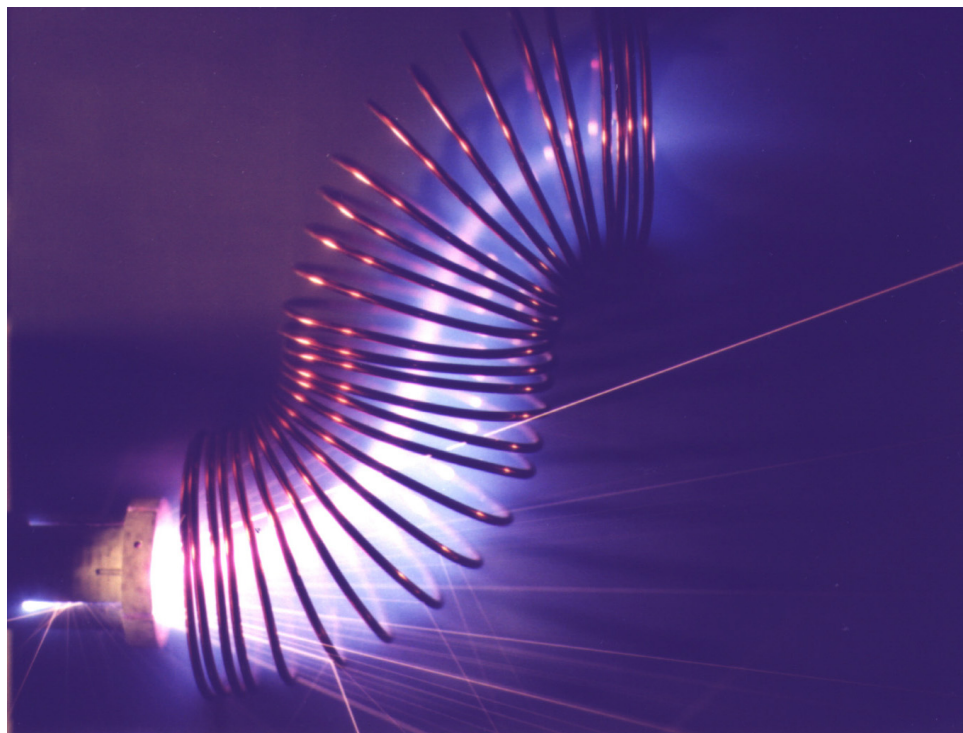
Figure 3.4. Open-walled S-duct filter in operation [103].
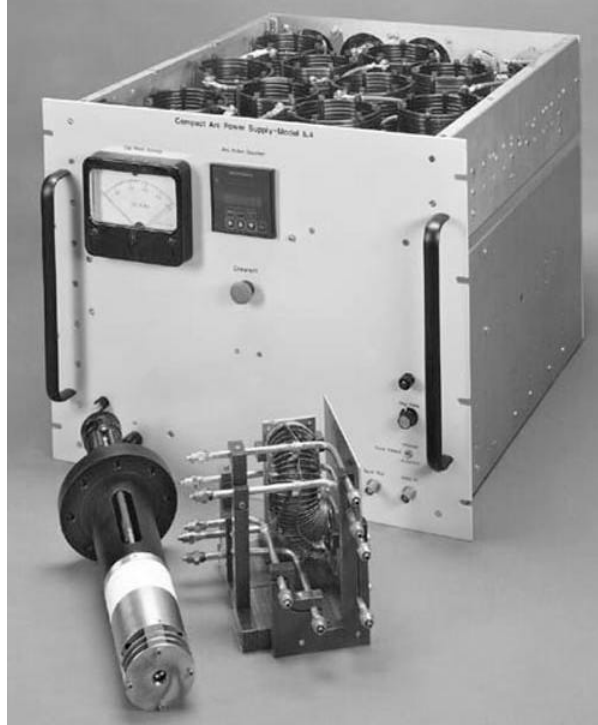
Figure 3.5. Fourth generation macroparticle filter: the twist filter [27].
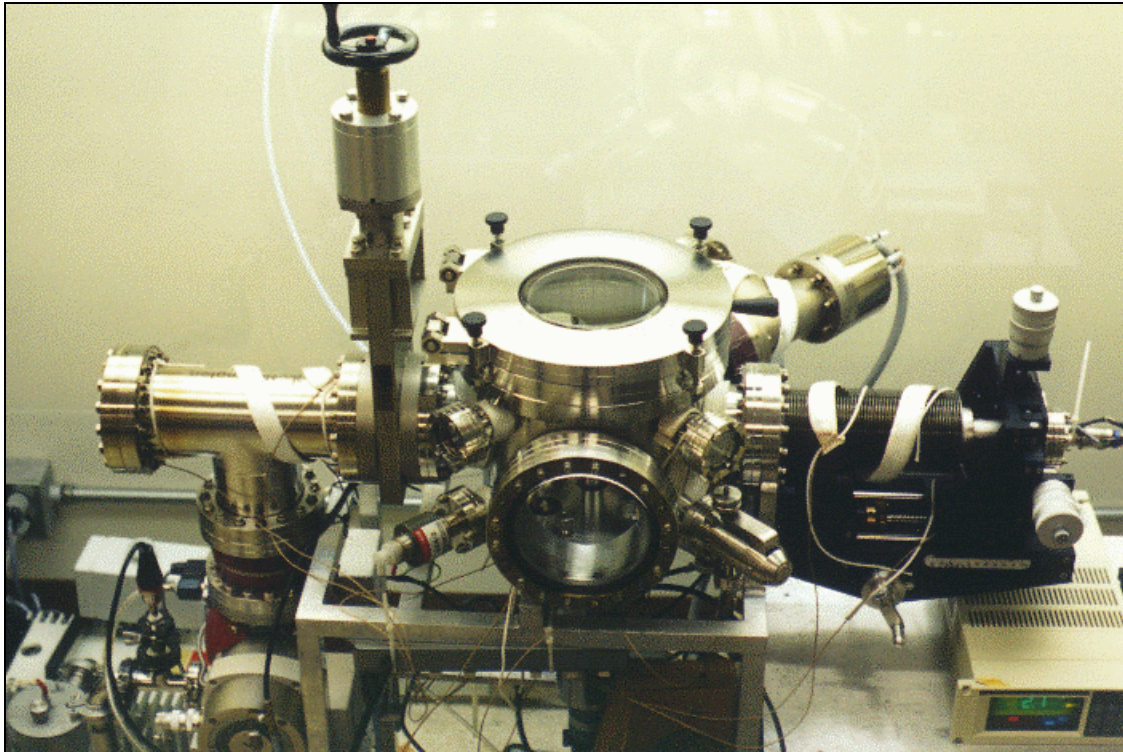
Figure 3.6. Ultra High Vacuum (UHV) tribochamber.

(a)   (b)
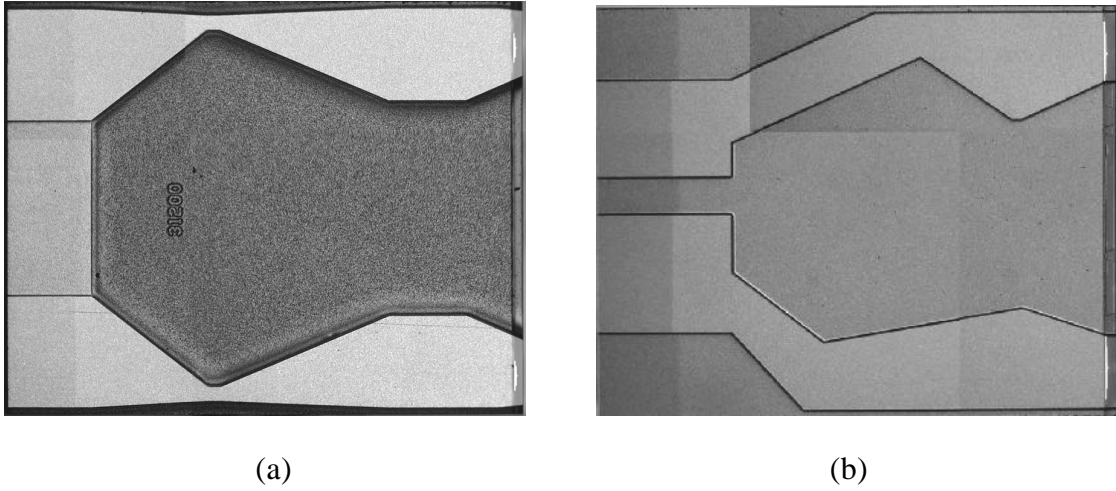
Figure 3.7. 50% slider air bearing surfaces.
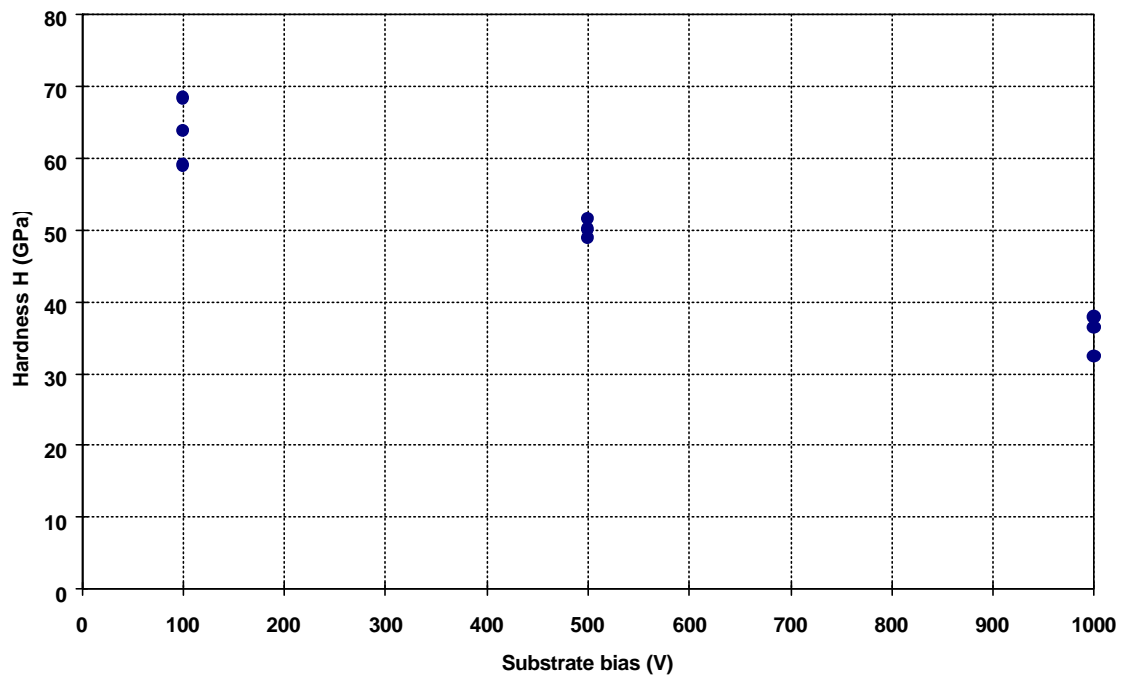
Figure 3.8. Plot of hardness H vs. substrate bias during deposition.
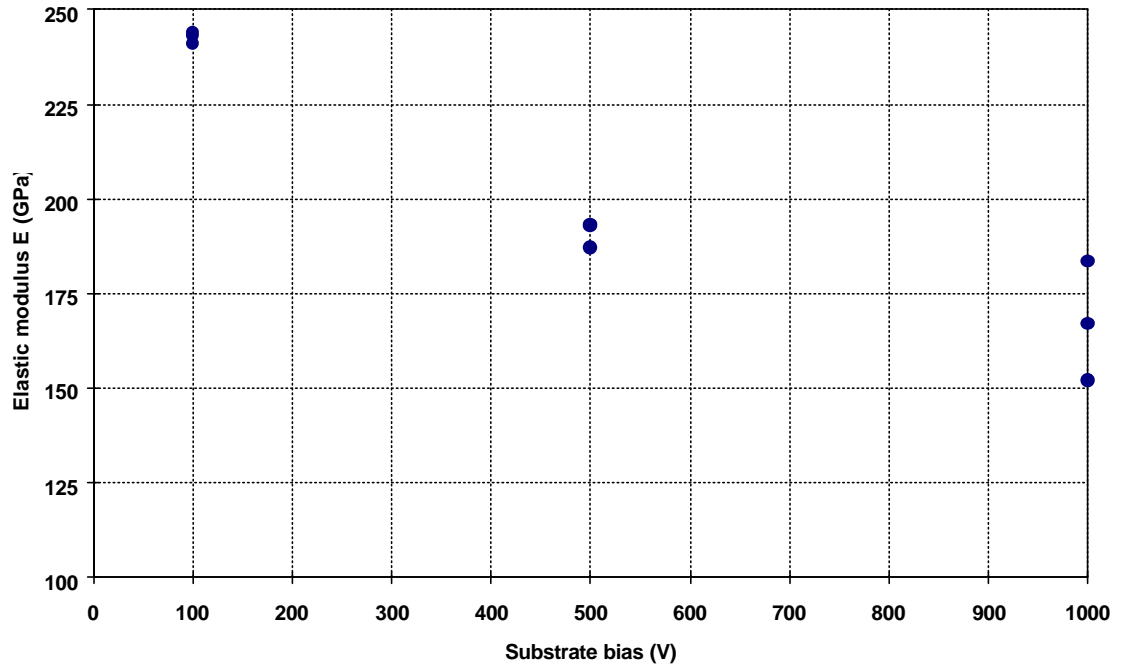
Figure 3.9. Plot of elastic modulus E vs. substrate bias during deposition.
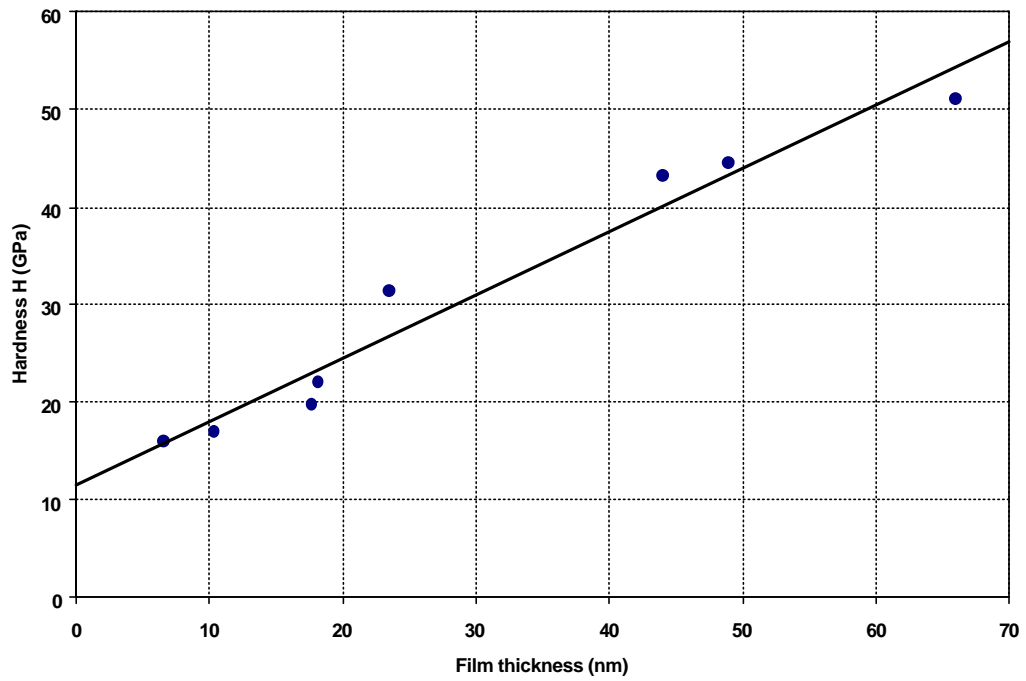
Figure 3.10. Plot of hardness H vs. film thickness.
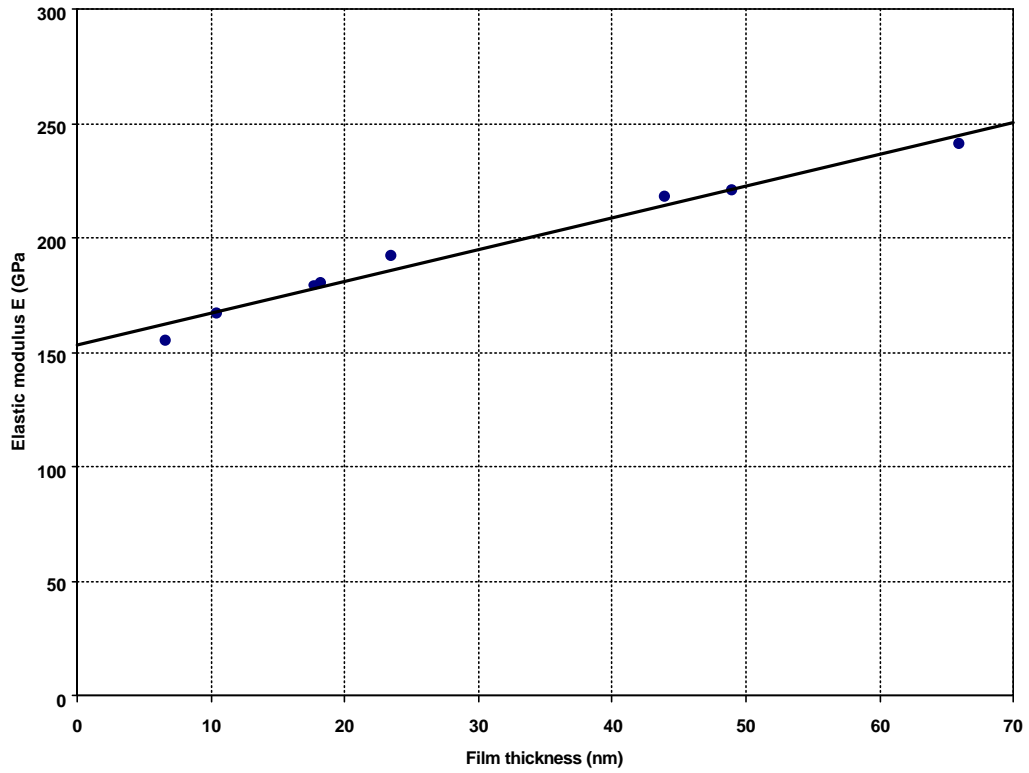
Figure 3.11. Plot of elastic modulus E vs. film thickness.
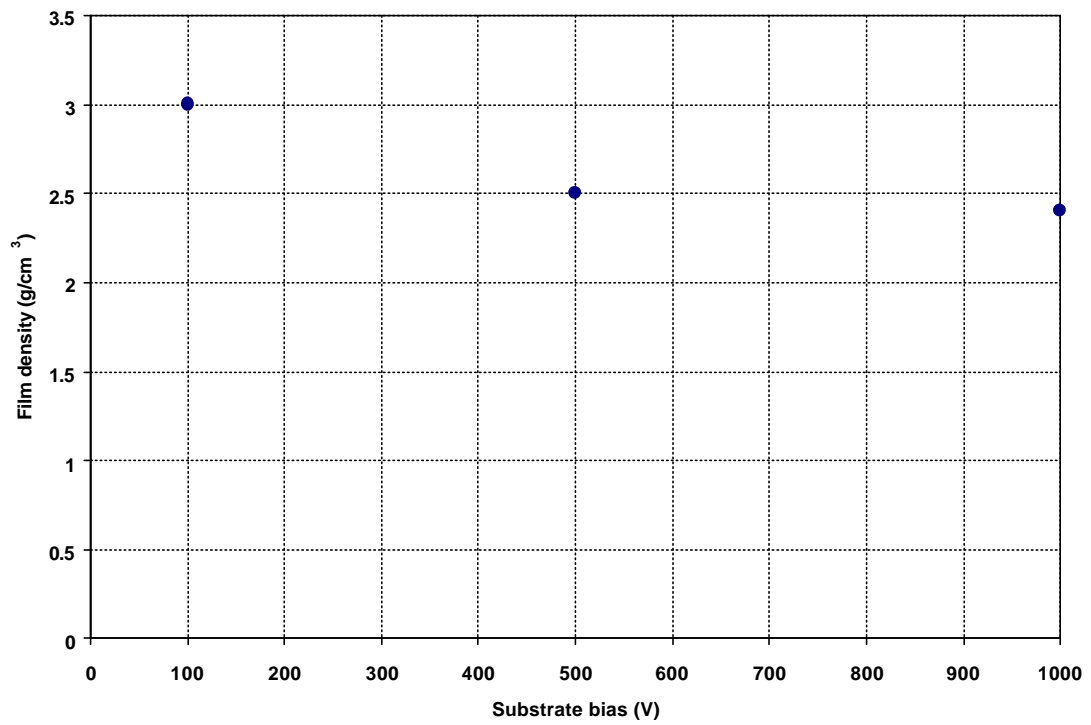
Figure 3.12. Film density vs. substrate bias during deposition.
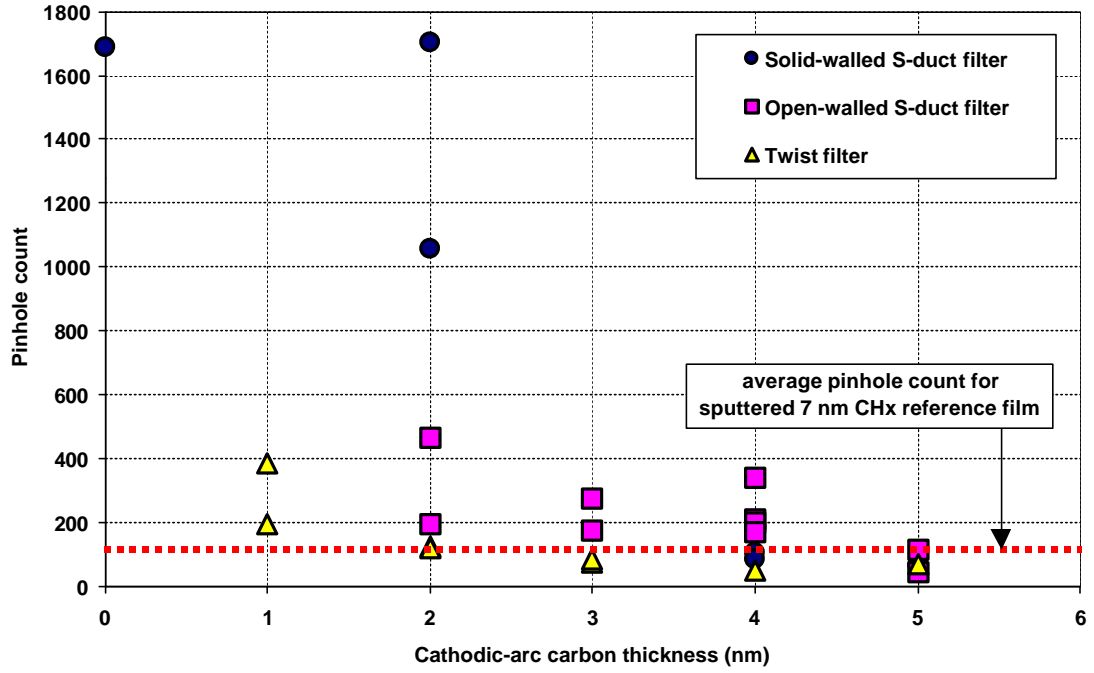
Figure 3.13. Corrosion pit count vs. film thickness.
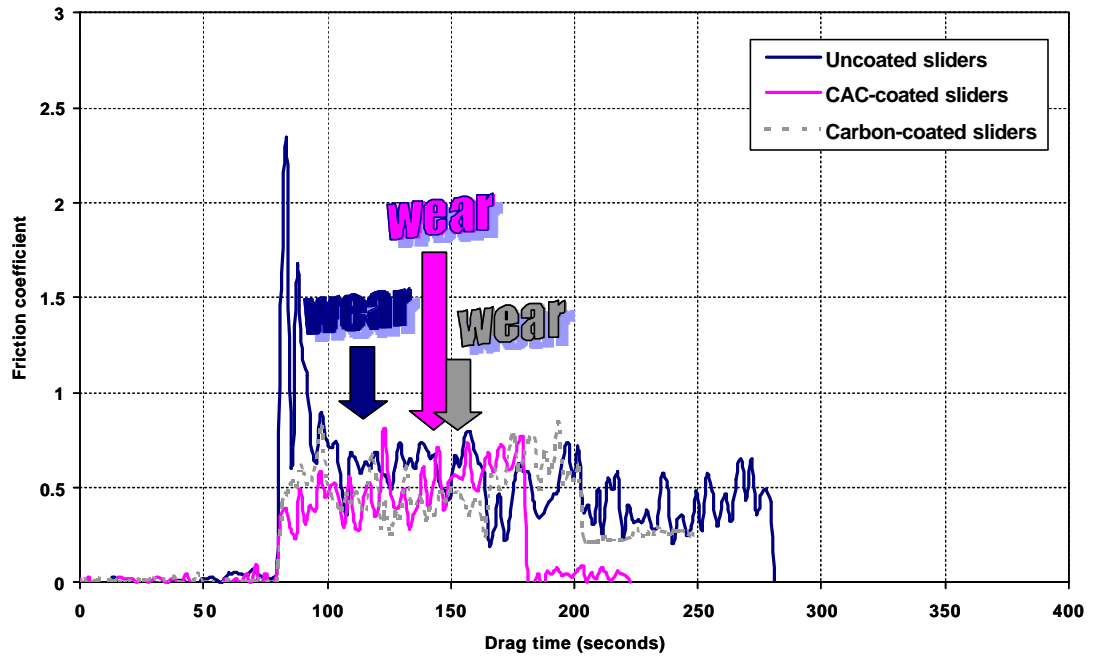
Figure 3.14. Friction coefficient vs. drag time for 5 nm CAC disk lubricated with ZDOL.
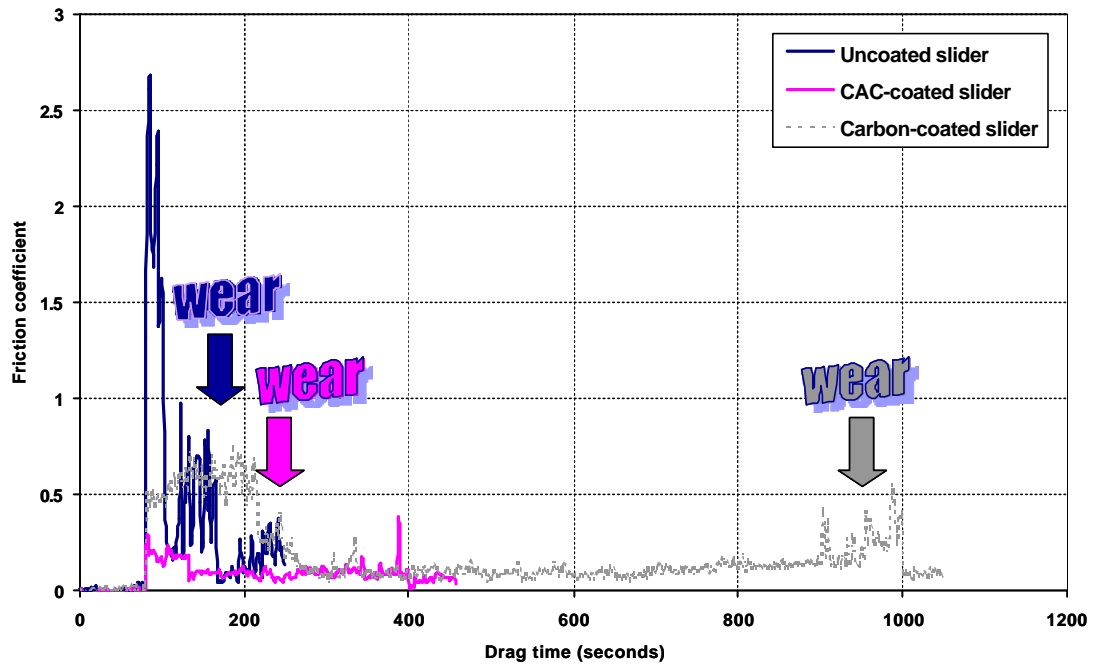
Figure 3.15. Friction coefficient vs. drag time for 5 nm CH_x disk lubricated with ZDOL.
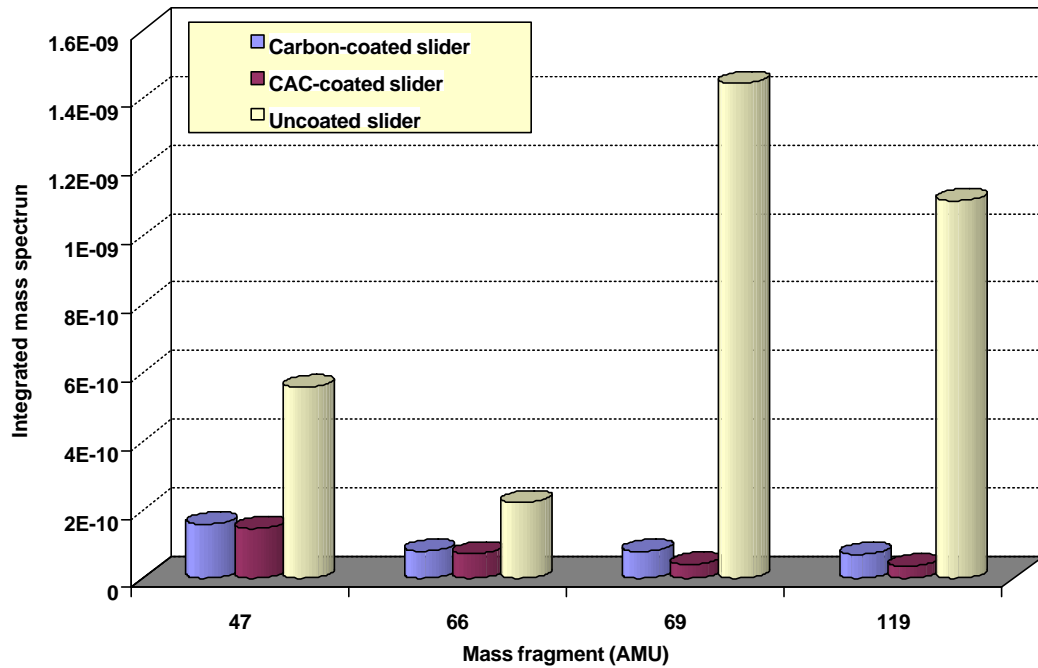
Figure 3.16. Integrated mass spectrum for drag tests with 5 nm CH_x disk.

93
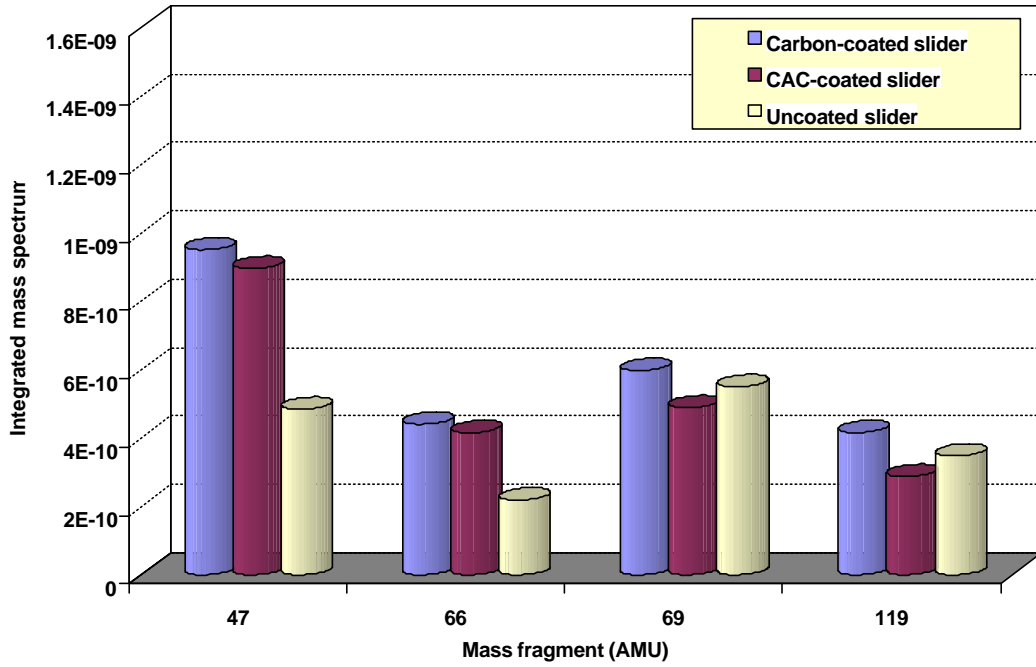
Figure 3.17. Integrated mass spectrum for drag tests with 5 nm CAC disk.
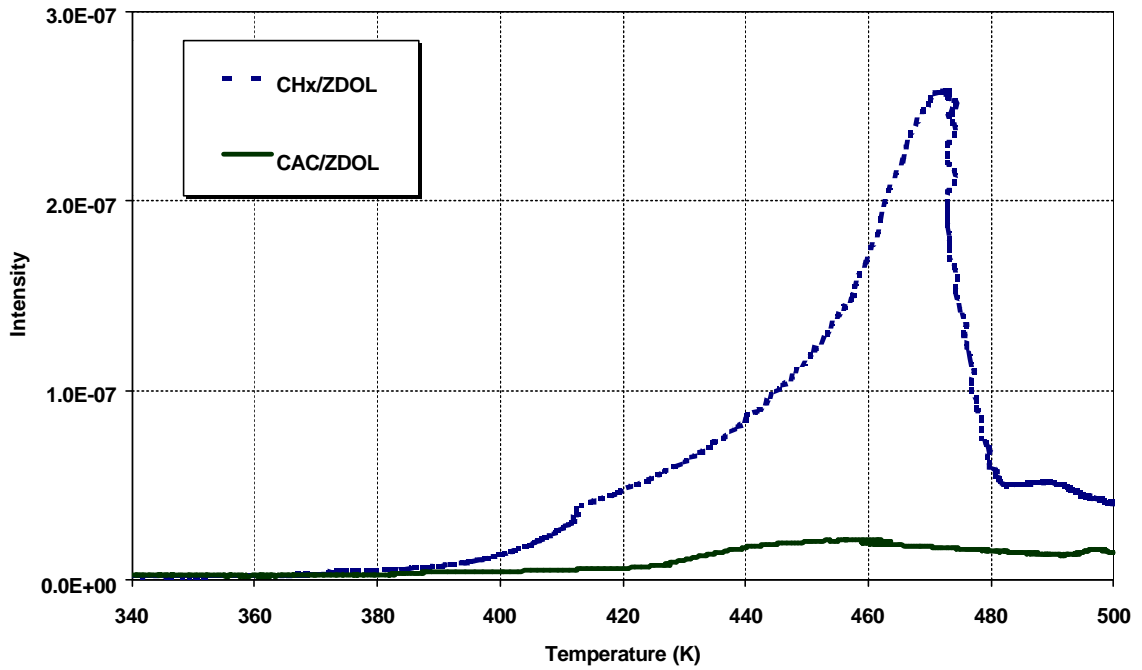
Figure 3.18. Thermal desorption profile for H_2.
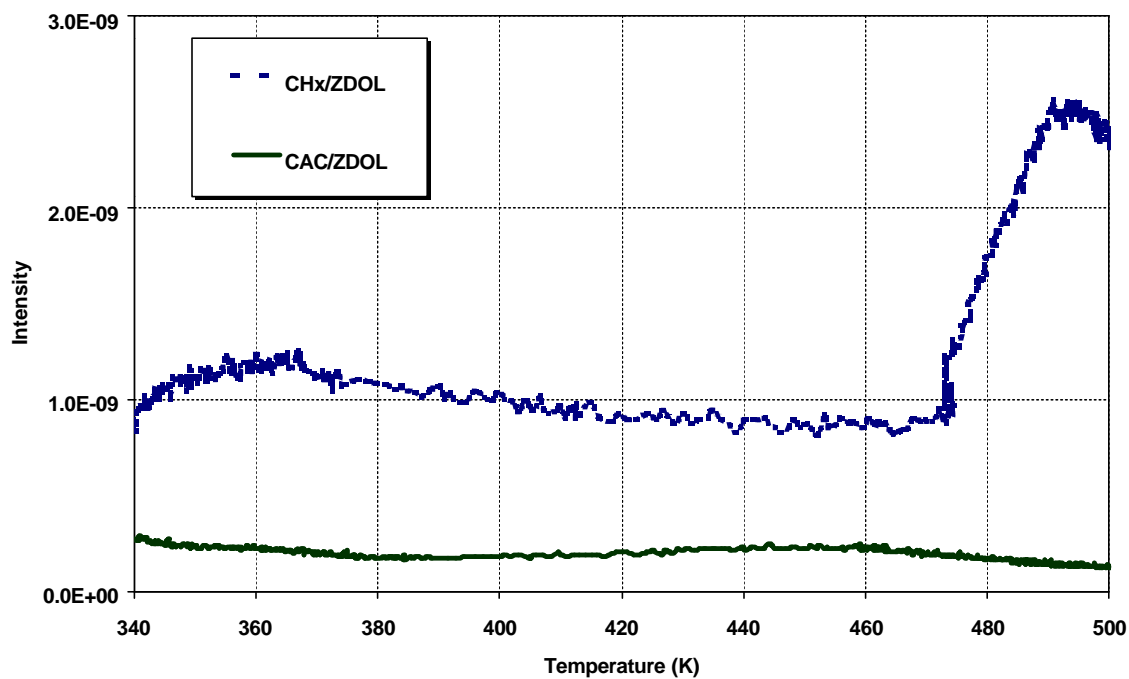
Figure 3.19. Thermal desorption profile for F.
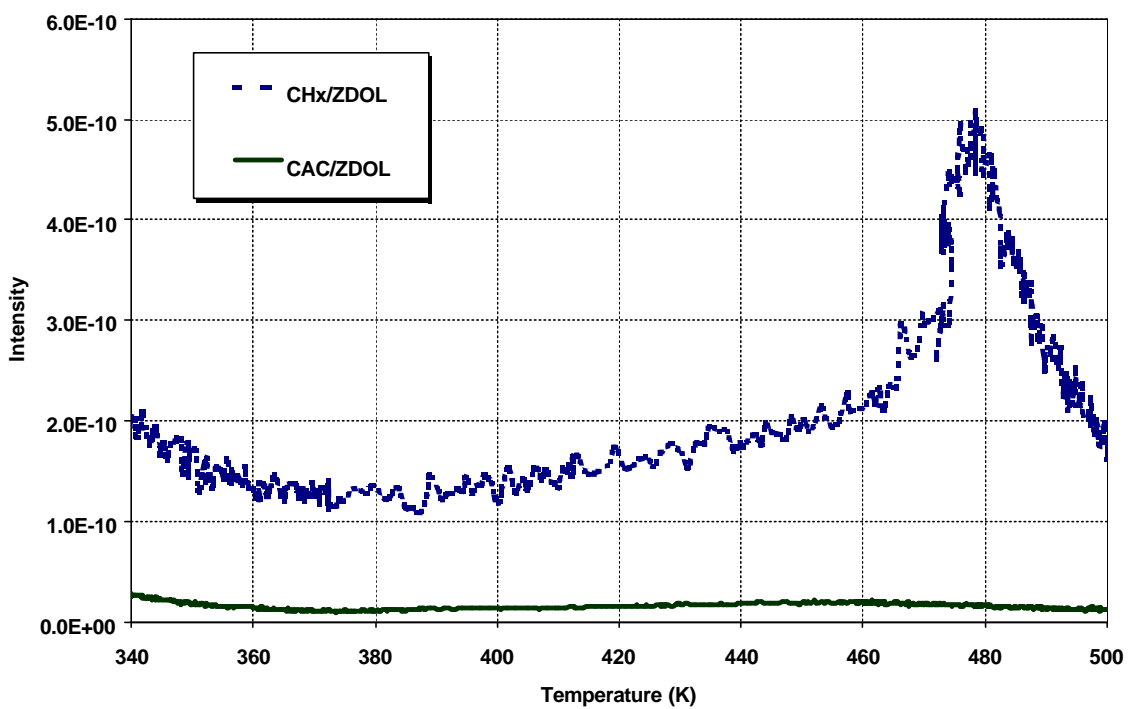
Figure 3.20. Thermal desorption profile for HF.
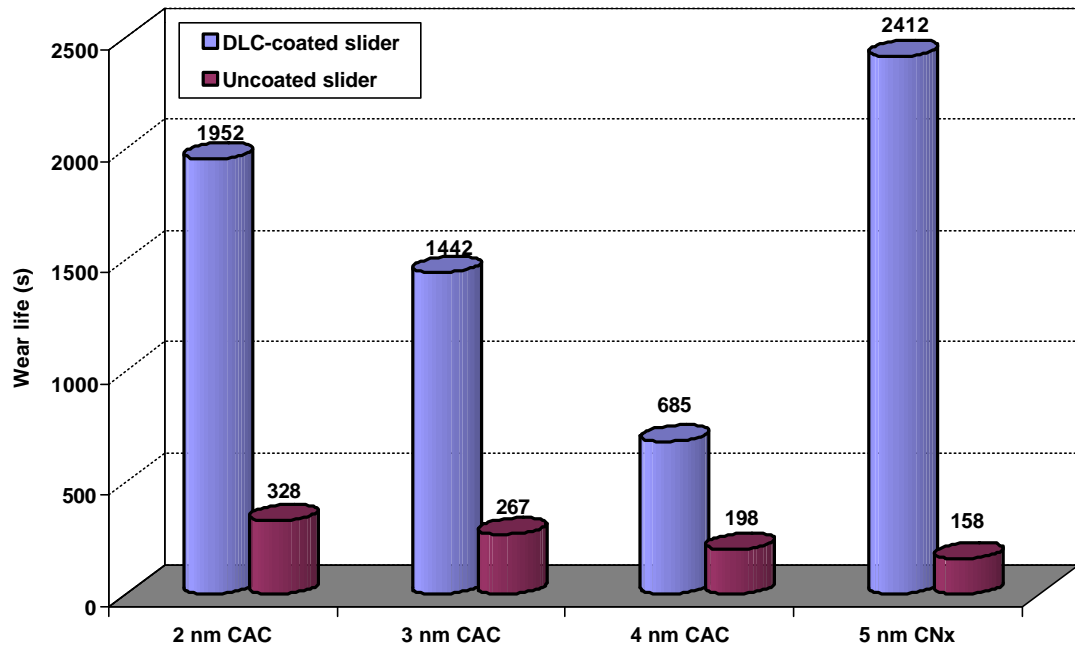
Figure 3.21. Wear life vs. carbon overcoat thickness for tests with DLC-coated and uncoated sliders.
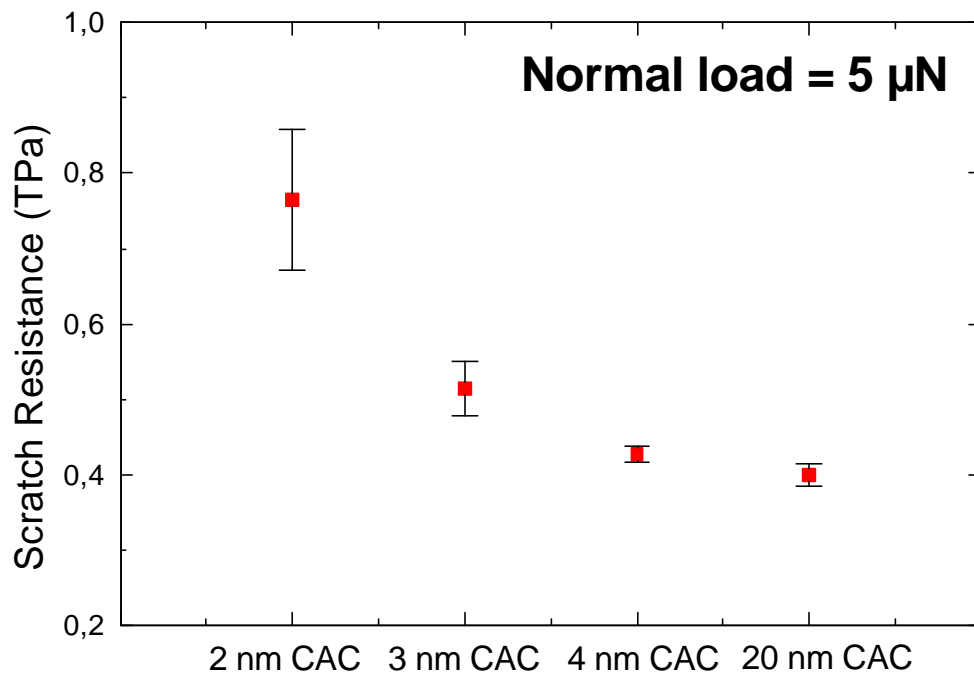
Figure 3.22. Nano-scratch resistance vs. CAC film thickness [125].
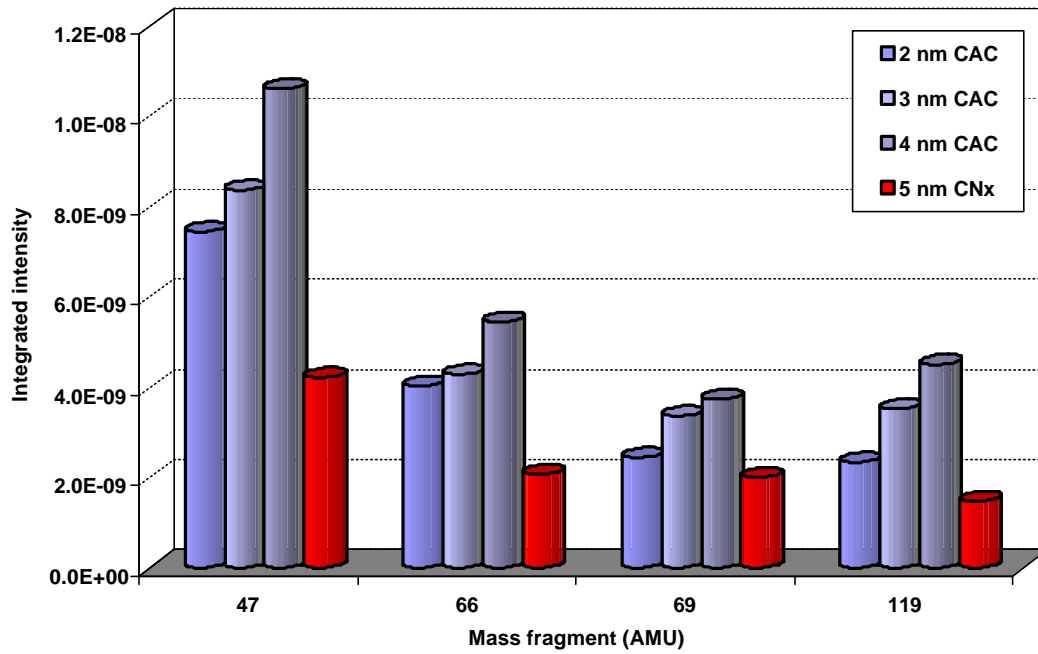
Figure 3.23. Integrated mass spectrum for drag tests with DLC-coated sliders.
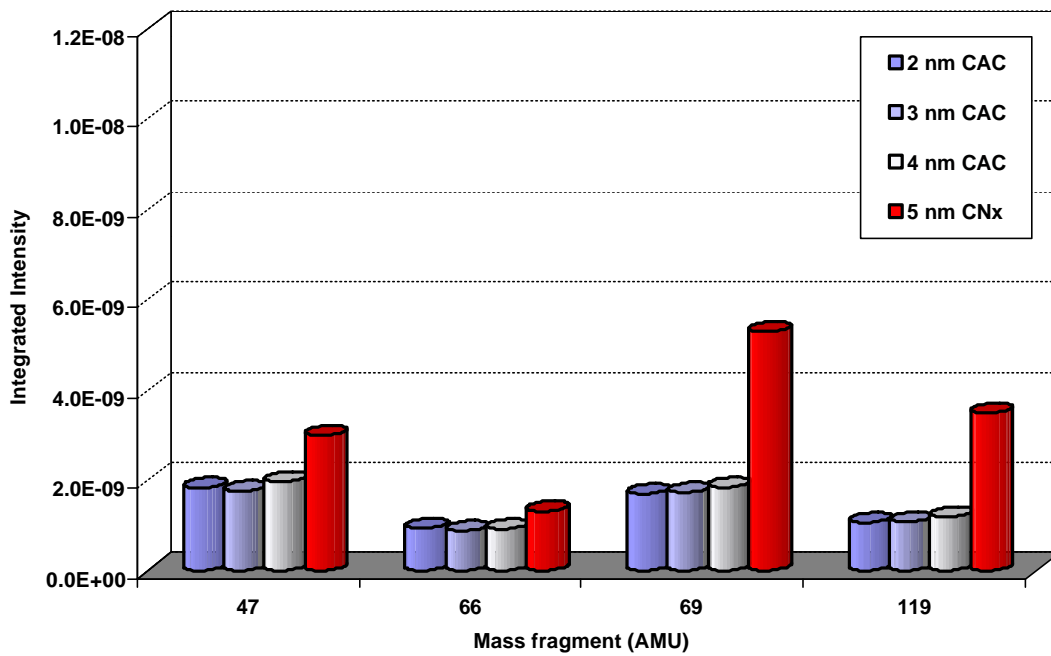
Figure 3.24. Integrated mass spectrum for drag tests with uncoated sliders.

CHAPTER 4

SUMMARY AND CONCLUSION

As the demand for increased areal densities in disk drive products continues to grow to 100 Gb/in^2 and further to 1 Tb/in^2, new technologies will be needed to decrease the magnetic spacing between the head and disk. On the slider side, lower flying height slider designs will be implemented, eventually evolving into pseudo-contact and contact designs. On the media side, protective carbon overcoats and lubricant layers will become thinner. All these developments insure more frequent and intimate contact between the head and disk surfaces and place extraordinary demands on the reliability of the head-disk interface. The tribology of the HDI, in addition to the tribochemistry, becomes critical in the selection of carbon overcoats to reduce friction, wear, lubricant migration, and lubricant decomposition. Understanding the mechanical and chemical properties of the carbon films will allow engineers and scientists to develop ultra-thin protective overcoats that are compatible with the lubricant layer for a tribologically-robust system for this application.

In this dissertation, the research focus is on amorphous carbon films deposited by RF-sputtered and filtered cathodic-arc methods. RF-sputtered, nitrogenated carbon (CN_x) films are currently used as protective overcoats on disk media at thicknesses greater than 10 nm and this research provides a picture of the mechanical and chemical behavior that occurs at the HDI to extend its use for ultra-thin applications. In Chapter 2, we utilized the ultra-high vacuum tribochamber to understand the effects of nitrogen content, a

simple variable in the deposition process, in the carbon film on wear durability in drag tests. A battery of characterization techniques was used to measure the material properties of the overcoat and its interaction with the lubricant layer. It is found that increasing the nitrogen content in the carbon films changes several properties of the overcoat: (1) it increases the wear resistance of the CN_x overcoat due to an increase in the sp^3/sp^2 ratio, (2) it decreases the surface mobility of ZDOL due to an increased dangling bond density in the carbon film, and (3) it decreases the catalytic decomposition of ZDOL in the presence of Al_2O_3 slider material. An insight into the catalytic decomposition process is also presented, which explains the role of hydrogen and nitrogen in carbon films in this phenomenon.

From these results, an optimal design point for ultra-thin CN_x overcoats with this sputtering process would be located at higher nitrogen contents, where the resulting film addresses some of the foreseeable requirements of the HDI - the need for improved wear durability due to increased slider-disk contacts from lower flying height slider designs and a reduction of the lubricant's inevitable catalytic decomposition due to exposure of the Al_2O_3 slider material with thinner carbon films on the ABS, either worn-away during normal operation or incomplete in its coverage initially. In addition, the reduced surface mobility of the ZDOL molecule counteracts the lubricant spin-off that plagues server drives with high spindle speeds (needed for fast access times to data) in continuous operation. Some mobility of the lubricant layer is needed though to insure adequate repair of areas where the lubricant is removed due to slider-disk contacts and a compromise must be carefully made by choosing a nitrogen content that satisfies these two competing

requirements. Finally, the potential to fail at providing adequate corrosion protection of the magnetic layer still exists, but recent results by other researchers have suggested that success with 1 nm CN_x overcoats may be found in this respect by varying other aspects of the deposition process, which may be incorporated easily into our sputtering conditions without changing the film's existing properties.

As an alternative to RF-sputtered CN_x and CH_x films, we also explored the use of cathodic-arc carbon films in Chapter 3 because they offer the promise of dense films for corrosion protection of the magnetic layer and easily tuned material properties during room temperature deposition. In the characterization of these films, it is found that the most diamond-like properties (hardness, elastic modulus, density) occur at ion energies of 120 eV and that there is a correlation between film thickness and hardness/elastic modulus. The CAC films significantly outperformed the CH_x films in corrosion protection and provided continuous coverage at a film thickness of 2 nm. In ultra-high vacuum drag tests, the 5 nm CAC overcoats prevented the catalytic decomposition of ZDOL lubricant in the presence of Al_2O_3 slider material, but did not outperform the CH_x overcoats in terms of wear durability. By optimizing the deposition parameters for wear durability, 2 nm CAC overcoats on disk media demonstrated performance in drag tests close to 5 nm CN_x films.

These CAC films also fulfill the needs outlined above for HDI requirements – good wear durability, excellent corrosion protection, and reduced catalytic decomposition of ZDOL lubricant in the presence of Al_2O_3 – all demonstrated on 2 nm overcoats. However, we

have yet to confirm if the optimized wear durability films offer the same excellent corrosion protection as our room temperature deposited-films. If not, future work leading to the successful incorporation of these two properties will produce an amazingly robust overcoat for this application.

Based on the research presented, careful selection of the deposition parameters of RF-sputtered CN_x and CAC overcoats is required to provide good mechanical performance AND chemical properties that are compatible with the lubricant layer and beneficial to the overall tribology and tribochemistry at the head-disk interface. We conclude that both of these carbon overcoats are suitable contenders for this role – once optimized, either one would be an excellent candidate for future ultra-thin overcoats in disk drive applications.

REFERENCES

[1]   Daniel, E. D., Mee, C. D., and Clark, M. H., *Magnetic Recording The First 100 Years*. New Jersey: IEEE Press, 1999.

[2]   Jorgensen, F., *The Complete Handbook of Magnetic Recording*. United States of America: McGraw-Hill, 1996.

[3]   Mee, C. D. and Daniel E. D., *Magnetic Recording Handbook: Technology & Applications*. United States of America: McGraw-Hill, 1990.

[4]   Western Digital Corporation website, http://www.wdc.com/company/branding/digitalphotos.asp.

[5]   IBM website, http://www.almaden.ibm.com/sst.

[6]   Fujitsu Limited website, http://hdd.fujitsu.com/global/drive/mam3xxx/catalog.html.

[7]   Seagate website, http://www.seagate.com/cda/newsinfo/newsroom/releases/article/0,1121,1305,00.html.

[8]   Wallace, R. L., "The Reproduction of Magnetically Recorded Signals," *Bell Syst. Tech. J.*, Vol. 30, 1951, p. 1145.

[9]   Thornton, B. H., Bogy, D. B., and Bhatia, C. S., "NSIC 7 nm Slider Design: Flyability/Flying-Height Modulation," National Storage Industry Consortium Annual Meeting, Monterey, CA, June 2001.

[10]   Wood, R., "EHDR Joint Session Summary of Strategy Team Results", National Storage Industry Consortium Spring Meeting, Tucson, AZ, March 12-13, 2002.

[11]   Zeng, Q. H. and Bogy, D.B., "Effects of certain design parameters on load/unload performance," *IEEE Transactions on Magnetics*, Vol. 36, No. 1, Pt.1, January 2000, pp.140-147.

[12]   Ranjan, R., Lambeth, D. N., Tromel, M., Goglia, P., and Li, Y., "Laser texturing for low-flying-height media," *Journal of Applied Physics*, Vol. 69, No. 8, Pt. 2B, April 1991, pp.5745-5747.

[13]   Yamamoto, T., Yokohata, T., and Kasamatsu, Y., "Stiction free slider for lightly textured disks," *IEEE Transactions on Magnetics*, Vol. 34, No. 4, Pt. 1, July 1998, pp.1753-1755.

[14] Yong Hu, "Design and analysis of slider's landing pads for fast take-off performance in magnetic hard disk drives," *Journal of Tribology*, Vol. 121, No. 4, October 1999, pp.955-960.

[15] Coughlin, T. and Wald, D., "SANs/SSPs Drive Storage Demand," *DATA Storage*, February 2001.

[16] Grochowski, E., "IBM Leadership in Disk Storage Technology," http://www.almaden.com/sst/html/leadership/g02.htm.

[17] Mee, C. and Daniel, E., *Magnetic Recording*. United States of America: McGraw-Hill, Inc, 1987.

[18] Bhatia, C. S., Polycarpou, A. A., and Menon, A, *Forward of Proceedings of the Symposium on Interface Tribology Towards 100 Gb/in^2 and Beyond*, ASME Trib-Vol. 10, Seattle, WA, Oct. 2000, p. iii.

[19] Wood, R., "The Feasibility of Magnetic Recording at 1 Terabit per Square Inch," *IEEE Transactions on Magnetics*, Vol. 36, No. 1, January 2000, pp. 36-42.

[20] Tsai, H. and Bogy, D. B., "Characterization of Diamondlike Carbon Films and Their Application as Overcoats on Thin-film Media for Magnetic Recording," *J. Vac. Sci. Technol. A*, Vol. 5, No. 6, November/December 1987, pp. 3287-3312.

[21] Huang, L., Hung, Y., and Chang, S., "Structure of Nitrogenated Carbon Overcoats on Thin-Film Hard Disks," *IEEE Transactions on Magnetics*, Vol. 33, No. 6, November 1997, pp. 4551-4559.

[22] Sivertsen, J. M., Wang, G., Chen, G., and Judy, J., "Evaluation of Amorphous Diamond-Like Carbon-Nitrogen Films as Wear Protective Coatings on Thin Film Media and Thin Film Head Sliders," *IEEE Transactions on Magnetics*, Vol. 33., No. 1, January 1997, pp. 926-931.

[23] Bhushan, B., "Chemical, Mechanical and Tribological Characterization of Ultra-thin and Hard Amorphous Carbon Coatings as Thin as 3.5 nm: Recent Developments," *Diamond and Related Materials*, Vol. 8, 1999, pp. 1985-2015.

[24] Akita, N., Konishi, Y., Ogura, S., Imamura, M., Hu, Y. H., and Shi, X., "Comparison of deposition methods for ultra thin DLC overcoat film for MR head," *Diamond and Related Materials*, Vol. 10, 2001, pp. 1017-1023.

[25] Druz, B., Zaritskiy, I., Hoehn, J., Polyakov, V. I., Rukovishnikov, A. I., and Novotny, V., "Direct ion beam deposition of hard (>30 GPa) diamond-like films from RF inductively coupled plasma source," *Diamond and Related Materials*, Vol. 10, 2001, pp. 931-936.

[26]   Fong, W., *Fabrication and evaluation of 5 nm cathodic-arc carbon films for disk drive applications*, M.S. Project Report, University of California, Berkeley, CA, October 1999.

[27]   Anders, A., Fong, W., Kulkarni, A., Ryan, F., and Bhatia, C. S., "Ultrathin Diamond-like Carbon Films Deposited by Filtered Cathodic Arcs," accepted for publication in *IEEE Transactions on Plasma Sciences*, Vol. 29, No. 5, 2001.

[28]   Anders, S., Bhatia, C. S., Fong, W., Lo, R., Bogy, D. B., "Application of cathodic-arc deposited amorphous hard carbon films to the head/disk tribology," Materials Research Society Symposium Proceedings, High-Density Magnetic Recording and Integrated Magneto-Optics: Materials and Devices, Vol. 517, 1998, pp. 371-382.

[29]   Thornton, B. H., Nayak, A., and Bogy, D. B., "Flying Height Modulation Due to Disk Waviness of Sub-5nm Flying Height Air Bearing Sliders," *Journal of Tribology*, accepted for publication.

[30]   Marchon, B., Vo, P. N., Khan, M. R., and Ager III, J. W., "Structure and Mechanical Properties of Hydrogenated Carbon Films Prepared by Magnetron Sputtering," *IEEE Transactions on Magnetics*, Vol. 27, No. 6, November 1991, pp. 5160-5162.

[31]   Lee, H. J., Zubeck, R., Hollars, D., Lee, J. K., Smallen, M., and Chao, A., "Material Properties and Tribological Performance of Hydrogenated Sputter Carbon Overcoat on Rigid Disk," *J. Vac. Sci. Technol. A.*, Vol. 11, No. 6, November/December 1993, pp. 3007-3013.

[32]   Lee, J. K., Smallen, M., Enguero, J., Lee, H. J., and Chao, A., "The Effect of Chemical and Surface Properties of Hydrogenated Carbon Overcoats on the Tribological Performance of Rigid Magnetic Disks," *IEEE Transactions on Magnetics*, Vol. 29, No. 1, January 1993, pp. 276-281.

[33]   Lal, B. B., Yang, M., Chao, J., and Russak, M. A., "Asymmetric DC-Magnetron Sputtered Carbon-Nitrogen Thin-Film Overcoat for Rigid-Disk Applications," *IEEE Transactions on Magnetics*, Vol. 32., No. 5, September 1996, pp. 3774-3776.

[34]   Cutiongco, E. C., Li, D., Chung, Y. W., and Bhatia, C. S., "Tribological Behavior of Amorphous Carbon Nitride Overcoats for Thin-Film Rigid Disks," *Journal of Tribology*, Vol. 118, July 1996, pp. 543-548.

[35]   Wang, R. H., Meeks, S. W., White, R. L., Weresin, W. E., "The Effect of Hydrogen in Carbon Overcoats on the Tribology of the Head-Disk Interface," *IEEE Transactions on Magnetics*, Vol. 31, No. 6, November 1995, pp. 2919-2921.

[36]   Agarwal, S., Li, E., and Heiman, N., "Structure and Tribological Performance of Carbon Overlayer Films," *IEEE Transactions on Magnetics*, Vol. 29, No. 1, January 1993, pp. 264-269.

[37]   White, R., Bhatia, S. S., Meeks, S., Friedenberg, M., and Mate, C. M., "RF-Sputtered Amorphous CNx for Contact Recording Applications," Tribology of Contact/Near-Contact Recording for Ultra High Density Magnetic Storage (TRIB-Vol.6), Proceedings of 1996 ASME/STLE International Tribology Conference and Exposition, San Francisco, CA, USA, October 13-18, 1996, p.33-38.

[38]   Bhushan, B. and Koinkar, V. N., "Microscale Mechanical and Tribological Characterization of Hard Amorphous Carbon Coatings as Thin as 5 nm for Magnetic Disks," *Surface and Coatings Technology*, Vol. 76-77, 1995, pp. 655-669.

[39]   Broitman, E., Hellgren, N., Wänstrand, O., Johansson, M. P., Berlind, T., Sjöström, H., Sundgren, J. E., Larsson, M., and Hultman, L., "Mechanical and Tribological Properties of CN_x Films Deposited by Reactive Magnetron Sputtering," *Wear*, Vol. 248, 2001, pp. 55-64.

[40]   Lu, W. and Komvopoulos, K., "Dependence of Growth and Nanomechanical Properties of Ultrathin Amorphous Carbon Films on Radio Frequency Sputtering Conditions," *Journal of Applied Physics*, Vol. 86, No. 4, August 1999, pp. 2268-2277.

[42]   Ott, R. D., Scharf, T. W., Yang, D., and Barnard, J. A., "Tribological and Mechanical Properties of CN Ultra-Thin Overcoat Films," *IEEE Transactions on Magnetics*, Vol. 34, No. 4, July 1998, pp. 1735-1737.

[43]   Scharf, T. W., Ott, R. D., Yang, D., and Barnard, J. A., "Structural and Tribological Characterization of Protective Amorphous Diamond-like Carbon and Amorphous CN*x* Overcoats for Next Generation Hard Disks," *Journal of Applied Physics*, Vol. 85, No. 6, March 199, pp. 3142-3154.

[44]   Wienss, A., Neuhäuser, M., Schneider, H. H., Persch-Schuy, G., Windeln, J., Witke, T., and Hartmann, U., "Mechanical Properties of D.C. Magnetron-Sputtered and Pulsed Vacuum Arc Deposited Ultra-Thin Nitrogenated Carbon Coatings," *Diamond and Related Materials*, Vol. 10, 2001, pp. 1024-1029.

[45]   Chia, R. W. J., Wang, C. W., Lee, J. J. K., and Tang, W. T., "Overview of corrosion on thin film magnetic media and its implication on head disk interface," *Proceedings of the Fifth International Symposium on Magnetic Materials, Processes, and Devices Applications to Storage and Microelectromechanical*

Systems (MEMS), Boston, MA, Nov. 1-6, 1998. Pennington, New Jersey: Electrochem. Soc, 1999, pp. 255-68.

[46]   Sjöstrom, H., Hultman, L, Sundgren, J. E., Hainsworth, S. V., Page, T. F., and Theunissen, G. S. A. M., "Structural and Mechanical Properties of Carbon Nitride CNx (0.2≤x≤0.35) Films," *J. Vac. Sci. Technol. A*, Vol. 14, No. 1, January/February 1996, pp. 56-62.

[47]   Hellgren, N., *Sputtered Carbon Nitride Thin Films*, Linköping Studies in Science and Technology, Dissertation No. 604, Linköping University, Sweden 1999.

[48]   Guruz, M. U., Dravid, V. P., Chung, Y. W., Lacerda, M. M., Bhatia, C. S., Yu, Y. H., and Lee, S. C., "Corrosion Performance of Ultrathin Carbon Nitride Overcoats Synthesized by Magnetron Sputtering," *Thin Solid Films*, Vol. 381, 2001, pp. 6-9.

[49]   Li, D., Guruz, M. U., and Chung, Y. W., "Ultrathin CN_x Overcoats for 1 Tb/in^2 Hard Disk Drive Systems," submitted for publication.

[50]   Bhatia, C. S., Fong, W., Chen, C. Y., Wei, J., Bogy, D. B., Anders, S., Stammler, T., Stöhr, J., "Tribo-chemistry at the Head/Disk Interface," *IEEE Transactions on Magnetics*, Vol. 35, No. 2, Part 1, March 1999, pp. 910-915.

[51]   Kasai, P. H., Tang, W. T., Wheeler, P., "Degradation of Perflouropolyethers Catalyzed by Aluminum Oxide," *Applied Surface Science*, Vol. 51, September 1991, pp. 201-211.

[52]   Yun, X., Bogy, D. B., and Bhatia, C. S., "Wear of Hydrogenated Carbon Coated Disks by Carbon Coated and Uncoated Al_2O_3/TiC Sliders in Ultra High Vacuum," *IEEE Transactions on Magnetics*, Vol.32, No.5, Pt.1, September 1996, pp. 3669-3671.

[53]   Chen, C. Y., *Tribochemistry of the Decomposition Mechanisms of Perfluoropolyether Lubricants at the Head-Disk Interface of Hard Disk Drives in UHV*, Ph.D. Dissertation, University of California, Berkeley, CA, Fall 1999.

[54]   Wang, R. H., White, R. L., Meeks, S. W., Min, B. G., Kellock, A., Homola, A., Yoon D., "The Interaction of Perfluoro-Polyether Lubricant with Hydrogenated Carbon," *IEEE Transactions on Magnetics*, Vol. 32, No. 5, September 1996, pp. 3777-3779.

[55]   Ruhe, J., Novotny, V., Clarke, T., and Street, G. B., "Ultrathin Perfluoropolyether Films – Influence of Anchoring and Mobility of Polymers on the Tribological Properties," *Journal of Tribology*, Vol. 118, July 1996, pp. 663-668.

[56]   Ma, X., Gui, J., Grannen, K. J., Smoliar, L. A., Marchon, B., Jhon, M. S., and Bauer, C. L., "Spreading of PFPE lubricants on carbon surfaces: effect of hydrogen and nitrogen content," *Tribology Letters*, Vol. 6, 1999, pp. 9-14.

[57]   Pacansky, J., Waltman, R. J., and Pacansky, G., "Electron Beam Induced Degradation of Poly(perfluoropolyethers) and Poly(olefin sulfones)," *Chem. Mater.*, Vol. 5, 1993, pp. 1526-1532.

[58]   Lin, J. L., Bhatia, C. S., Yates, Jr., J. T., "Thermal and Electron-stimulated Chemistry of Fomblin-Zdol Lubricant on a Magnetic Disk," *J. Vac. Sci. Technol. A*, Vol. 13, No. 2, March/April 1995, pp. 163-168.

[59]   Pit, R., Marchon, B., Meeks, S., and Velidandla, V., "Formation of Lubricant "Moguls" at the Head/Disk Interface," *Tribology Letters*, Vol. 10, No. 3, 2001, pp. 133-142.

[60]   Wang, R. H., Meeks, S. W., White, R. L., and Weresin, W. E., "The Effect of Hydrogen in Carbon Overcoats on the Tribology of the Head-disk Interface," *IEEE Transactions on Magnetics*, Vol. 31, No. 6, Pt. 1, November 1995, pp.2919-2921.

[61]   Waltman, R. J., Pocker, D. J., Tyndall, G. W., "Studies on the Interactions Between ZDOL Perflouropolyether Lubricant and the Carbon Overcoat of Rigid Magnetic Media," *Tribology Letters*, Vol. 4, 1998, pp. 267-275.

[62]   Waltman, R. J., Tyndall, G. W., Pacansky, J., Berry, R. J., "Impact of Polymer Structure and Confinement on the Kinetics of Zdol 4000 Bonding to Amorphous-hydrogenated Carbon," *Tribology Letters*, Vol. 7, 1999, pp. 91-102.

[63]   Waltman, R. J., "Experimental and Theoretical Investigation of the Effect of Lubricant Structure on the Bonding Kinetics of Perfluoroalkylethers on CH_x Amorphous Hydrogenated Carbon," *Chem. Mater.*, Vol. 12, 2000, pp. 2039-2049.

[64]   Waltman, R. J., "Computer-modeling Study of the Interactions of Zdol with Amorphous Carbon Surfaces," *Langmuir*, Vol. 15, 1999, pp. 6470-6483.

[65]   Kasai, P. H. and Spool, A. M., "Z-DOL and Carbon Overcoat: Bonding Mechanism," *IEEE Transactions on Magnetics*, Vol. 37, No. 2, March 2001, pp. 929-933.

[66]   Kasai, P. H., Wass, A., and Yen, B. K., "Carbon Overcoat: Structure and Bonding of Z-DOL," *Journal of Information Storage and Processing Systems*, Vol. 1, No. 3, July 1999, pp. 245-58.

[67]   Lo, R. and Bogy, D. B., "On the Measurements of Nano-hardness and Elastic Modulus of Ultra-thin Overcoats: Effect of W-doping and Annealing on the

Properties of DLC," *Technical Report 97-017 (Blue Series)*, Computer Mechanics Laboratory, University of California, Berkeley, CA, September 1997.

[68]   Meeks, S. W., Weresin, W. E., and Rosen, H. J., "Optical Surface Analysis of the Head-Disk-Interface of Thin Film Disks," *Journal of Tribology*, Vol. 117, No. 1, January 1995, pp. 112-118.

[69]   Yun, X. H. and Bogy, D. B., *Tribochemical Study of Hydrogenated and Nitrogenated Overcoats at the Head Disk Interface in Magnetic Disk Drives*, Ph.D. Dissertation, University of California, Berkeley, CA, June 1996.

[70]   Wienss, A., Persch-Schuy, G., Hartmann, R., Joeris, P., and Hartmann, U., "Subnanometer scale tribological properties of nitrogen containing carbon coatings used in magnetic storage devices," *J. Vac. Sci. Technol. A*, Vol. 18, No. 4, Jul/Aug 2000, pp. 2023-2026.

[71]   Ma, X., Gui, J., Marchon, B., Jhon, M. S., Bauer, C. L., and Rauch, G. C., "Lubricant Replenishment on Carbon Coated Discs," *IEEE Transactions on Magnetics*, Vol. 35, No. 5, September 1999, pp. 2454-2456.

[72]   Kasai, P. H. and Spool, A. M., "Z-DOL and Carbon Overcoat: Bonding Mechanisms," *IEEE Transactions on Magnetics*, Vol. 37, No. 2, March 2001, pp. 929-933.

[73]   Yanagisawa, M., "Adsorption of Perfluoro-Polyethers on Carbon Surfaces," *Tribology and Mechanics of Magnetic Storage Systems*, Vol. IX, 1994, pp. 25-32.

[74]   Tyndall, G. W., Waltman, R. J., and Pocker, D. J., "Concerning the Interactions between Zdol Perfluoropolyether Lubricant and an Amorphous-Nitrogenated Carbon Surface," *Langmuir*, Vol. 14, 1998, pp. 7527-7536.

[75]   Paserba, K., Shukla, N., Gellman, A. J., Gui, J., and Marchon, B., "Bonding of Ethers and Alcohols to a-CN$_x$ Films," *Langmuir*, Vol. 15, 1999, pp. 1709-1715.

[76]   Cornaglia, L. and Gellman, A., "Fluoroether bonding to carbon overcoats," *Journal of Vacuum Science & Technology A*, Vol. 15, No. 5, September - October 1997, pp. 2755-2765.

[77]   Waid, D. and Ajk, Toren, "Magnetic Storage: What Does the Future Hold?," *IDEMA Insight*, May/June 1999, pp. 7 and 38.

[78]   Hsia, Y. and Donovan, M., "The Design and Tribology of Tripad Sliders for Pseudo-Contact Recording in Magnetic Hard Disk Drives," Tribology of Contact/Near-Contact Recording for Ultra High Density Magnetic Storage (TRIB-Vol.6), Proceedings of 1996 ASME/STLE International Tribology

Conference and Exposition, San Francisco, CA, USA, October 13-18, 1996, p.17-23.

[79]   Bhushan, B., *Tribology and Mechanics of Magnetic Storage Devices*, Springer, New York, 1990.

[80]   Ohring, M., *The Materials Science of Thin Films*, Academic Press, San Diego, 1992.

[81]   Robertson, J., "Deposition and Properties of Diamond-Like Carbons," to be published in *Properties and Processing of Vapor-Deposited Coatings, Proceedings of 1998 Fall Meeting of Materials Research Society Symposium*, Boston, Massachusetts, USA, November 30 - December 2, 1998, Vol. 555.

[82]   Weiler, M., Lang, K., Li, E., and Robertson, J., "Deposition of tetrahedral hydrogenated amorphous carbon using a novel electron cyclotron wave resonance reactor," *Applied Physics Letters*, Vol. 72, No. 11, March 1998, pp. 1314-1316.

[83]   Robertson, J., "Properties of Diamond-Like Carbon," *Surface and Coatings Technology*, Vol. 50, 1992, pp. 185-203.

[84]   Anders, A., "Metal Plasma Immersion Ion Implantation and Deposition: A Review," *Surface and Coatings Technology*, Vol. 93, 1997, pp. 158-167.

[85]   Anders, S., Anders, A., Brown, I., Wei, B., Komvopoulos, K., Ager III, J. W., and Yu, K. M., "Effect of Vacuum Arc Deposition Parameters on the Properties of Amorphous Carbon Thin Films," *Surface and Coatings Technology*, Vol. 68/69, 1994, pp. 388-393.

[86]   Veerasamy, V. S., Amaratunga, G. A. J., Milne, W. I., Robertson, J., and Fallon, P. J., "Influence of Carbon Ion Energy on Properties of Highly Tetrahedral Diamond-Like Carbon," *Journal of Non-Crystalline Solids*, Vol. 164-166, 1993, pp. 1111-1114.

[87]   Sanders, D., Boercker, D., and Falabella, S., "Coating Technology Based on the Vacuum Arc – A Review," *IEEE Transactions on Plasma Science*, Vol. 18, No. 16, December 1990, pp. 883-894.

[88]   Brown, I., "Vacuum Arc Ion Sources," *Rev. Sci. Instrum.*, Vol. 65, No. 10, October 1994, pp. 3061-3081.

[89]   Anders, A., Anders, S., and Brown, I., "Transport of Vacuum Arc Plasmas Through Magnetic Macroparticle Filters," *Plasma Sources Sci. Technology*, Vol. 4, 1995, pp. 1-12.

[90]   Pharr, G. M., Callahan, D. L., McAdams, S. D., Tsui, T. Y., Anders, S., Anders, A., Ager , J. W., Brown, I. G., Bhatia, C. S., Silva, S. R. P., and Robertson, J., "Hardness, Elastic Modulus, and Structure of Very Hard Carbon Films Produced by Cathodic-Arc Deposition with Substrate Pulse Biasing," *Appl. Phys. Lett.*, Vol. 68, No. 6, February 1996.

[91]   Ager III, J. W., Anders, S., Anders, A., and Brown, I., "Effect of Intrinsic Growth Stress on the Raman Spectra of Vacuum-arc-deposited Amorphous Carbon Films," *Applied Physics Letters*, Vol. 66, No. 25, June 1995, pp. 3444-3446.

[92]   Tay, B. K., Shi, X., Tan, H. S., Yang, H. S., Sun, Z., "Raman Studies of Tetrahedral Amorphous Carbon Films Deposited by Filtered Cathodic Vacuum Arc," *Surface and Coatings Technology*, Vol. 105, 1998, pp. 155-158.

[93]   Davis, C. A., Knowles, K. M., and Amaratunga, G. A. J., "Cross-sectional Structure of Tetrahedral Amorphous Carbon Thin Films," *Surface and Coatings Technology*, Vol. 76-77, 1995, pp. 316-321.

[94]   Lossy, R., Pappas, D. L., Roy, R. A., Doyle, J. P., Cuomo, J. J., and Bruley, J., "Properties of Amorphous Diamond Films Prepared by a Filtered Cathodic Arc," *J. Appl. Phys.*, Vol. 77, No. 9, May 1995, pp. 4750-4756.

[95]   Coll, B. F., Sathrum, P., Aharonov, R., and Tamor, M. A., "Diamond-like Carbon Films Synthesized by Cathodic Arc Evaporation," *Thin Solid Films*, Vol. 209, 1992, pp. 165-173.

[96]   McKenzie, D. R., Yin, Y., Marks, N. A., Davis, C. A., Pailthorpe, B. A., Amaratunga, G. A. J., Veerasamy, V. S., "Hydrogen-free Amorphous Carbon Preparation and Properties," *Diamond and Related Materials*, Vol. 3, 1994, pp. 353-360.

[97]   McKenzie, D. R., Yin, Y., Marks, N. A., Davis, C. A., Kravtchinskaia, E., Pailthorpe, B. A., Amaratunga, G. A. J., "Tetrahedral Amorphous Carbon Properties and Applications," *Journal of Non-Crystalline Solids*, Vol. 164-166, 1993, pp. 1101-1106.

[98]   McKenzie, D. R., Muller, D., and Pailthorpe, B. A., "Compressive-Stress-Induced Formation of Thin-Film Tetrahedral Amorphous Carbon," *Physical Review Letters*, Vol. 67, No. 6, August 1991, pp. 773-776.

[99]   Anders, S., Callahan, D. L., Pharr, G. M., Tsui, T. Y., Bhatia, C. S., "Multilayers of Amorphous Carbon Prepared by Cathodic Arc Deposition," *Surfaces and Coating Technology*, Vol. 94-95, No. 1-3, October 1997, pp. 189-194.

[100]   Friedmann, T. A., Sullivan, J. P., Knapp, J. A., Tallant, D. R., Follstaedt, D. M., Medlin D. L., and Mirkarimi, P. B., "Thick Stress-Free Amorphous-Tetrahedral

Carbon Films with Hardness Near that of Diamond," *Appl. Phys. Lett.*, Vol. 71, No. 26, December 1997.

[101] Gerstner, E. G., McKenzie, D. R., Puchert, M. K., Timbrell, P. Y., and Zou, J., "Adherent Carbon Film Deposition by Cathodic Arc with Implantation," *J. Vac. Sci. Technol. A*, Vol. 13, No. 2, March/April 1995, pp. 406-411.

[102] Anders, A., Anders, S., Brown, I., Dickinson, M. R., MacGill, R. A., "Metal Plasma Immersion Ion Implantation and Deposition Using Vacuum Arc Plasma Sources," *J. Vac. Sci. Technol. B*, Vol. 12, No. 2, March/April 1994, pp. 815-820.

[103] Anders, A., "Approaches to Rid Cathodic Arc Plasmas of Macro and Nanoparticles: A Review," to be published in *Surface and Coatings Technology*.

[104] Anders, S., Anders, A., Dickinson, M. R., MacGill, R. A., Brown, I.G., "S-shaped Magnetic Macroparticle Filter for Cathodic Arc Deposition," *IEEE Trans. Plasma Sci.*, Vol. 25, August 1997, pp. 670-674.

[105] Anders, A., personal communication, August 30, 1999.

[106] Sneddon, I. N., "The Relation Between Load and Penetration in the Axisymmetric Boussinesq Problem for a Punch of Arbitrary Profile," *Int. J. Eng. Sci.*, Vol. 3, 1965, pp. 47-57.

[107] Lo, R. and Bogy, D. B., "Compensating for elastic deformation of the indenter in hardness tests of very hard materials," *Journal of Materials Research*, Vol. 14, No. 6, June 1999, pp. 2276-2282.

[108] Anders, S., Brown, I., and Bogy, D., "Wanted: Hard, Thin Coatings for Near-Contact Recording," *Data Storage*, Vol. 4, No. 9, October 1997, pp. 31-34.

[109] Chen, C. Y., Wei, J., Fong, W., Bogy, D. B., and Bhatia, C. S., "The Decomposition Mechanisms and Thermal Stability of ZDOL Lubricant on Hydrogenated Carbon Overcoats," *Journal of Tribology*, Vol. 122, No. 2, April 2000, pp. 458-464.

[110] Chen, C. Y., Fong, W., Bogy, D. B., and Bhatia, C. S., "Initiation of lubricant catalytic decomposition by hydrogen evolution from contact sliding on CHx and CNx overcoats," *Tribology Letters*, Vol. 8, No. 1, 2000, pp. 25-34.

[111] Chen, C. Y., Bogy, D. B., and Bhatia, C. S., "Tribochemistry of monodispersed ZDOL with hydrogenated carbon overcoats," *Journal of Vacuum Science & Technology A (Vacuum, Surfaces, and Films)*, Vol. 18, No. 4, July-August 2000, pp. 1809-1817.

[112] Wei, J., Fong, W., Bogy, D. B., and Bhatia, C. S., "The Decomposition Mechanisms of a Perfluoroether at the Head/Disk Interface of Hard Disk Drives," *Tribology Letters*, Vol. 5, No. 2-3, 1998, pp. 203-209.

[113] Product data for Fomblin Z lubricants, Ausimont, undated.

[114] Fallon, P. J., Veerasamy, V. S., Davis, C. A., Robertson, J., Amaratunga, G. A. J., Milne, W. I., and Koskinen, K., "Properties of Filtered-Ion-Beam-Deposited Diamondlike Carbon as a Function of Ion Energy," *Physical Review B*, Vol. 48, 1993, p. 4777.

[115] Weiler, M., Sattel, S., Jung, K., Ehrhardt, H., Veerasamy, V. S., and Robertson, J., "Highly Tetrahedral, Diamond-Like Amorphous Hydrogenated Carbon Prepared from a Plasma Beam Source," *Applied Physics Letters*, Vol. 64, No. 21, May 1994, pp. 2797-2799.

[116] Brookes, C. A., Properties of Diamond, Academic Press, New York, 1979.

[117] Lo, R., Fong, W., Bogy, D. B., and Bhatia, C. S., "Thickness Dependence of Hardness and Elastic Modulus of Cathodic-Arc Amorphous Carbon Films," *Technical Report 98-012 (Blue Series)*, Computer Mechanics Laboratory, University of California, Berkeley, CA, November 1998.

[118] Robertson, J., "Deposition Mechanism of a-C and a-C:H," *Journal of Non-Crystalline Solids*, Vol. 164-166, 1993, pp. 1115-1118.

[119] Davis, C. A., "A Simple Model for the Formation of Compressive Stress in Thin Films by Ion Bombardment," *Thin Solid Films*, Vol. 226, No. 1, April 1993, pp. 30-34.

[120] Tsui, T. Y., Pharr, G. M., Oliver, W. C., Bhatia, C. S., White, R. L., Anders, S., Anders, A., and Brown, I. G., "Nanoindentation and Nanoscratching of Hard Carbon Coatings for Magnetic Disks," Proceedings of 1995 Materials Research Society Mechanical Behavior of Diamond and Other Forms of Carbon Symposium, San Francisco, CA, USA, April 17-21, 1995, p.447-52.

[121] Bogy, D. B., Yun, X., and Knapp, B. J., "Enhancement of Head-Disk Interface Durability by Use of Diamond-Like Carbon Overcoats on Slider's Rail," *IEEE Transactions on Magnetics*, Vol. 30, No. 2, pp. 369-374.

[122] Varanasi, S. S., Lauer, J. L., Talke, F. E., Wang, G., and Judy, J. H., "Friction and Wear Studies of Carbon Overcoated Thin Films Magnetic Sliders: Application of Raman Microspectroscopy," *Journal of Tribology – Transactions of the ASME*, Vol. 119, No. 3, July 1997, pp. 471-475.

[123] Bhatia, C. S., Anders, S., Brown, I. G., Bobb, K., Hsiao, R., and Bogy, D.B., "Ultra-thin Overcoats for the Head/Disk Interface Tribology," *Journal of Tribology – Transactions of the ASME*, Vol. 120, No. 4, October 1998, pp. 795-799.

[124] Chen, C. Y., Fong, W., Bogy, D. B., and Bhatia, C. S., "Lubricant thickness effect on tribological performance of ZDOL lubricated disks with hydrogenated overcoats," *Tribology Letters*, Vol. 7, No. 1, 1999. pp. 1-10.

[125] Ohr, R., to be published.

[126] Chhowalla, M., Robertson, J., Chen, C. W., Silva, S. R. P., Davis, C. A., Amaratunga, G. A. J., and Milne, W. I., "Influence of ion energy and substrate temperature on the optical and electronic properties of tetrahedral amorphous carbon (ta-C) films," *Journal of Applied Physics*, Vol. 81, No. 1, January 1997, pp. 139-145.

[127] Kleinsorge, B., Ferrari, A. C., Robertson, J., Milne, W. I., Waidmann, S., and Hearne, S., "Bonding regimes of nitrogen in amorphous carbon," *Diamond and Related Materials*, Vol. 9, 2000, pp. 643-648.